

Spatially organized tumor-stroma boundary determines the efficacy of immunotherapy in colorectal cancer patients



Open Access This file is licensed under a Creative Commons Attribution 4.0 International License, which permits use, sharing, adaptation, distribution and reproduction in any medium or format, as long as you give appropriate credit to the original author(s) and the source, provide a link to the Creative Commons

license, and indicate if changes were made. In the cases where the authors are anonymous, such as is the case for the reports of anonymous peer reviewers, author attribution should be to 'Anonymous Referee' followed by a clear attribution to the source work. The images or other third party material in this file are included in the article's Creative Commons license, unless indicated otherwise in a credit line to the material. If material is not included in the article's Creative Commons license and your intended use is not permitted by statutory regulation or exceeds the permitted use, you will need to obtain permission directly from the copyright holder. To view a copy of this license, visit

<http://creativecommons.org/licenses/by/4.0/>.

REVIEWER COMMENTS

Reviewer #1, expertise in colorectal cancer TME, CAFs (Remarks to the Author):

Feng et al use a combination of integrated spatial enhanced resolution sequencing (Stereo-seq) with scRNA Seq to characterize mismatch repair proficient as well as mismatch repair deficient human colon cancer samples. In the case of dMMR they also analyze tumor samples from patients undergoing anti PD1-PDL-1 treatment and displaying either partial or complete response or stable disease. Thus, this study aims to provide answers why dMMR patients often respond to ICB therapies whereas pMMR do not. This is an urgent open question to be resolved and is of high scientific and clinical interest.

However, there are several major concerns concerning this study, which need to be resolved for publication in Nat Comm.

Major points

- 1.) Table S1: Patient cohort and clinical description: The description of partial response, complete remission and stable disease is not sufficient to describe the clinical response to therapy. The tumor response grade (e.g. by Dvorak) is missing and needs to be provided by a pathologist and integrated into the table and the stratification of the patients. There are different responses, which are not sufficiently covered by the distinction in stable disease, partial response and complete response. This needs to be updated.
- 2.) Figure 1: The authors state in the introduction that the current spatial resolution (about 50 μm) of available techniques is not sufficient to recapitulate the cellular topological complexity in a tumor, especially of immune cells, which are about 6-14 μm of size. The authors state that they have developed Stereo-seq to overcome this problem and published a paper on this. However, in the results section the resolution of Stereo-seq in this study again only reached 50 μm resolution. Thus, the resolution is not better than of established methods so far. What is the reason for this and why the study is not performed at a higher resolution as stated in the introduction for the Stereo-seq method?
- 3.) Figure 1: Please indicate in much more detail how the tumor stroma boundary was defined. For me the expression analysis in Figure 1B reveals that the tumor stroma boundary does not represent a specific state in the spatial distribution of cells but more is a mixture of (tumor) epithelial gene expression and stromal gene expression signatures, which are mixed due to the nature of the spatial resolution of 50 μm , which implicates the contribution of at least two or more cell types for this expression pattern. This needs to be clarified. Is the tumor stroma boundary defined by a certain cell state of epithelial cells and/or stromal cells, which are different because of their close interaction or is it simply a mixture of gene expression patterns of two or more cell types sitting close together and are not properly resolved spatially in the experiment. Shen et al. showed in a Nat. Comm paper in 2014 in micropatterned in vitro tumor stromal assays that gene expression changes in the tumor stromal interaction area. These data and possibly data from follow up studies should be integrated and might help to better define boundary signatures. Thus, there is need to demonstrate that the boundary region is defined by cells expressing a specialized program and not just a mixture of gene expression signatures of different cell types not sufficiently resolved at the topological level.
- 4.) Figure 1D and S1D: the authors state that naïve dMMR and pMMR contain similar tumor stroma boundary proportions (lane 131): However, the data in Figure S1D show a very pronounced population of these boundary cells in pMMR, whereas in dMMR these cells (in greenish grey) were underrepresented. How does this fit to the statement??? In dPR/dCR and dSD/PD these cells are also barely visible.
- 5.) Lane 171-172: The authors state that RCTD revealed that the tumor stroma boundary where mostly composed of epithelial and stromal cells: this supports my notion that it is might be just a mixture of gene expression patterns of tumor and stromal cells not sufficiently resolved by spatial profiling.

6.) Figure 2D: The distribution of immune cells in the tumor areas, the boundary and stromal areas (-1000 to +1000 μ m) is overloaded with the many different immune cell types defined in Fig. 2A. These results should be shown increased by a factor of 5 in the supplemental files, whereas the major immune cell type distinction of Fig. 2bB should be shown instead in the main Figure. The many different but very similar color codes for the cells makes this extremely difficult to read. Importantly, the obvious controls displaying the distribution of epithelial (tumor) cells and stromal cells is missing in Figure 2D. This is essential to demonstrate that the epithelia cells should only appear right to 0 of the graph and stromal cells left to 0. This control would convincingly demonstrate the proper distribution and the proper integration and deconvolution of the scRNA Seq data into the spatial data.

7.) Figure 2F: The line graph of the different immune cell subsets is very convincing; however, a clearer representation of the data is additionally needed for intuitive understanding of the differences. In addition to the boundary region (which is fine) the Stromal and Tumor region should be divided in a (-)250 to (-)500 and a (-)500 to (-)1000 region and the accumulated values of these areas shown in bar graphs (as in Fig 2H). Bar graphs in Fig 2H are too small, need to be increased

8.) The authors tend to overinterpret their solely descriptive data and they make statements which are not supported by the results shown.

Lane 188: there is no validation of a structural barrier by IHC or IF of matrix proteins accumulating exactly at these areas as defined by spatial sequencing: thus, this statement is not valid. The term barrier even implements that a functional assay must be performed to demonstrate that the presence of this area indeed hinders immune cells from entering.

Lane 201: Mac_SPP1 myeloid cells cannot be stated to be remarkably reduced after PD-1 treatment based on the presented data: this is only valid if the same tumors would have been assessed before and after treatment. Avoid these statements

Lane 6: same ...led to decreased...is misleading. Instead: anti PD1 treated tumors showed low frequencies of ...

Lane 229: replace "led" by "was associated with higher abundance"

Lane 241: "tended to accumulate" replace with "were more abundant"

Lane 258: "accumulate"....replace

Lane 292: "accumulated" replace by "present at higher level"

Lane 325: "accumulation" replace by "elevated"

same for Lane 344, 346, 347, 383, 404

In summary there are a lot of conclusions made in this manuscript which are highly speculative and lack substantial functional support, in fact here are no functional data shown at all

9.) Figure S6G: What is the rationale to focus on CXCL12 CAFs and why the 5 subsets were defined in this group?

10.) Lane 398, 404: again no functional evidence: IHC and IF and functional evidence needed

11.) There is need for at least some functional evaluation of the hypotheses generated by the descriptive data. One such option would be the in vitro characterization of the CXCL14 CAFs and the proposed signaling cascades involved. And the ligand/receptor interactions

Reviewer #2, expertise in colorectal cancer TME, CAFs immunotherapy (Remarks to the Author):

In the manuscript entitled "Spatially organized tumor-stroma boundary determines the efficacy of immunotherapy in colorectal cancer patients", Feng and collaborators use spatial transcriptomics to investigate the composition of the TME, in particular from an immune cell point of view, in dMMR and pMMR patients and their response to immune checkpoint blockade therapy. To achieve their study, the authors use an internally

developed spatial transcriptomics method called Stereo-Seq, which, according to their claim, exhibits advantages such as in particular a high spatial resolution other alternative commercially available solution. The study, which is purely descriptive, is in line with the current scientific focus pushing the scRNA-Seq field to take into account the precise spatial localization and neighborhood of each cell-type. It nicely shows that the tumor-stroma boundary shows distinct features between dMMR, ICB responder and pMMR, ICB non-responder and suggests that cell interactions at the boundary region might drive immune checkpoint therapy resistance.

I nevertheless have some concerns that should be addressed before recommending the article as suitable for publication.

The authors claim that one of the main advantages of the developed Stereo-Seq method is the higher resolution down to 500 nm (line 93) compared to spatial transcriptomics competitors. However, it is confusing how this technical advantage is maintained in the current manuscript as the authors report that once processed, the end resolution of their Stereo-Seq transcriptomics data is 50 μm (lines 120 & 766). The statement on line 88 justifying the use of Stereo-Seq (line 88) should be revised as it finally doesn't apply to this manuscript.

The authors defined and labeled spatial clusters (figure 1) but do not describe or provide any detail on the rationale behind this labeling. For instance, tumor spatial clusters are either "tumor_CEA" or "tumor_MKI67". While MKI67 might be self-intuitive, it is not clear to me how the authors defined the "tumor_CEA" spatial cluster. I suppose that CEA is referring to the expression of CEA cell adhesion molecules but Figure 1b shows only the expression of CEACAM1 while "CEA" is also known as the former gene symbol of CEACAM5. The authors should clearly describe how they characterized the different spatial clusters shown in figure 1b.

The authors should include a clear description of how the subtypes of each major cell type have been identified in the materials and methods section. I assume it is through DGE analysis looking at Table S2, but this should be clearly referenced.

In general, the authors should make sure to carefully describe the labeling/characterization of all cell clusters. The Material and Methods part needs to be revised thoroughly.

In Extended Data Figure 2a, the authors should show the major cell type instead of cell subtypes to better relate this to the conclusion drawn from Figure 1e.

In Figure 2b, the authors should include a distribution plot of major cell types from scRNA-Seq in each patient and within dMMR, pMMR, dSD and dPR/dCR groups similar to the one shown in Extended Data Figure 4f.

In Extended Data Figure 3, the author should include a dot plot showing the marker genes used to identify the major cell types shown in Figure 2b.

The color scale used in figures 2a and 2c is not easy to read. In figure 2c it is in particular difficult to grasp which is the dominating cell type (distinguishing hues of green colors).

In Figure 2d, it would be valuable that the authors provide the same plot with major cell type annotations to clearly show the abundance of those cells over tumor-stroma boundaries.

While a reduction in myeloid cells and in particular SPP1+ macrophages is visible in dCR and dPR in figure 2h, these patients show increased proportions of plasma cells and to a

lesser extent B cells. The authors do not mention and interpret this increase which of course affects the proportion of remainder cell types. Could the authors comment this observation and how this affects the proportion of the remaining ones?

Although the characterized cluster are nicely and convincingly shown on the UMAP plot (figure S3c), the mean gene expression of major cell type markers shown in figure Extended Data Figure 3b doesn't look convincing. Indeed, the average expression of each marker seems to reach the maximum value (of 1, coded as dark red / brown) in Extended Data Figure 3b. As the UMAP plot (Extended Data Figure 3c) suggests a higher variance (much more lighter dots are visible for every marker except JCHAIN), the mean will unlikely reach such a high value.

The authors use the COAD bulk RNA-Seq dataset from TCGA to support their findings. However, the manuscript does not provide any detail on how the data was fetched and processed. In particular, the number of reported COAD samples (n=275) highly deviates from the currently available participants in the COAD project on the TCGA/GDC portal (n=461). The authors should clearly state why they only used a subset of patients. What was the rationale?

Overall, figures are of good quality but the authors should make sure to provide exhaustive legends. For example, Extended Data Figure 6f shows the mean expression as a scale but it is not clear if the values were normalized (capped to 1 and similar to the min/max scale shown in panel d?). The same Extended Data Figure 6g shows boxes which are not described in the legend nor in the manuscript and their purpose can only be guessed out of the main manuscript.

In addition, the flow of Extended Data Figure 6 is misleading as the panels appear in the following order: a, b, d, c, f, e and g.

The authors suggest that DC and T-cells crosstalk to accumulate in the tumor-stroma boundary (line 291). While the correlation plots (albeit some exhibiting poor correlation coefficients) support the spatial co-occurrence, the analysis could benefit from a ligand receptor pair analysis (such as performed by the authors in figure 3) to identify potential crosstalk signaling pathways.

Several typos subsist in the manuscript (batch: Bacth, line 152; bath line 153). Further language editing will improve the reading.

The raw sequencing data kindly provided for reviewing purposes is not accessible or likely outdated (pointing to a "Wrong share code OR this preview is Cancelled." webpage).

Reviewer #3, expertise in colorectal cancer TME, immunogenomics, scRNAseq and ST (Remarks to the Author):

Feng and colleagues' manuscript, which integrates spatial and single-cell transcriptomics along with multiplex immunofluorescence to explore the factors influencing response to immune checkpoint blockade (ICB) in colorectal cancer, represents a significant effort. However, there are substantial concerns regarding the study's design and the occasionally overstated conclusions drawn from the data:

1. The study's primary comparison between mismatch repair deficient (dMMR) and proficient (pMMR) colorectal cancer cases may not accurately reflect the nuances of ICB response. It would be more appropriate to analyze separate cohorts of dMMR and pMMR patients, further divided into responders and non-responders. Additionally, comparing treatment-naïve pMMR cases with treated dMMR cases introduces a confounding factor.

A more focused analysis solely on dMMR cases in the current cohort may still not provide a sufficient sample size to draw robust conclusions.

2. The use of the term "determinants of efficacy of immunotherapy" in the title and throughout the paper is misleading. Ideally, these determinants should be assessed before the administration of immunotherapy, not post-treatment.

3. There's a lack of clarity regarding the equal number of responders and non-responders in dMMR cases, especially given the previously reported high response rates. Clarification is needed on whether the cohort was specifically enriched for non-responders.

4. For methodological transparency, it's recommended to indicate in Table S1 or Figure 1 which patients underwent specific analytical processes. Were all patients analyzed with single-cell RNA sequencing also subject to spatial transcriptomics? And were RCTD analyses consistently performed on paired samples? If there's a mismatch in sample processing, this could affect the validity of the RCTD findings.

Additional Comments:

1. Certain claims, such as those in the abstract about unraveling the "black box" of ICB response, should be moderated. The primary known determinant in this context is the mutational burden, particularly in distinguishing between MMRd and MMRp CRCs. The term "black box" seems to oversimplify the current understanding of these mechanisms.

2. In the Results section, the authors' claim about the resolution of spatial transcriptomic data requires further justification, especially when compared to similar technologies like Visium. The significance of choosing this particular technology for its resolution, as stated in the introduction, remains unclear.

3. In the Results section the authors claim that they are able to analyse the spatial transcriptomic data at 50 um resolution, which is not that different from technologies like Visium. I therefore do not understand the significance of the last paragraph from the introduction where the authors claim that they have opted for this technology because of its resolution.

4. The interpretation of immune cell infiltration patterns in dSD versus dCR patients (line 183) appears speculative, especially in the absence of a tumor border in dCR patients. The observed patterns might simply reflect the presence of tumor cells, which inherently limits immune cell infiltration.

5. For consistency in data presentation, Figure 2D should have a uniform Y-axis.

6. The claim of treatment-induced changes (line 346) lacks a pre-treatment comparative analysis, which is crucial for substantiating such conclusions.

7. The discrepancy in the classification of responders between Figures 2 and 4 needs clarification. Why are only dPR patients considered responders in Figure 4, whereas dCR patients are also included in Figure 2?

Point-to-point respond letter to NCOMMS-23-41464A

Reviewer #1: expertise in colorectal cancer TME, CAFs

Overall comments	Feng et al use a combination of integrated spatial enhanced resolution sequencing (Stereo-seq) with scRNAseq to characterize mismatch repair proficient as well as mismatch repair deficient human colon cancer samples. In the case of dMMR they also analyze tumor samples from patients undergoing anti-PD1-PDL1 treatment and displaying either partial or complete response or stable disease. Thus, this study aims to provide answers to why dMMR patients often respond to ICB therapies whereas pMMR does not. This is an urgent open question to be resolved and is of high scientific and clinical interest. However, there are several major concerns concerning this study, which need to be resolved for publication in Nat Comm.
Author Response	We appreciate the reviewer for highlighting the scientific and clinical interest of our findings and for providing constructive comments to guide us on strengthening our manuscript. We acknowledge the shortcomings raised by the reviewer and have addressed them in the revised manuscript.
Major revisions	<ol style="list-style-type: none"> 1. Add new information to clarify the clinical features and ICB response assessment of our patient cohort. 2. Revise the description about the resolution of our stereo-seq platform by performing additional analysis and include discussion about the limitations of our study. 3. Add new analysis on the distribution curves of tumor cells, stromal cells and published marker genes in defining tumor-stroma boundary in the spatial map. 4. Add new <i>in vitro</i> experiments to support our analysis at least partially.

Ref 1.1 Clarification of clinical response to ICB therapy

Reviewer Comment	Table S1: Patient cohort and clinical description: The description of partial response, complete remission and stable disease is not sufficient to describe the clinical response to therapy. The tumor response grade (e.g. by Dvorak) is missing and needs to be provided by a pathologist and integrated into the table and the stratification of the patients. There are different responses, which are not sufficiently covered by the distinction in stable disease, partial response and complete response. This needs to be updated.
Author Response	We thank the reviewer for highlighting the importance of further clarifying the clinical response to ICB therapy in our patient cohort. We have now updated Table S1 and revised the description of patient samples and clinical study in the Methods part. As mentioned by the reviewer, the Dworak system is commonly used to assess the effectiveness of neoadjuvant therapy for CRC patients based on histopathological examination, in particular for neoadjuvant chemoradiotherapy ¹ . In the context of neoadjuvant immunotherapy, both image-based evaluation such as endoscopy or MRI using Response Evaluation Criteria in Solid Tumors (RECIST) version 1.1, as well as pathological-based evaluation using National Comprehensive Cancer Network (NCCN) Tumor Regression Grade (TRG) system, are commonly used for patient stratification ^{2,3} . According to the guidelines in our hospital, we considered both the NCCN TRG system and RECIST to define the treatment response. For the NCCN TRG system, patients were grouped into complete response (TRG 0: no remaining viable cancer cells), partial response

(TRG 1: only small clusters or single cancer cells remaining), and stable disease (TRG 2: residual cancer remaining) briefly⁴. The information is now integrated into the revised table S1.

Excerpt from revised manuscript

(P. 27:)

Method lane 810

Tumor tissues were collected from 23 patients with CRC who underwent colon resection with or without neoadjuvant ICB treatment at Sun Yat-Sen University Cancer Center. Tumors were staged with the 8th edition of the American Joint Committee of Cancer (AJCC) tumor node-metastasis (TNM) staging classification for CRC. Enhanced CT scans of the chest and abdomen, and MRI scans of the rectum, were used to ascertain the TNM stage. Transrectal ultrasonography or endoscopic ultrasound was used to ascertain the tumor and nodal stage for patients unsuitable for MRI tests because of metal implants or other reasons. Mismatch repair was determined by immunohistochemistry (IHC) for mismatch repair proteins and microsatellite instability status was determined by PCR for microsatellite instability markers. Patient response to neoadjuvant ICB treatment was determined by image-based evaluation such as endoscopy or MRI using Response Evaluation Criteria in Solid Tumors (RECIST) version 1.1 as well as postoperative pathological evaluation according to the criteria from National Comprehensive Cancer Network (NCCN) Tumor Regression Grade (TRG) system. The clinical information including age, gender, MMR/MSI status, TNM stage, anti-PD1 monoclonal antibodies used, course of treatment and tumor response grade, as well as the stratification of the patients in the current study were listed in **table S1**. This study was done in accordance with the Declaration of Helsinki (B2023-178-01). The protocol was reviewed and approved by The Institutional Review Board of BGI Ethical (BGI-IRB21083-T1). All participants provided written informed consent and the clinical information was collected at Sun Yat-Sen University cancer center.

Table S1: Clinical information of the patients

Table S1. Clinical information of the patients.

stereo-seq													
patients No.	age	gender	MMR status	MSI status	pre-surgery TNM stage	post-surgery TNM stage	treatment	apd1 drug	course of treatment	timepoint for sampling	response on NCCN TRG	response on RECIST	group label in this study
24	69	F	dMMR	MSI-H	cT4N2M0	pT0N0M0	apD1	Pembrolizumab	4	post-treatment	0	CR	dCR
25	34	M	dMMR	MSI-H	cT4N2M0	pT0N0M0	apD1	Pembrolizumab	8	post-treatment	0	CR	dCR
56	55	F	dMMR	MSI-H	cT4N2M1	pT4N2M1	NA	NA	NA	treatment-naive	NA	NA	dMMR
61	51	F	dMMR	MSI-H	cT4N2M0	pT0N0M0	apD1	Camrelizumab	4	post-treatment	1	CR	dCR
95	71	M	dMMR	MSI-H	cT3N0M0	pT3N0M0	apD1	Camrelizumab	4	post-treatment	not evaluated	SD	dSD
99	39	M	dMMR	MSI-H	cT4N2M0	pT4N2M0	NA	NA	NA	treatment-naive	NA	NA	dMMR
100	55	M	dMMR	MSI-H	cT4N2M0	pT3N0M0	NA	NA	NA	treatment-naive	NA	NA	dMMR
104	53	F	dMMR	undetermined	cT3N1M0	pT3N0M0	apD1	Sintilimab	4	post-treatment	2	SD	dSD
107	79	F	dMMR	undetermined	cT4N1M0	pT3N0M0	NA	NA	NA	treatment-naive	NA	NA	dMMR
112	34	F	dMMR	MSI-H	cT4N2M1	pT1N0M0	apD1	Sintilimab	6	post-treatment	1	PR	dPR
50	57	F	pMMR	MSS	cT3N0M0	pT3N1M0	NA	NA	NA	treatment-naive	NA	NA	pMMR
55	46	F	dMMR	MSS	cT3N0M0	pT3N0M0	NA	NA	NA	treatment-naive	NA	NA	pMMR
59	74	F	pMMR	MSS	cT4N1M0	pT3N0M0	NA	NA	NA	treatment-naive	NA	NA	pMMR
61	74	F	pMMR	MSS	cT3N0M0	pT3N0M0	NA	NA	NA	treatment-naive	NA	NA	pMMR
73	51	M	pMMR	MSS	cT3N0M0	pT3N0M0	NA	NA	NA	treatment-naive	NA	NA	pMMR

stRNA-seq													
patients No.	age	gender	MMR status	MSI status	pre-surgery TNM stage	post-surgery TNM stage	treatment	apd1 drug	course of treatment	timepoint for sampling	response on NCCN TRG	response on RECIST	group label in this study
146	76	F	dMMR	MSI-H	cT4N2M0	pT3N2M0	apD1	Pembrolizumab	3	post-treatment	2	SD	dSD
147	38	M	dMMR	MSI-H	cT4N2M1	pT4N2M1	apD1+chemo	Nivolumab	6	post-treatment	2	SD	dSD
148	34	F	dMMR	MSI-H	cT4N2M0	pT3N1M0	apD1	Tislelizumab	3	post-treatment	1	PR	dPR
60	39	M	dMMR	MSI-H	cT4N2M0	pT4N2M0	apD1	Camrelizumab	8	post-treatment	2	SD	dSD
74	69	F	dMMR	MSI-H	cT4N2M0	pT0N0M0	apD1	Pembrolizumab	4	post-treatment	0	CR	dCR
27	61	F	pMMR	MSS	cT3N1M0	pT3N1M0	NA	NA	NA	treatment-naive	NA	NA	pMMR
20	67	M	dMMR	MSS	cT3N0M0	pT3N0M0	NA	NA	NA	treatment-naive	NA	NA	pMMR
32	56	F	pMMR	MSS	cT3N0M0	pT3N0M0	NA	NA	NA	treatment-naive	NA	NA	pMMR
34	70	M	pMMR	MSS	cT3N0M0	pT3N0M0	NA	NA	NA	treatment-naive	NA	NA	pMMR
37	63	M	dMMR	MSS	cT3N0M0	pT3N1M0	NA	NA	NA	treatment-naive	NA	NA	pMMR

nCR: near complete response

Ref 1.2 Clarification of spatial resolution of the Stereo-seq platform

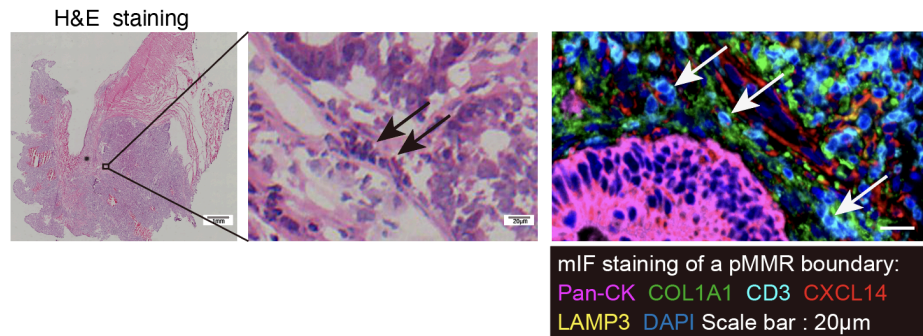
Reviewer Comment

Figure 1: The authors state in the introduction that the current spatial resolution (about 50 μm) of available techniques is not sufficient to recapitulate the cellular topological complexity in a tumor, especially of immune cells, which are about 6-14 μm of size. The authors state that they have developed Stereo-seq to overcome this problem and published a paper on this. However, in the results section the resolution of Stereo-seq in this study again only reached 50 μm resolution. Thus,

	<p>the resolution is not better than established methods so far. What is the reason for this and why the study is not performed at a higher resolution as stated in the introduction for the Stereo-seq method?</p>								
<p>Author Response</p>	<p>We acknowledge the issue of spatial resolution used in this study raised by the reviewer. The Stereo-seq platform we developed is based on combined DNA nanoball (DNB)-patterned arrays and in situ RNA capture. By aggregating neighboring DNA nanoballs (forming a square bin) or assigning DNA nanoballs to individual cell via image-based cell segmentation (cell bin), our previous studies have nicely demonstrated the achievement of high sensitivity and single-cell resolution (500nm) <i>in situ</i> through Stereo-seq in mouse embryos ⁵ and axolotl brain ⁶. We therefore applied Stereo-seq to analyze the tumor tissues collected from CRC patients in the current study. Unfortunately, when we set the cell bin for single-cell segmentation, we could only generate fewer than 300 genes per bin (new Supplementary Fig. 1b). Compared to scRNA-seq datasets generated from CRC patients in our in-house and published datasets⁷ (new Supplementary Fig. 1b), ~300 genes/cell was insufficient for cell type annotation and follow-up analysis. One probable explanation may be the difference on the average cell size and the complexity among different tissues. This observation indicated the limitation of our Stereo-seq platform, which may not be universally applicable, particularly in tissues enriched with small-sized immune cells, such as tumors, spleen and thymus. In addition, it is common to observe the co-localization of different cells within the three-dimensional (3D) structure of tumors. For example, we observed that the immune cells (e.g. CD3⁺) were co-localized with fibroblasts (COL1A1⁺) as shown by H&E and mIF staining (Fig. R1). However, our current spatial transcriptomic analysis can only generate 2D sequencing data from single slide analysis ⁸. As a result, when cells were segmented into single cell resolution, it was common to find transcripts mixed with fibroblasts (such as COL1A1), immune cells (such as CD3E, PTPRC, FCGR3A), and epithelial cells (such as EPCAM) (Fig. R2). These cells would be classified as doublets in scRNA-seq analyses due to their ambiguous nature ⁹. Therefore, a general challenge faced in Stereo-seq analysis, which may also be applicable to other spatial transcriptomic platforms, is how to balance the resolution and mRNA capture efficiency. To overcome these limitations, we employed parallel scRNA-seq analysis alongside Stereo-seq and set the resolution into 50 μm (bin 100) in our current study. This combination allowed us to distinguish transcriptionally similar cell types and analyze their spatial localization. We have now incorporated this information into the discussion section and modified the introduction in our revised manuscript.</p> <div data-bbox="411 1541 670 1848" data-label="Figure"> <p>b Gene counts per cell</p> <table border="1"> <thead> <tr> <th>Method</th> <th>Approximate Median Gene Counts</th> </tr> </thead> <tbody> <tr> <td>cell bin</td> <td>~10²</td> </tr> <tr> <td>in house scRNA-seq</td> <td>~10³</td> </tr> <tr> <td>external scRNA-seq</td> <td>~10³</td> </tr> </tbody> </table> </div> <p>New Supplementary Fig. 1b. Violin plots of the gene counts per cell in cell bin segmented of Stereo-seq data from a representative patient #59, our in house</p>	Method	Approximate Median Gene Counts	cell bin	~10 ²	in house scRNA-seq	~10 ³	external scRNA-seq	~10 ³
Method	Approximate Median Gene Counts								
cell bin	~10 ²								
in house scRNA-seq	~10 ³								
external scRNA-seq	~10 ³								

scRNA-seq data and a representative public scRNA-seq data (GSE178341) are shown.

FigR1



FigR2

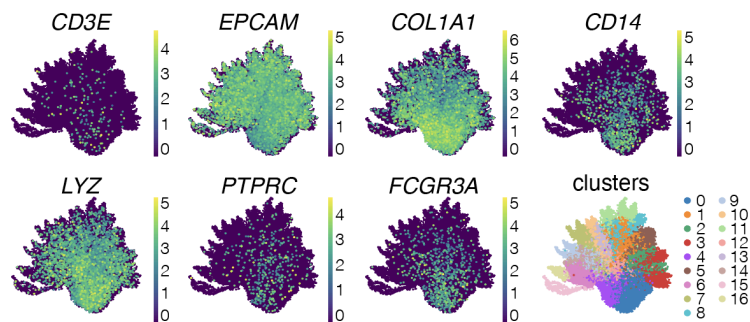


Fig R1. Possible co-localization of immune cells and fibroblasts is shown by H&E staining (left) or mIF staining (right).

Fig R2. The UMAP of the unsupervised clustering of the cell bins and marker genes from the spatial transcriptome of patient #59.

Excerpt from revised manuscript

(P. 5:)

Introduction lane 88

We therefore developed the spatial enhanced resolution omics-sequencing (Stereo-seq). It is a DNA nanoball (DNB)-patterned array embedded with coordinate identity¹³ and unique molecular identifiers (MID) co-barcoded poly-T probe, capable of capturing mRNA *in situ* at a resolution of 500 nanometer (nm). Using this platform, we successfully constructed 2-dimensional (2D) spatial transcriptomic maps at single cell level in mouse embryos and axolotl brain^{13,14}. Considering the complexity and smaller size of immune cells in the tumors, here we applied integrative analysis of scRNA-seq and Stereo-seq to in-depth dissect the gene regulatory programs and cell-cell interactions underlying ICB response in CRC patients. Through analysis in 25 tumor specimens from CRC patients of treatment naïve dMMR, pMMR and anti-PD1-treated dMMR patients that included responders (complete response (CR)/PR) and non-responders (stable disease, SD), we generated a CRC spatial transcriptomic atlas and uncovered a 300 micrometer (µm) boundary region (0±150 µm) that regulated immune cell influx to the tumor center region (>150 µm).

(P. 6:)

Results lane 118

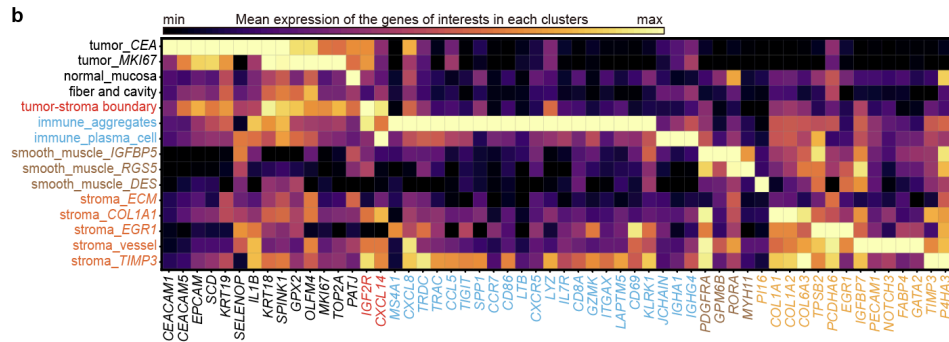
After pre-processing on the raw data generated by Stereo-seq (see Methods), the spatial transcriptome map was lassoed out and matched to the tissue edge

	<p>(https://www.stomics.tech/sap/home.html). <u>As the single-cell resolution was insufficient to generate an adequate number of genes per bin for cell type annotation and follow-up analysis in tumor tissues (Supplementary Fig. 1b), we adjusted the bin size to bin100, which allowed us to obtain a sufficient gene count for transcriptomic analysis at a resolution of 50µm (Supplementary Fig. 1b-d).</u></p> <p>(P. 21:) Discussion lane 601 <u>Secondly, the Stereo-seq technique has not reached the single-cell resolution when analyzing heterogenous and complex tumor specimens in the current study. The nanoscale resolution (capture spot diameter: 220 nm; center-to-center distance: 500 nm) of Stereo-seq merely supported an estimate of 1-10 cells in each bin in CRC tumor tissues compared to previous analysis in mouse embryos and axolotl brain^{13,14,63}. One probable explanation may be the difference on the average cell size and the complexity among different tissues. This observation indicated the limitation of our Stereo-seq platform, which may not be universally applicable, particularly in tissues enriched with small-sized immune cells, such as tumors, spleen and thymus. A more precise spatial map, if we can develop in the future, will be essential for better understanding of how to therapeutically target the spatiotemporal heterogeneity of the complex TME of CRCs, as well as other cancers. For example, enrichment of the variable regions of T and B cell receptor mRNA accompanied with the current Stereo-seq platform would present a compelling strategy for mapping the immune cells, at least T cell and B cells at single cell resolution in tumors <i>in situ</i>.</u></p>
--	---

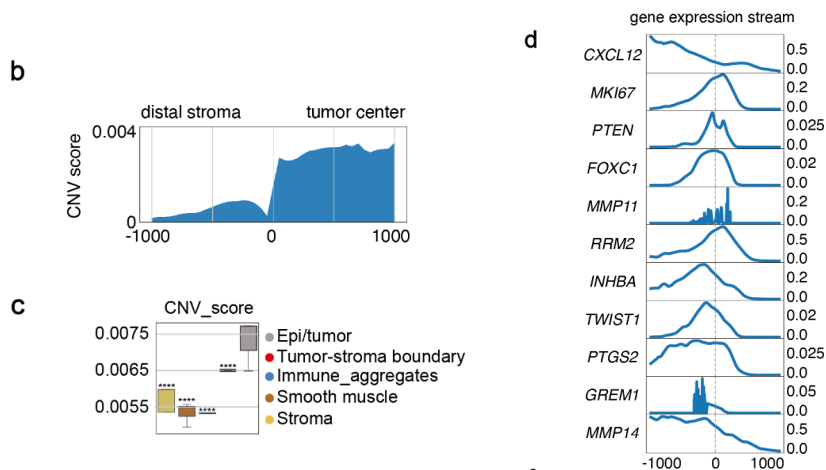
Ref 1.3 Definition of tumor stroma boundary

<p>Reviewer Comment (i)</p>	<p>Figure 1: Please indicate in much more detail how the tumor stroma boundary was defined. For me the expression analysis in Figure 1B reveals that the tumor stroma boundary does not represent a specific state in the spatial distribution of cells but mor is a mixture of (tumor) epithelial gene expression and stromal gene expression signatures, which are mixed due to the nature of the spatial resolution of 50 µm, which implicates the contribution of at least two or more cell types for this expression pattern. This needs to be clarified. Is the tumor stroma boundary defined by a certain cell state of epithelial cells and/or stromal cells, which are different because of their close interaction or is it simply a mixture of gene expression patterns of two or more cell types sitting close together and are not properly resolved spatially in the experiment. Shen et al. showed in a Nat. Comm paper in 2014 in micropatterned in vitro tumor stromal assays that gene expression changes in the tumor stromal interaction area. These data and possibly data from follow up studies should be integrated and might help to better define boundary signatures. Thus, there is need to demonstrate that the boundary region is defined by cells expressing a specialized program and not just a mixture of gene expression signatures of different cell types not sufficiently resolved at the topological level.</p>
<p>Author Response (i)</p>	<p>We agree with the reviewer that much more details about how the tumor-stroma boundary was defined are needed. The tumor-stroma boundary is commonly recognized as a niche composed of malignant cells in the outermost circle of solid tumor and non-malignant cells that are closely adjacent in spatial architecture, bridging these distinct spatial regions ¹⁰. By using Leiden algorithm ¹¹, we clustered the regional transcriptome in an unsupervised manner and annotated each region based on both the differentially expressed genes (DEGs) and the</p>

anatomical structures presented by the H&E staining (as shown in **original Fig. 1b, Fig 1d** and **Supplementary Fig. 2a**). As a result, we identified 6 major anatomical structures: normal epithelia/tumor (epi/tumor), smooth muscle, tumor-stroma boundary, stroma, immune aggregates and low mRNA-enriched (fiber and cavity) regions by Stereo-seq analysis (**revised Fig. 1b**). To further distinguish the tumor center and tumor-stroma boundary, we assessed the copy number variation (CNV) score in the spatial transcriptomic data ^{12,13} (<https://github.com/broadinstitute/infercnv>). We found CNV scores were significantly higher in the epi/tumor region, whereas lower CNV scores were observed in the tumor-stroma boundary and stromal regions (**new Supplementary Fig. 2b-c**). In addition, as mentioned by the reviewer, Shen et al. have provided a comprehensive analysis of tumor-stroma interactions by evaluating 11 pertinent genes within and adjacent to the tumor mass in breast cancer ¹⁴. We also assessed the expression patterns of these genes in our spatial transcriptomic data. Our data suggested that 8 out of 11 genes (MKI67, PTEN, FOXC1, MMP11, RRP2, INHBA, TWIST1, GREM1) were significantly enriched at the boundary region (**new Supplementary Fig. 2d**), further supporting that our boundary definition is robust. We have now incorporated this information into our revised manuscript.



Revised Fig. 1b. The top differential express gene (DEG) expressions in each spatial cluster are shown in the matrix plot.



New Supplementary Fig. 2b-c. **b** The stacked stream plot of the CNV scores from the distal stroma (-1000µm, left) to the tumor center (1000µm, right) is shown. The mean CNV score in each 1mm interval is smoothed using slinger model. The distance of boundary was set to 0µm. **c** The box plots of the CNV scores in each major spatial cluster are shown. The asterisk represents the comparison of the

	<p>epi/tumor clusters towards other spatial clusters. Data are represented as mean±SD and analyzed by unpaired Student-t test. ****, p<0.0001. d The stacked stream plots of the indicated gene expressions from the distal stroma (-1000µm, left) to the tumor center (1000µm, right) are shown. The mean expression level in each 1mm interval is smoothed using slinger model. The distance of boundary was set to 0µm.</p>
<p>Excerpt from revised manuscript (i)</p>	<p>(P. 6:) Results lane 128 <u>Using Leiden algorithm¹⁶, we next performed an integration of unsupervised clustering analysis of the spatial transcriptomics data with H&E staining image. This approach led to the generation of signature score and enrichment score, enabling the deconvolution of the cellular composition of spatially defined bins. As a result, we identified 15 spatial clusters, which captured a wide spectrum of regions of the 6 major anatomical structures: normal epithelia/tumor (epi/tumor), smooth muscle, tumor-stroma boundary, stroma, immune aggregates and low mRNA-enriched (fiber and cavity) regions in the tissues from 15 patients by Stereo-seq analysis (Fig. 1b and Supplementary Fig. 2a). Further assessment of copy number variation (CNV) score^{15,17} (https://github.com/broadinstitute/infercnv/) clearly showed that the tumor region exhibited higher CNV scores compared to other regions (Supplementary Fig. 2b-c). In addition, we observed a similar gene expression pattern in the gene set used to define the tumor-stroma boundary in breast cancer¹⁸ within our spatial cluster (Supplementary Fig. 2d), supporting the robustness of our spatial cluster definition.</u></p>
<p>Reviewer Comment (ii)</p>	<p>Lane 171-172: The authors state that RCTD revealed that the tumor stroma boundary where mostly composed of epithelial and stromal cells: this supports my notion that it is might be just a mixture of gene expression patterns of tumor and stromal cells not sufficiently resolved by spatial profiling.</p>
<p>Author Response (ii)</p>	<p>The tumor-stroma boundary is indeed defined as a niche composed of malignant cells and non-malignant cells that are closely adjacent in spatial architecture ¹⁰. As mentioned by the reviewer, the cell type composition analysis in the tumor-stroma boundary reflected epi/tumor and fibroblasts was the predominant cell type (original Supplementary Fig. 4f). Nevertheless, we did observe clear differences of other cell types in the tumor-stroma boundary between dMMR and pMMR as shown in the revised Fig. 2d. Therefore, we focused on this region for our follow up analysis.</p> <div data-bbox="414 1568 1085 1881" data-label="Figure"> <p>d</p> </div> <p>Revised Fig. 2d. The stacked stream plots of immune cell distribution patterns from distal stroma (-1000µm, left) to tumor center (1000µm, right) in indicated patient groups are shown. The mean RCTD frequencies of each immune cell in</p>

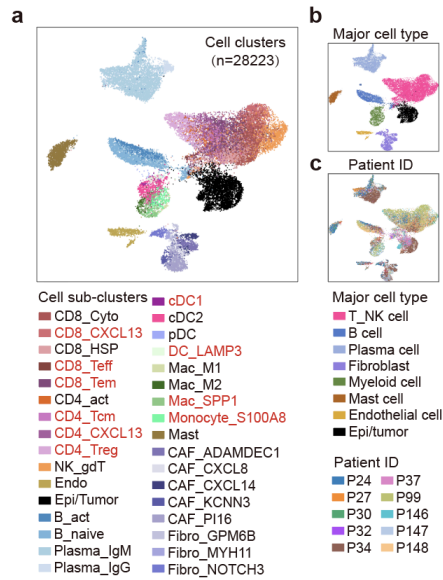
	each 1mm interval was smoothed using slinger model and colored by cell sub-clusters in accordance with a.
Excerpt from revised manuscript	(P. 8:) Result lane 192 As expected, the majority of cell types accumulated in the tumor-stroma boundary were epithelial/tumor cells, followed by fibroblasts in either dMMR or pMMR, except for patient #25 and #61 who showed complete response to the anti-PD1 therapy (Supplementary Fig. 4f). <u>This finding is consistent with previous report that describes the tumor-stroma boundary as a niche composed of malignant cells in the outermost circle of solid tumor and non-malignant cells that are closely adjacent in spatial architecture, bridging these distinct spatial regions²².</u>

Ref 1.4 Labelling errors on Figure 1D and S1D

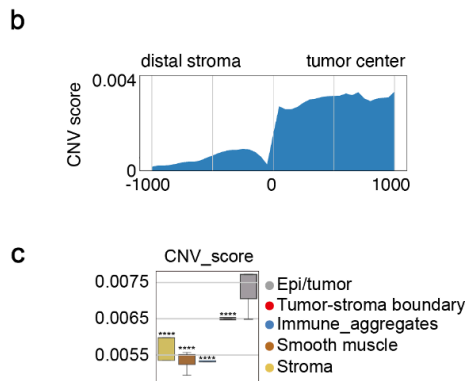
Reviewer Comment	Figure 1D and S1D: the authors state that naïve dMMR and pMMR contain similar tumor stroma boundary proportions (lane 131): However, the data in Figure S1D show a very pronounced population of these boundary cells in pMMR, whereas in dMMR these cells (in greenish grey) were underrepresented. How does this fit to the statement??? In dPR/dCR and dSD/PD these cells are also barely visible.
Author Response	<p>We apologize for any confusion caused by the information presented in Fig. 1D and Supplementary Fig 1D. We double-checked our data and confirmed that the proportions of tumor-stroma boundary in naïve dMMR and pMMR in Fig. 1D are correct. For the Supplementary Fig. 1D, we previously made a mistake and wrongly labeled the groups of pMMR and dPR/dCR. In addition, we initially labelled the tumor-stroma boundary by greenish-grey dots, which may overlap with the other greenish dots and made it difficult to distinguish. In the revised Supplementary Fig. 1e, we modified the labelling color of the tumor-stroma boundary into red dots and corrected the numbers.</p> <p>e</p> <p> <ul style="list-style-type: none"> ● boundary ● tumor_CEA ● tumor_MKI67 ● normal_mucosa ● fiber and cavity ● immune_aggregates ● immune_plasma_cell ● smooth_muscle_DES ● smooth_muscle_IGFBP5 ● smooth_muscle_RGS5 ● stroma_COL1A1 ● stroma_ECM ● stroma_EGR1 ● stroma_TIMP3 ● stroma_vessel </p> <p>Revised Supplementary Fig. 1e. UMAP of the spatial transcriptome data from 205,362 bins from 15 CRC patients are shown. Bins are colored by spatial cell clusters, split by clinical information.</p>

Ref 1.5 Revision of the labelling colors and distribution curves of cell types in Fig. 2

<p>Reviewer Comment (i)</p>	<p>Figure 2D: The distribution of immune cells in the tumor areas, the boundary and stromal areas (-1000 to +1000μm) is overloaded with the many different immune cell types defined in Fig. 2A. These results should be shown increased by a factor of 5 in the supplemental files, whereas the major immune cell type distinction of Fig. 2B should be shown instead in the main Figure. The many different but very similar color codes for the cells make this extremely difficult to read. Importantly, the obvious controls displaying the distribution of epithelial (tumor) cells and stromal cells are missing in Figure 2D. This is essential to demonstrate that the epithelia cells should only appear right to 0 of the graphs and stromal cells left to 0. This control would convincingly demonstrate the proper distribution and the proper integration and deconvolution of the scRNA Seq data into the spatial data.</p>
<p>Author Response (i)</p>	<p>We thank the reviewer for this helpful suggestion and apologize for the confusion caused by the color labelling. It is indeed extremely difficult to read more than 30 different colors on a single panel of the UMAP data. We therefore assigned a principal color to each major cell type: green for myeloid cell clusters, red for NK_T cell clusters, blue for B/plasma cell clusters, violet for fibroblasts, dark brown for mast cell, orange for endothelial cell and black for epi/tumor cell, in consistence with the main cell type labelling in the revised Fig. 2b. Next, we fine-tuned the shades of myeloid cells to ensure that subsets within each major category are similar yet distinct in the revised Fig. 2a.</p> <p>As suggested by the reviewer, we agree that including the distribution analysis by RCTD of epi/tumor and stromal cells will be useful. However, it is quite difficult to separate the tumor cells and tumor-adjacent normal epithelial cells on the spatial map only based on RNA expression. That was also the reason why we named epi/tumor as one spatial cluster (Fig. 2a-b). With a focus on tumor cells, we further generated an additional RCTD curve using CNV scores as described above ^{12,13} (https://github.com/broadinstitute/infercnv). The result showed that the CNV scores mainly appeared 0 to right (new Supplementary Fig. 2b-c), suggesting an accumulated tumor cells in the annotated tumor edge and tumor center (original fig 2e).</p> <p>Since it is not applicable to integrate the CNV curve (representing tumor cells) into the RCTD curve (representing all other cells except for tumor cells) in one figure, we generated a new RCTD curve (Fig. R3) to indicate the distributions of the other major cell types, i.e. stromal cell and immune cell types in Fig. 2b. As we mentioned, the majority of cell types accumulated in the tumor-stroma boundary were epithelial/tumor cells, followed by fibroblasts (Supplementary Fig. 4f). The distribution of immune cells is difficult to distinguish in the new RCTD curve (Fig. R3). Therefore, we separately described the distribution patterns of immune cells and stromal cells (focused on fibroblasts) in Fig. 2 and Fig. 5, respectively.</p>



Revised Fig. 2a-b. **a** Uniform manifold approximation and projection (UMAP) of the transcriptome of 28,223 single cells from 10 CRC patients (5 pMMR; 2 dPR/CR; 3 dSD). Cells are colored by single cell subclusters, **b** major cell types. The names of the cell of interests are highlighted in red.



New Supplementary Fig. 2b-c. **b** The stacked stream plot of the CNV scores from the distal stroma (-1000µm, left) to the tumor center (1000µm, right) is shown. The mean CNV score in each 1mm interval is smoothed using slinger model. The distance of boundary was set to 0µm. **c** The box plots of the CNV scores in each major spatial cluster are shown. The asterisk represents the comparison of the epi/tumor clusters towards other spatial clusters. Data are represented as mean±SD and analyzed by unpaired Student-t test. ****, $p < 0.0001$.

	<p>Fig R3. The stacked stream plot of the distribution patterns of immune cells and stromal cells from stroma (-1000µm, left) to tumor (1000µm, right).</p>
<p>Reviewer Comment (ii)</p>	<p>Figure 2F: The line graph of the different immune cell subsets is very convincing; however, a clearer representation of the data is additionally needed for intuitive understanding of the differences. In addition to the boundary region (which is fine) the Stromal and Tumor region should be divided in a (-)250 to (-)500 and a (-)500 to (-)1000 region and the accumulated values of these areas are shown in bar graphs (as in Fig 2H). Bar graphs in Fig 2H are too small, need to be increased.</p>
<p>Author Response (ii)</p>	<p>We thank the reviewer for the good suggestion. Based on our initial analysis as described in result part 1, we focused on the in-depth analysis of cellular composition in the tumor-stroma boundary. Therefore, we highlighted this region, i.e. 0±150µm in the line graph, although the immune cell distribution from -1000 to +1000 µm could also be observed in Fig. 2f. The results suggested that the immune cell subsets, including CD8_Teff, CD8_Tem, CD8_CXCL13, CD4_CXCL13, CD4_Treg, CD4_Tcm, cDC1 and DC_LAMP3 showed significant enrichment peaks within the tumor-stroma region in treatment naïve dMMR compared to pMMR (Fig. 2f), which were also significantly higher in dPR/dCR compared to dSD (Fig. 2g). As suggested by the reviewer, we also generated bar graphs of different immune cell subsets by calculating accumulated values as Fig. 2h based on divided regions as follows: distal stroma (-500 to -1000µm), proximal stroma (-150 to -500µm), tumor-stromal boundary (-150 to +150µm), proximal tumor (+150 to +500µm), and distal tumor (+500 to +1000µm) (Fig. R4). Consistently, we observed that CD8_Teff, CD8_Tem, CD8_CXCL13, CD4_CXCL13, CD4_Treg, CD4_Tcm, cDC1 and DC_LAMP3 showed significant enrichment peaks within the tumor-stroma region in treatment naïve dMMR compared to pMMR, which were also significantly higher in dPR/dCR compared to dSD. Although we also observe distinct values of immune cell subsets in other regions (Fig. R4), our focus in the current study is on the characteristics of the tumor-stroma boundary, which showed potential implications for immunotherapy response. These observations hold promise for informing future research. The size of the bar graphs in Fig. 2i is revised.</p>

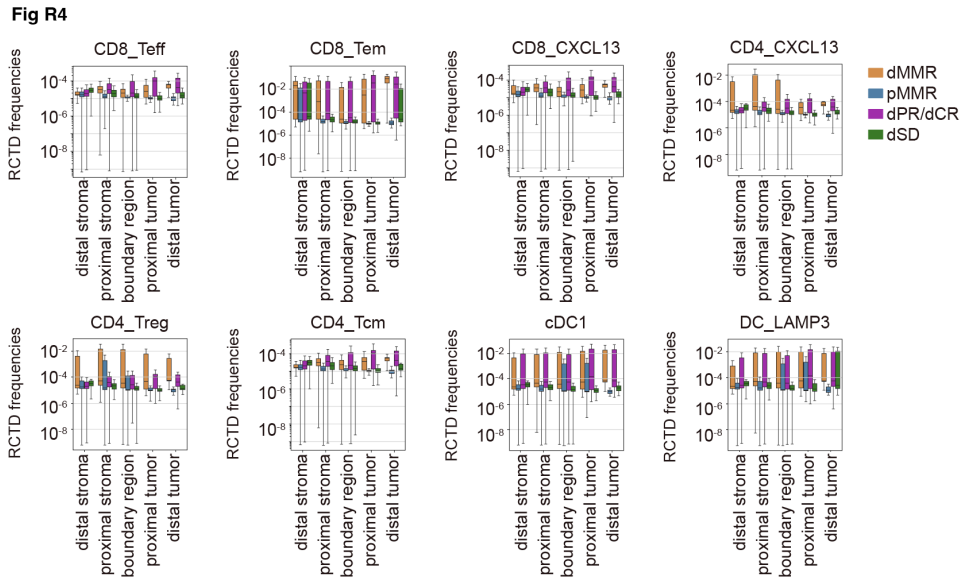
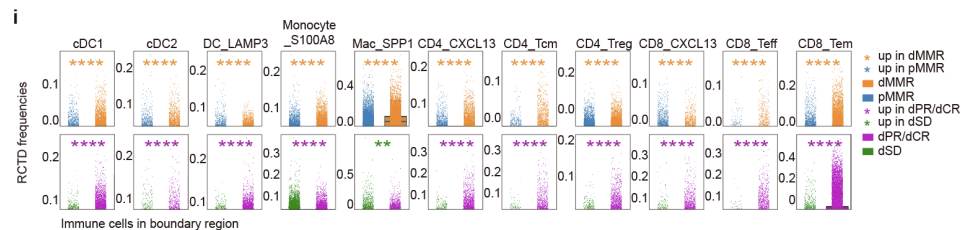


Fig R4. The RCTD frequencies of CD8_Teff, CD8_Tem, CD8_CXCL13, CD4_CXCL13, CD4_Treg, CD4_Tcm, cDC1 and DC_LAMP3 covering $0 \pm 1000 \mu\text{m}$, including distal stroma (-500 to $-1000 \mu\text{m}$), proximal stroma (-150 to $-500 \mu\text{m}$), tumor-stromal boundary (-150 to $+150 \mu\text{m}$), proximal tumor ($+150$ to $+500 \mu\text{m}$), and distal tumor ($+500$ to $+1000 \mu\text{m}$) regions in the spatial map.



Enlarged Fig. 2i. The RCTD frequencies of indicated immune cell subclusters in the tumor-stroma boundary of the four groups of patients. Data are analyzed by unpaired Student-t test. **, $p < 0.01$; ****, $p < 0.0001$.

Ref 1.6 Statement rephrase and experimental validation

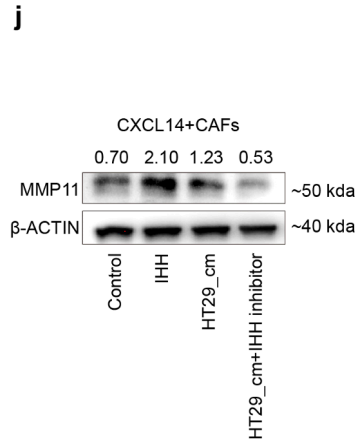
Reviewer Comment

The authors tend to overinterpret their solely descriptive data and they make statements which are not supported by the results shown.

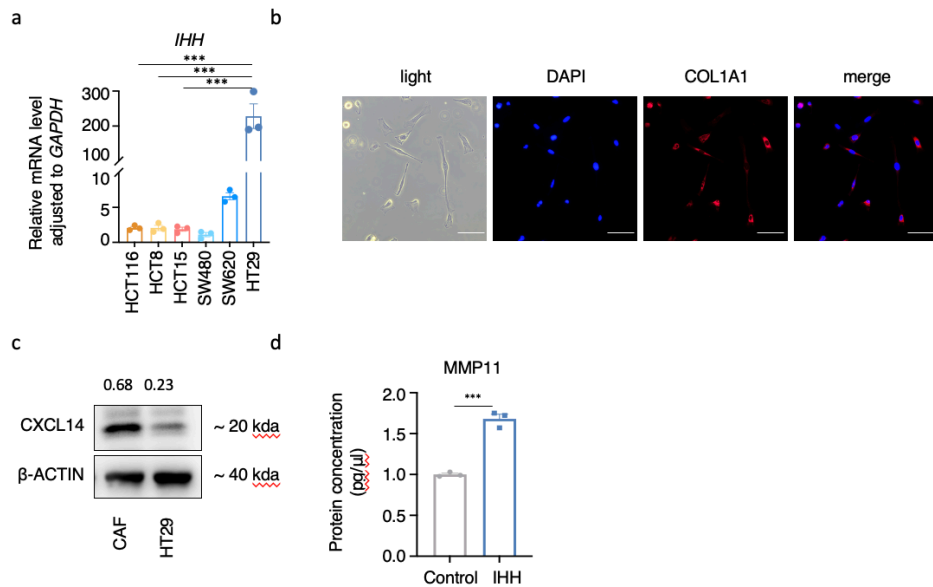
Lane 188: there is no validation of a structural barrier by IHC or IF of matrix proteins accumulating exactly at these areas as defined by spatial sequencing: thus, this statement is not valid. The term barrier even implements that a functional assay must be performed to demonstrate that the presence of this area indeed hinders immune cells from entering.

Lane 201: Mac_SPP1 myeloid cells cannot be stated to be remarkably reduced after PD-1 treatment based on the presented date: this is only valid if the same tumors would have been assessed before and after treatment. Avoid these statements.

	<p>Lane 206: same ...led to decreased...is misleading. Instead: anti PD1 treated tumors showed low frequencies of</p> <p>Lane 229: replace “led” by “was associated with higher abundance “</p> <p>Lane 241: “tended to accumulate” replace with “were more abundant”</p> <p>Lane 258: “accumulate”replace</p> <p>Lane 292: “accumulated” replace by “present at higher level”</p> <p>Lane 325: “accumulation” replace by “elevated”</p> <p>same for Lane 344, 346, 347, 383, 404</p> <p>In summary there are a lot of conclusions made in this manuscript which are highly speculative and lack substantial functional support, in fact here are no functional data shown at all.</p>
<p>Author Response</p>	<p>We acknowledge the reviewer's comments regarding our inaccurate descriptions and lack of functional data support. We have now included new experimental data to support our bioinformatic analysis at least partially: 1) new sets of multiplex immunofluorescences staining of CXCL14+CAFs on patient specimens (new Fig. 5i); 2) new Masson's trichrome staining to indicate the collagen fibers deposition in dMMR and pMMR (new Fig. 5h); 3) <i>in vitro</i> assay to indicate the possible role of IHH/PTCH1 pathway on CAFs (New Fig. 6j and Supplementary Fig. 9). These data are now included in the revised manuscript, respectively. In addition, we have revised our descriptions accordingly.</p> <div data-bbox="427 1167 1329 1554" data-label="Image"> <p>Figure 5h-i consists of two panels. Panel h shows two representative images of Masson's trichrome staining. The top image is labeled 'dMMR' and the bottom image is labeled 'pMMR'. Both images show a dense network of collagen fibers stained in blue, with a scale bar of 50µm. Panel i shows a 2x2 grid of multiplexed immunofluorescence (mIF) images. The top row shows 'dMMR' (left) and 'pMMR' (right). The bottom row shows 'dPR/dCR' (left) and 'dSD' (right). Each image displays a complex pattern of colored signals representing different markers: Pan-CK (magenta), COL1A1 (green), CD3 (red), CXCL14 (cyan), and DAPI (blue). A legend at the bottom of panel i reads: 'Multi-plexed IF staining of tumor-stroma boundary: Pan-CK COL1A1 CD3 CXCL14 DAPI Scale bar : 20µm'.</p> </div> <p>Fig. 5h-i. h Representative images of Masson's trichrome staining from treatment naive dMMR and pMMR patients. Scale bar = 50µm. i Representative mIF images of panCK, COL1A1, CD3 and CXCL14 in indicated patient groups. DAPI was used as a positive control for cell nuclei staining. Scale bars, 50 µm.</p>



New Fig. 6j. Western blot analysis of MMP11 in indicated group is shown. β -actin serves as loading control. Number indicates the relative expression towards β -actin.



New Supplementary Fig. 9. a The relative expression of *IHH* to *GAPDH* in the 6 human CRC cell lines. Data are represented as mean \pm SD and analyzed by unpaired Student-t test. **b** The representative images of the morphology and IF staining of COL1A1 in the CAFs are shown. DAPI was used as a positive control for cell nuclei staining. Scale bars, 20 μ m. **c** Western blot analysis of CXCL14 in CAF and HT29 cell lines is shown. β -actin serves as loading control. Number indicates the relative expression towards β -actin. **d** The relative expression of *MMP11* to *GAPDH* in HT29 cells treated with PBS or IHH recombinant protein. Data are represented as mean \pm SD and analyzed by unpaired Student-t test. ***, $p < 0.001$.

Excerpt from revised manuscript

(P. 9:)

Result lane 210:

These data suggested that: 1) the abundance of immune cell clusters in the tumor-stroma boundary may contribute to a better anti-PD1 response; 2) the limited infiltration of immune cells in the tumor region may be associated with a restricted anti-PD1 response in pMMR and dSD, potentially attributable to the spatial features of the tumor-stroma boundary.

Result lane 225:

Interestingly, when we compared the RCTD frequencies of these immune cell subsets in the centre of boundary (0 μ m), we observed that the majority of immune cells were Mac *SPP1* in both treatment naïve dMMR and pMMR (Fig. 2h). In addition, the proportion of Mac *SPP1* was higher in treatment naïve dMMR compared to pMMR, while lower in dPR/CR compared to dSD (Fig. 2h-i).

Result lane 233:

Of note, decreased RCTD frequencies of myeloid clusters (inner donut, dark green) and increased T cell clusters (inner donut, light pink) were observed in patients with dPR/dCR compared to dSD (Fig. 2h).

(P. 10:)

Result lane 257:

Anti-PD1 treatment was associated with the increased abundance of these subsets (excluded CD4_Tcm) into the tumor centre in dPR/dCR (Supplementary Fig. 5), suggesting their potential contributions to a better ICB response in CRCs.

Result lane 267:

Since we have pointed out the potential importance of *cDC1*, *DC_LAMP3*, *CD4_CXCL13*, *CD4_Treg*, *CD8_Teff*, *CD8_Tem* and *CD8_CXCL13* in ICB response, we next explored the potential mechanism of why these cell subsets were more abundant in the tumor-stroma boundary of dMMR but not pMMR.

(P. 11:)

Result lane 285:

Next, we detected the expressions of corresponding receptors toward *CCL2/5/21* and *CXCL9/10/13* on the immune cells that displayed higher abundance in treatment naïve dMMR or dPR/dCR using scRNA-seq dataset.

(P. 12:)

Result lane 319:

Next, we explored the potential crosstalk among *cDC1*, *DC_LAMP3*, *CD4_CXCL13*, *CD4_Treg*, *CD8_Teff*, *CD8_Tem* and *CD8_CXCL13* cells that presented at higher levels in the tumor-stroma boundary of treatment naïve dMMR by calculating their Pearson's correlations and spatial distances.

(P. 13:)

Result lane 354:

When further applied these exhausted signatures and PD1-PD-L1 axis into our spatial transcriptomics FOV analysis, our data confirmed an elevation of *PDCD1/CD274* and T cell exhaustion signature in the tumor-stroma boundary of treatment naïve dMMR patients (Fig. 3h-i).

(P. 14:)

Result lane 374

When applied these immune states into patient groups, we found that the proportion of state 0 was higher in treatment naïve pMMR, whereas dMMR displayed the enrichment towards 95% of state 1 (Fig. 4a and 4b).

Result lane 376

In addition, anti-PD1 treatment was associated with the reduction of state 1 and expansion of state 2 in dPR/dCR, but an elevation of state 0 in dSD (Fig. 4a and 4b).

(P. 15:)

	<p>Result lane 416 <u><i>CXCL14</i>⁺CAF <i>may contribute to the well-organized matrix structure and T cell exclusion in TME of ICB non-responders</i></u></p> <p>(P. 16:) Result lane 441 Therefore, our data suggested that <i>CXCL14</i>⁺CAF <u>may contribute to</u> the formation of structural barrier by the reprogramming ECM organization and structure, thereby leading to a T cell-exclusive TME of ICB non-responders.</p>
--	---

Ref 1.7 CAF definition

Reviewer Comment	Figure S6G: What is the rationale to focus on CXCL12 CAFs and why the 5 subsets were defined in this group?
Author Response	<p>We thank the reviewer for the question. Fibroblast is commonly recognized as cell that synthesizes the extracellular matrix and collagen, and expresses marker genes like <i>COL1A1</i>, <i>COL1A2</i>, <i>COL5A1</i>¹⁵. As <i>COL1A1</i> showed distinguished expression in fibroblast clusters compared to other cell clusters (Supplementary Fig. 3c), we first defined the fibroblasts by <i>COL1A1</i> expression accordingly. Next, we further analyzed the differentially expressed genes in the fibroblast clusters and identified 8 subsets according to the markers listed in the new Fig. 4d. Among the 8 subsets, 5 CAFs were identified based on their higher expression of <i>CXCL12</i> and <i>PDGFRA</i>, which represented the mesenchymal-derived CAF phenotype¹⁶. Nevertheless, the functional roles of <i>CXCL12</i>-expressing CAFs in different cancers remain to be controversial^{17,18}. Therefore, we further defined the CAFs into 5 subsets by <i>ADAMDEC1</i>, <i>CXCL8</i>, <i>CXCL14</i>, <i>KCNN3</i> and <i>PI16</i>, respectively (revised Fig. 4e-f). As our trajectory analysis indicated two distinctive differentiation paths into CAF_<i>CXCL8</i> or CAF_<i>CXCL14</i>, we then focused on these two CAF subsets for the follow-up study.</p> <div style="text-align: center;"> </div> <p>New Fig. 4d. Bubble plots of marker gene expressions in fibroblast subsets from the scRNA-seq dataset are shown. The plots are sized by the fraction of cells with positive gene expression, while the color represents the gene expression level. The name of the two CAFs are highlighted in red.</p>
Excerpt from revised manuscript	<p>(P. 14:) Result lane 397 We thus identified 5 cancer-associated fibroblasts (CAFs) subsets from other fibroblast clusters <u>by their distinguished expressions</u> of <i>CXCL12</i> and <i>PDGFRA</i>,</p>

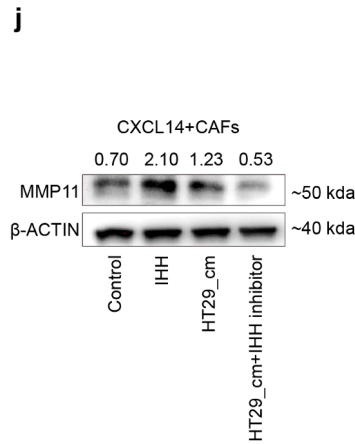
which represented the mesenchymal-derived CAF phenotype (Fig. 4d) ^{28,43-45}. We then re-embedded these cells in a new UMAP for trajectory inference (Fig. 4e). These 5 CAF subsets were marked by *ADAMDEC1*, *CXCL8*, *CXCL14*, *KCNN3* and *PI16*, respectively (Fig. 4e-f).

Ref 1.8 Experimental data support on *CXCL14_CAF*

<p>Reviewer Comment (i)</p>	<p>Lane 398, 404: again, no functional evidence: IHC and IF and functional evidence needed.</p>
<p>Author Response (i)</p>	<p>We agree with the reviewer that at least some functional evidence is necessary to support our bioinformatic analysis. We therefore included new experimental data to support our analysis at least partially. First, we included new sets of image data using Masson's trichrome staining to evaluate the collagen fiber deposition and mIF staining to assess the CXCL14+CAF in tumor tissues. The result clearly showed the existence of well-organized matrix structures in pMMR, but not in dMMR by Masson's trichrome staining (new Fig. 5h). In parallel, a higher number of CXCL14+COLA1+cells, represented CXCL14+CAFs was observed in the tumor-stroma boundary region of pMMR compared to dMMR (new Fig. 5i). In addition, obvious co-expressions of CXCL14 and COLA1 were observed in the tumor-stroma boundary region of dSD, while COLA1+fibroblasts displayed limited expression of CXCL14 in dCR/dPR (new Fig. 5i).</p> <div data-bbox="443 1041 1348 1444" data-label="Image"> <p>Figure 5h-i consists of two panels. Panel h shows Masson's trichrome staining of tumor tissues from dMMR and pMMR patients. The dMMR image shows a less organized matrix structure, while the pMMR image shows a well-organized matrix structure. Both images include a 50µm scale bar. Panel i shows multi-plexed IF staining of the tumor-stroma boundary in four patient groups: dMMR, pMMR, dPR/dCR, and dSD. The staining is for Pan-CK (magenta), COL1A1 (green), CD3 (red), CXCL14 (cyan), and DAPI (blue). The pMMR and dSD images show higher levels of COL1A1+CXCL14+ cells compared to dMMR and dPR/dCR. A 20µm scale bar is provided for the IF images.</p> </div> <p>Fig. 5h-i. h Representative images of Masson's trichrome staining from treatment naïve dMMR and pMMR patients. Scale bar = 50µm. i Representative mIF images of panCK, COL1A1, CD3 and CXCL14 in indicated patient groups. DAPI was used as a positive control for cell nuclei staining. Scale bars, 50 µm.</p>
<p>Excerpt from revised manuscript (i)</p>	<p>(P. 15:) Result lane 431 <u>To further evaluate the distribution of collagen fiber and CAF <i>CXCL14</i>, Masson's trichrome staining and mIF staining were performed. As expected, a well-organized matrix structure and higher level of COL1A1+CXCL14+cells were clearly observed in the tumor-stroma boundary of treatment naïve pMMR but not dMMR (Fig. 5h-i). In addition, higher frequency of COL1A1+CXCL14+cells was also detected in the tumor-stroma boundary of dSD compared to dPR/dCR (Fig. 5i).</u></p>

	<p>(P. 16:) Result lane 441 Therefore, our data suggested that <i>CXCL14</i>⁺CAF <u>may contribute to</u> the formation of structural barrier by the reprogramming ECM organization and structure, thereby leading to a T cell-exclusive TME of ICB non-responders.</p>																													
<p>Reviewer Comment (ii)</p>	<p>There is need for at least some functional evaluation of the hypotheses generated by the descriptive data. One such option would be the <i>in vitro</i> characterization of the <i>CXCL14</i> CAFs and the proposed signaling cascades involved. And the ligand/receptor interactions.</p>																													
<p>Author Response</p>	<p>As mentioned, we proposed a possible signaling cascade IHH/PTCH1 in regulating the function of <i>CXCL14</i>⁺CAF, represented by MMP11 expression in pMMR. To validate our hypothesis, we did some <i>in vitro</i> assays as suggested by the reviewer. First, we selected a pMMR CRC cell line HT29 for the <i>in vitro</i> experiment based on its higher expression of IHH over dMMR CRC cell lines via qRT-PCR (new Supplementary Fig. 9a). We attempted to isolate CAF from fresh tumor tissues from pMMR CRC patients who underwent colon surgery in our hospital. Unfortunately, the viability and features of the CAF did not sustain in culture due to our limited experience and time. Alternatively, we utilized commercially available primary CAF cells from patient with pancreatic cancer (Guangzhou Saliat Stem cell Science and Technology Co., Ltd, Cat No. iCell-0030a), which displayed a clear fibroblast morphology, COL1A1 and <i>CXCL14</i> expression (new Supplementary Fig. 9b-c). Consistent with our hypothesis, recombinant IHH recombinant protein (MCE, Cat. No. HY-P7204, 5 μg/mL) treatment significantly upregulated the expression of MMP11 by the CAF cells (new Supplementary Fig. 9d). Similarly, CAF treated with conditional medium (CM) from HT29 cells displayed a higher level of MMP11, which could be reverted by IHH inhibitor (Selleckchem, Vismodegib (GDC-0449), 25 μM) (new Fig 6j). Collectively, our data suggested a possible link between pMMR tumor and CAF via IHH/PTCH1.</p> <div data-bbox="427 1294 1364 1877"> <p>a</p> <table border="1"> <caption>Relative mRNA level of IHH adjusted to GAPDH in CRC cell lines</caption> <thead> <tr> <th>Cell Line</th> <th>Relative mRNA level (approx.)</th> </tr> </thead> <tbody> <tr> <td>HCT116</td> <td>~10</td> </tr> <tr> <td>HCT8</td> <td>~15</td> </tr> <tr> <td>HCT15</td> <td>~20</td> </tr> <tr> <td>SW480</td> <td>~25</td> </tr> <tr> <td>SW620</td> <td>~50</td> </tr> <tr> <td>HT29</td> <td>~200</td> </tr> </tbody> </table> <p>b</p> <p>light, DAPI, COL1A1, merge</p> <p>c</p> <table border="1"> <caption>Western blot analysis of CXCL14 and β-ACTIN</caption> <thead> <tr> <th>Sample</th> <th>CXCL14 (0.68)</th> <th>β-ACTIN (0.23)</th> </tr> </thead> <tbody> <tr> <td>CAF</td> <td>~20 kda</td> <td>~40 kda</td> </tr> <tr> <td>HT29</td> <td>~20 kda</td> <td>~40 kda</td> </tr> </tbody> </table> <p>d</p> <table border="1"> <caption>MMP11 protein concentration in CAF</caption> <thead> <tr> <th>Treatment</th> <th>Protein concentration (pp/μl)</th> </tr> </thead> <tbody> <tr> <td>Control</td> <td>~1.0</td> </tr> <tr> <td>IHH</td> <td>~1.7</td> </tr> </tbody> </table> </div> <p>New Supplementary Fig. 9. a The relative expression of <i>IHH</i> to <i>GAPDH</i> in the 6 human CRC cell lines. Data are represented as mean±SD and analyzed by unpaired Student-t test. b The representative images of the morphology and IF staining of COL1A1 in the CAFs are shown. DAPI was used as a positive control for cell nuclei</p>	Cell Line	Relative mRNA level (approx.)	HCT116	~10	HCT8	~15	HCT15	~20	SW480	~25	SW620	~50	HT29	~200	Sample	CXCL14 (0.68)	β-ACTIN (0.23)	CAF	~20 kda	~40 kda	HT29	~20 kda	~40 kda	Treatment	Protein concentration (pp/μl)	Control	~1.0	IHH	~1.7
Cell Line	Relative mRNA level (approx.)																													
HCT116	~10																													
HCT8	~15																													
HCT15	~20																													
SW480	~25																													
SW620	~50																													
HT29	~200																													
Sample	CXCL14 (0.68)	β-ACTIN (0.23)																												
CAF	~20 kda	~40 kda																												
HT29	~20 kda	~40 kda																												
Treatment	Protein concentration (pp/μl)																													
Control	~1.0																													
IHH	~1.7																													

staining. Scale bars, 20 μ m. **c** Western blot analysis of CXCL14 in CAF and HT29 cell lines is shown. b-actin serves as loading control. Number indicates the relative expression towards b-actin. **d** The relative expression of *MMP11* to *GAPDH* in HT29 cells treated with PBS or IHH recombinant protein. Data are represented as mean \pm SD and analyzed by unpaired Student-t test. ***, p<0.001



New Fig. 6j. Western blot analysis of MMP11 in indicated group is shown. β -actin serves as loading control. Number indicates the relative expression towards β -actin.

Excerpt from revised manuscript

(P. 17:)
Result lane 480
Interestingly, we observed higher expression of *IHH* in pMMR CRC cell lines HT29 and SW620 compared to dMMR CRC cell lines, including HCT116, HCT8 and HCT15⁵² (Supplementary Fig. 9a). Treatment of CXCL14+CAFs (Guangzhou Saliat Stem cell Science and Technology Co., Ltd) with IHH recombinant protein resulted in a notable increase in MMP11 release (Supplementary Fig. 9b-d). Furthermore, exposure of CXCL14+CAFs to conditional medium (CM) from pMMR CRC HT29 cells also let to a similar upregulation of MMP11. Importantly, this upregulation could be suppressed by IHH inhibitor Vismodegib (Selleckchem) (Fig. 6j). Taken together, these results indicated the potential interaction between pMMR tumor cells and CAF_CXCL14 through *IHH_PTCH1* axis.

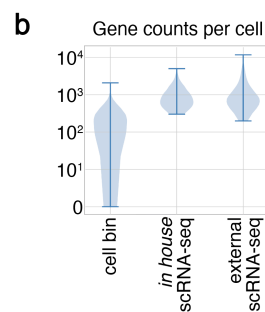
Reviewer #2: expertise in colorectal cancer TME, CAFs immunotherapy

Overall comments	In the manuscript entitled “Spatially organized tumor-stroma boundary determines the efficacy of immunotherapy in colorectal cancer patients”, Feng and collaborators use spatial transcriptomics to investigate the composition of the TME, in particular from an immune cell point of view, in dMMR and pMMR patients and their response to immune checkpoint blockade therapy. To achieve their study, the authors use an internally developed spatial transcriptomics method called Stereo-Seq, which, according to their claim, exhibits advantages such as in particular a high spatial resolution other alternative commercially available solution. The study, which is purely descriptive, is in line with the current scientific focus pushing the scRNA-Seq field to take into account the precise spatial localization and neighborhood of each cell-type. It nicely shows that the tumor-stroma boundary shows distinct features between dMMR, ICB responder and pMMR, ICB non-responder and suggests that cell interactions at the boundary region might drive immune checkpoint therapy resistance. I nevertheless have some concerns that should be addressed before recommending the article as suitable for publication.
Author Response	We are grateful for the reviewer’s insights and compliments on our study, and constructive suggestions to guide us on further strengthening our manuscript. We also acknowledge the shortcomings raised by the reviewer and have addressed them in the revised manuscript.
Major revisions	<ol style="list-style-type: none"> 1. Revise the description about the resolution of our stereo-seq platform by performing additional analysis, and include discussion about the limitations of our study. 2. Add new references and information to clarify the cell cluster annotation in both stereo-seq and scRNAseq analysis. 3. Add new ligand-receptor pair analysis. 4. Revise the analysis using a larger patient number from TCGA COAD cohort. 5. Revise the Methods and figure legends thoroughly.

Ref 2.1 Clarification of spatial resolution of stereo-seq platform

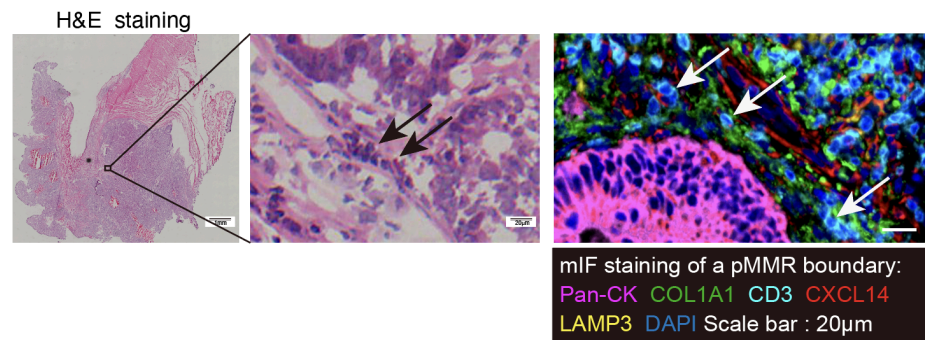
Reviewer Comment	1. The authors claim that one of the main advantages of the developed Stereo-Seq method is the higher resolution down to 500 nm (line 93) compared to spatial transcriptomics competitors. However, it is confusing how this technical advantage is maintained in the current manuscript as the authors report that once processed, the end resolution of their Stereo-Seq transcriptomics data is 50 µm (lines 120 & 766). The statement on line 88 justifying the use of Stereo-Seq (line 88) should be revised as it finally doesn’t apply to this manuscript.
Author Response	We acknowledge the issue of spatial resolution used in this study raised by the reviewer. The Stereo-seq platform we developed is based on combined DNA nanoball (DNB)-patterned arrays and in situ RNA capture. By aggregating neighboring DNA nanoballs (forming a square bin) or assigning DNA nanoballs to individual cell via image-based cell segmentation (cell bin), our previous studies have nicely demonstrated the achievement of high sensitivity and single-cell resolution (500nm) <i>in situ</i> through Stereo-seq in mouse embryos ⁵ and axolotl brain ⁶ . We therefore applied Stereo-seq to analyze the tumor tissues collected from CRC patients in the current study. Unfortunately, when we set the cell bin for single-cell segmentation, we could only generate fewer than 300 genes per bin (new Supplementary Fig. 1b). Compared to scRNA-seq datasets generated from

CRC patients in our in-house and published datasets⁷ (**new Supplementary Fig. 1b**), ~300 genes/cell was insufficient for cell type annotation and follow-up analysis. One probable explanation may be the difference on the average cell size and the complexity among different tissues. This observation indicated the limitation of our Stereo-seq platform, which may not be universally applicable, particularly in tissues enriched with small-sized immune cells, such as tumors, spleen and thymus. In addition, it is common to observe the co-localization of different cells within the three-dimensional (3D) structure of tumors. For example, we observed that the immune cells (e.g. CD3⁺) were co-localized with fibroblasts (COL1A1⁺) as shown by H&E and mIF staining (**Fig. R1**). However, our current spatial transcriptomic analysis can only generate 2D sequencing data from single slide analysis⁸. As a result, when cells were segmented into single cell resolution, it was common to find transcripts mixed with fibroblasts (such as COL1A1), immune cells (such as CD3E, PTPRC, FCGR3A), and epithelial cells (such as EPCAM) (**Fig. R2**). These cells would be classified as doublets in scRNA-seq analyses due to their ambiguous nature⁹. Therefore, a general challenge faced in Stereo-seq analysis, which may also be applicable to other spatial transcriptomic platforms, is how to balance the resolution and mRNA capture efficiency. To overcome these limitations, we employed parallel scRNA-seq analysis alongside Stereo-seq and set the resolution into 50 μ m (bin 100) in our current study. This combination allowed us to distinguish transcriptionally similar cell types and analyze their spatial localization. We have now incorporated this information into the discussion section and modified the introduction in our revised manuscript.



New Supplementary Fig. 1b. Violin plots of the gene counts per cell in cell bin segmented of Stereo-seq data from a representative patient #59, our in house scRNA-seq data and a representative public scRNA-seq data (GSE178341) are shown.

FigR1



FigR2

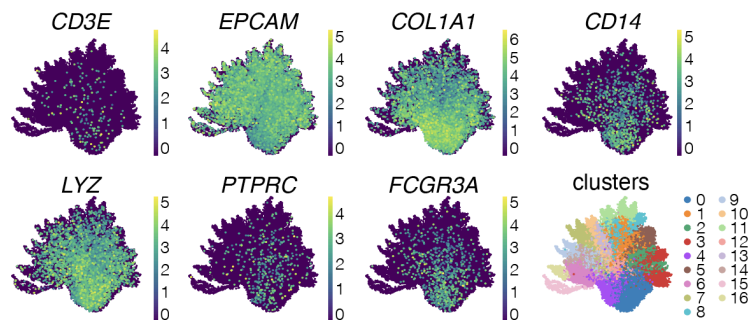


Fig R1. Possible co-localization of immune cells and fibroblasts is shown by H&E staining (left) or mIF staining (right).

Fig R2. The UMAP of the unsupervised clustering of the cell bins and marker genes from the spatial transcriptome of the patient #59.

Excerpt
from
revised
manuscript

(P. 5:)

Introduction lane 88

We therefore developed the spatial enhanced resolution omics-sequencing (Stereo-seq). It is a DNA nanoball (DNB)-patterned array embedded with coordinate identity¹³ and unique molecular identifiers (MID) co-barcoded poly-T probe, capable of capturing mRNA *in situ* at a resolution of 500 nanometer (nm). Using this platform, we successfully constructed 2-dimensional (2D) spatial transcriptomic maps at single cell level in mouse embryos and axolotl brain^{13,14}. Considering the complexity and smaller size of immune cells in the tumors, here we applied integrative analysis of scRNA-seq and Stereo-seq to in-depth dissect the gene regulatory programs and cell-cell interactions underlying ICB response in CRC patients. Through analysis in 25 tumor specimens from CRC patients of treatment naïve dMMR, pMMR and anti-PD1-treated dMMR patients that included responders (complete response (CR)/PR) and non-responders (stable disease, SD), we generated a CRC spatial transcriptomic atlas and uncovered a 300 micrometer (μm) boundary region (0±150 μm) that regulated immune cell influx to the tumor center region (>150 μm).

(P. 6:)

Results lane 118

After pre-processing on the raw data generated by Stereo-seq (see Methods), the spatial transcriptome map was lassoed out and matched to the tissue edge (<https://www.stomics.tech/sap/home.html>). As the single-cell resolution was insufficient to generate an adequate number of genes per bin for cell type

	<p><u>annotation and follow-up analysis in tumor tissues (Supplementary Fig. 1b), we adjusted the bin size to bin100, which allowed us to obtain a sufficient gene count for transcriptomic analysis at a resolution of 50µm (Supplementary Fig. 1b-d).</u></p> <p>(P. 21:)</p> <p>Discussion lane 601</p> <p><u>Secondly, the Stereo-seq technique has not reached the single-cell resolution when analyzing heterogenous and complex tumor specimens in the current study. The nanoscale resolution (capture spot diameter: 220 nm; center-to-center distance: 500 nm) of Stereo-seq merely supported an estimate of 1-10 cells in each bin in CRC tumor tissues compared to previous analysis in mouse embryos and axolotl brain^{13,14,63}. One probable explanation may be the difference on the average cell size and the complexity among different tissues. This observation indicated the limitation of our Stereo-seq platform, which may not be universally applicable, particularly in tissues enriched with small-sized immune cells, such as tumors, spleen and thymus. A more precise spatial map, if we can develop in the future, will be essential for better understanding of how to therapeutically target the spatiotemporal heterogeneity of the complex TME of CRCs, as well as other cancers. For example, enrichment of the variable regions of T and B cell receptor mRNA accompanied with the current Stereo-seq platform would present a compelling strategy for mapping the immune cells, at least T cell and B cells at single cell resolution in tumors <i>in situ</i>.</u></p>
--	---

Ref 2.2 Definition of spatial clusters in figure 1

<p>Reviewer Comment (i)</p>	<p>The authors defined and labeled spatial clusters (figure 1) but do not describe or provide any detail on the rationale behind this labeling. For instance, tumor spatial clusters are either “tumor_CEA” or “tumor_MKI67”. While MKI67 might be self-intuitive, it is not clear to me how the authors defined the “tumor_CEA” spatial cluster. I suppose that CEA is referring to the expression of CEA cell adhesion molecules but Figure 1b shows only the expression of CEACAM1 while “CEA” is also known as the former gene symbol of CEACAM5. The authors should clearly describe how they characterized the different spatial clusters shown in figure 1b.</p>
<p>Author Response (i)</p>	<p>We thank the reviewer for pointing out the incomplete description regarding the annotation of spatial clusters. As no published spatial transcriptomics data from CRC patients was available, the annotation of spatial clusters in the current study was mainly based on the DEG heatmap and our summarized literatures of scRNAseq data, image data as well as clinicopathological features. We labeled the spatial clusters based on the top and predominantly expressed DEGs. Therefore, as mentioned by the reviewer, “tumor_CEA” was labelled by its predominant expression of CEA cell adhesion molecules, i.e. CEACAM1 and CEACAM5 (revised Fig. 1b). We have now added the expression pattern of <i>CEACAM5</i> in the revised Fig. 1b, and the references and rationale of our cluster annotation in the revised manuscript.</p>

gene name	major producer	reference
<i>JCHAIN</i>	Plasma_ Ig M	Precursor B cells transformed by Epstein-Barr virus undergo sterile plasma-cell differentiation: J-chain expression without immunoglobulin ¹
<i>IGHA1</i>	Plasma_ Ig M	Intrahepatic inflammatory IgA+PD-L1high monocytes in hepatocellular carcinoma development and immunotherapy ²
<i>CLEC4C</i>	pDC	Altered ratio of dendritic cell subsets in skin-draining lymph nodes promotes Th2-driven contact hypersensitivity ³
<i>CSF2RB</i>	pDC	Granulocyte Macrophage-Colony Stimulating Factor Produces a Splenic Subset of Monocyte-Derived Dendritic Cells That Efficiently Polarize T Helper Type 2 Cells in Response to Blood-Borne Antigen ⁴
<i>TCF4</i>	pDC	Isoform-Specific Expression and Feedback Regulation of E Protein TCF4 Control Dendritic Cell Lineage Specification ⁵
<i>KLRK1</i>	NK_gdT	Altered NK cell development and enhanced NK cell-mediated resistance to mouse cytomegalovirus in NKG2D-deficient mice ⁶
<i>LYZ</i>	Monocyte_ S100A8	Aberrant LYZ expression in tumor cells serves as the potential biomarker and target for HCC and promotes tumor progression via csGRP78 ⁷
<i>S100A8</i>	Monocyte_ S100A8	S100A8 and S100A9 in Cancer ⁸
<i>S100A9</i>	Monocyte_ S100A8	S100A8 and S100A9 in Cancer ⁸
<i>FCN1</i>	Monocyte_ S100A8	Expansion of Fcγ Receptor IIIa-Positive Macrophages, Ficolin 1-Positive Monocyte-Derived Dendritic Cells, and Plasmacytoid Dendritic Cells Associated With Severe Skin Disease in Systemic Sclerosis ⁹
<i>GATA2</i>	Mast	GATA2 regulates mast cell identity and responsiveness to antigenic stimulation by promoting chromatin remodeling at super-enhancers ¹⁰
<i>TPSB2</i>	Mast	Sputum mast cell/basophil gene expression relates to inflammatory and clinical features of severe asthma ¹¹
<i>TPSAB1</i>	Mast	Single-cell RNA sequencing of mast cells in eosinophilic esophagitis reveals heterogeneity, local proliferation, and activation that persists in remission ¹²

<i>LYZ</i>	Mac_SPP1	Spatial transcriptomics reveals heterogeneity of macrophages in the tumor microenvironment of granulomatous slack skin ¹³
<i>SPP1</i>	Mac_SPP1	CXCL9:SPP1 macrophage polarity identifies a network of cellular programs that control human cancers ¹⁴
<i>SELENOP</i>	Mac_M2	Cellular crosstalk of macrophages and therapeutic implications in non-small cell lung cancer revealed by integrative inference of single-cell transcriptomics ¹⁵
<i>MRC1</i>	Mac_M2	Spatiotemporal Immune Landscape of Colorectal Cancer Liver Metastasis at Single-Cell Level ¹⁶
<i>IL10</i>	Mac_M2	IL-10 improves cardiac remodeling after myocardial infarction by stimulating M2 macrophage polarization and fibroblast activation ¹⁷
<i>CXCL8</i>	Mac_M1	Inhibition of the PI3K/AKT/mTOR signaling promotes an M1 macrophage switch by repressing the ATF3-CXCL8 axis in Ewing sarcoma ¹⁸
<i>IL1B</i>	Mac_M1	Tumor-promoting macrophages prevail in malignant ascites of advanced gastric cancer ¹⁹
<i>IL6</i>	Mac_M1	Blockade of interleukin-6 signaling inhibits the classic pathway and promotes an alternative pathway of macrophage activation after spinal cord injury in mice ²⁰
<i>IL1RN</i>	Mac_M1	Generation of bioactive MSC-EVs for bone tissue regeneration by tauroursodeoxycholic acid treatment ²¹
<i>NOTCH3</i>	Fibro_NOTCH3	Notch3: A New Culprit in Fibrotic Lung Disease ²²
<i>MYH11</i>	Fibro_MYH11	Histone deacetylase-mediated tumor microenvironment characteristics and synergistic immunotherapy in gastric cancer ²³
<i>GPM6B</i>	Fibro_GPM6B	AAV-mediated Gpm6b expression supports hair cell reprogramming ²⁴
<i>PECAM1</i>	Endo	PIEZO1 and PECAM1 interact at cell-cell junctions and partner in endothelial force sensing ²⁵
<i>CD86</i>	DC_LAMP3	Molecular signatures of maturing dendritic cells: implications for testing the quality of dendritic cell therapies ²⁶
<i>LAMP3</i>	DC_LAMP3	Overexpression of LAMP3/TSC403/DC-LAMP promotes metastasis in uterine cervical cancer ²⁷
<i>FSCN1</i>	DC_LAMP3	Integrated single-cell analysis-based classification of vascular mononuclear phagocytes in mouse and human atherosclerosis ²⁸
<i>CCR7</i>	DC_LAMP3	Single-cell transcriptome analysis of human skin identifies novel fibroblast subpopulation and enrichment of immune subsets in atopic dermatitis ²⁹
<i>CCL22</i>	DC_LAMP3	Molecular signatures of maturing dendritic cells: implications for testing the quality of dendritic cell therapies ²⁶

<i>CD274</i>	DC_LAMP3	TIM-3 Dictates Functional Orientation of the Immune Infiltrate in Ovarian Cancer ³⁰
<i>CD1D</i>	cDC2	CD1d-mediated lipid presentation by CD11c(+) cells regulates intestinal homeostasis ³¹
<i>CLEC10A</i>	Cdc2	CLEC10A Is a Specific Marker for Human CD1c(+) Dendritic Cells and Enhances Their Toll-Like Receptor 7/8-Induced Cytokine Secretion ³²
<i>CD1C</i>	Cdc2	Saponin-based adjuvants enhance antigen cross-presentation in human CD11c(+) CD1c(+) CD5(-) CD163(+) conventional type 2 dendritic cells ³³
<i>XCR1</i>	cDC1	XCR1(+) type 1 conventional dendritic cells drive liver pathology in non-alcoholic steatohepatitis ³⁴
<i>CLEC9A</i>	Cdc1	Secreted gelsolin inhibits DNGR-1-dependent cross-presentation and cancer immunity ³⁵
<i>BATF3</i>	Cdc1	Restoring tumor immunogenicity with dendritic cell reprogramming ³⁶
<i>IL7R</i>	CD8_Tem	Transcriptional programs of neoantigen-specific TIL in anti-PD-1-treated lung cancers ³⁷
<i>TCF7</i>	CD8_Tem	Human memory CD8 T cell effector potential is epigenetically preserved during in vivo homeostasis ³⁸
<i>IFNG</i>	CD8_Teff	Activation of CD8(+) T Cells in Chronic Obstructive Pulmonary Disease Lung ³⁹
<i>CD69</i>	CD8_Teff	CD69 Imposes Tumor-Specific CD8+ T-cell Fate in Tumor-Draining Lymph Nodes ⁴⁰
<i>HSPA6</i>	CD8_HSP	Excessive HSP70/TLR2 activation leads to remodeling of the tumor immune microenvironment to resist chemotherapy sensitivity of mFOLFOX in colorectal cancer ⁴¹
<i>HSPA8</i>	CD8_HSP	Alternative pathways for processing exogenous and endogenous antigens that can generate peptides for MHC class I-restricted presentation ⁴²
<i>LAG3</i>	CD8_CXC L13	Exploring Markers of Exhausted CD8 T Cells to Predict Response to Immune Checkpoint Inhibitor Therapy for Hepatocellular Carcinoma ⁴³
<i>CD8A</i>	CD8_CXC L13	Epigenetic plasticity of Cd8a locus during CD8(+) T-cell development and effector differentiation and reprogramming ⁴⁴
<i>GZMK</i>	CD8_CXC L13	Single-Cell Sequencing Reveals Trajectory of Tumor-Infiltrating Lymphocyte States in Pancreatic Cancer ⁴⁵
<i>GZMA</i>	CD8_CXC L13	Transcriptomic profiles of neoantigen-reactive T cells in human gastrointestinal cancers ⁴⁶
<i>PDCD1</i>	CD8_CXC L13	A single-cell map of intratumoral changes during anti-PD1 treatment of patients with breast cancer ⁴⁷

<i>TIGIT</i>	CD8_CXC L13	Intratumoral CXCL13(+)CD8(+)T cell infiltration determines poor clinical outcomes and immunoevasive contexture in patients with clear cell renal cell carcinoma ⁴⁸
<i>HAVCR2</i>	CD8_CXC L13	A single-cell map of intratumoral changes during anti-PD1 treatment of patients with breast cancer ⁴⁷
<i>CXCL13</i>	CD8_CXC L13	Intratumoral CXCL13(+)CD8(+)T cell infiltration determines poor clinical outcomes and immunoevasive contexture in patients with clear cell renal cell carcinoma ⁴⁸
<i>FOXP3</i>	CD4_Treg	Regulation of antitumour CD8 T-cell immunity and checkpoint blockade immunotherapy by Neuropilin-1 ⁴⁹
<i>IL2RA</i>	CD4_Treg	Cell-specific protein phenotypes for the autoimmune locus IL2RA using a genotype-selectable human bioresource ⁵⁰
<i>LAYN</i>	CD4_Treg	LAYN Is a Prognostic Biomarker and Correlated With Immune Infiltrates in Gastric and Colon Cancers ⁵¹
<i>RORA</i>	CD4_Tcm	RORalpha is a critical checkpoint for T cell and ILC2 commitment in the embryonic thymus ⁵²
<i>IL7R</i>	CD4_Tcm	IL-7 signalling represses Bcl-6 and the TFH gene program ⁵³
<i>CD69</i>	CD4_Tcm	The human liver microenvironment shapes the homing and function of CD4(+) T-cell populations ⁵⁴
<i>TCF7</i>	CD4_Tcm	Lineage tracing reveals clonal progenitors and long-term persistence of tumor-specific T cells during immune checkpoint blockade ⁵⁵
<i>CXCL13</i>	CD4_CXC L13	Single cell profiling of primary and paired metastatic lymph node tumors in breast cancer patients ⁵⁶
<i>HAVCR2</i>	CD4_CXC L13	A single-cell map of intratumoral changes during anti-PD1 treatment of patients with breast cancer ⁴⁷
<i>LAG3</i>	CD4_CXC L13	A single-cell map of intratumoral changes during anti-PD1 treatment of patients with breast cancer ⁴⁷
<i>PDCD1</i>	CD4_CXC L13	A single-cell map of intratumoral changes during anti-PD2 treatment of patients with breast cancer ⁴⁷
<i>NAMPT</i>	CD4_act	NAMPT is a metabolic checkpoint of IFNgamma-producing CD4(+) T cells in lupus nephritis ⁵⁷
<i>PI16</i>	CAF_PI16	Fibroblast-derived PI16 sustains inflammatory pain via regulation of CD206(+) myeloid cells ⁵⁸
<i>CXCL14</i>	CAF_CXC L14	Cancer-associated fibroblasts expressing CXCL14 rely upon NOS1-derived nitric oxide signaling for their tumor-supporting properties ⁵⁹
<i>ADAMDE C1</i>	CAF_ADA MDEC1	Cross-tissue organization of the fibroblast lineage ⁶⁰
<i>CD83</i>	B_act	The CD83 reporter mouse elucidates the activity of the CD83 promoter in B, T, and dendritic cell populations in vivo ⁶¹

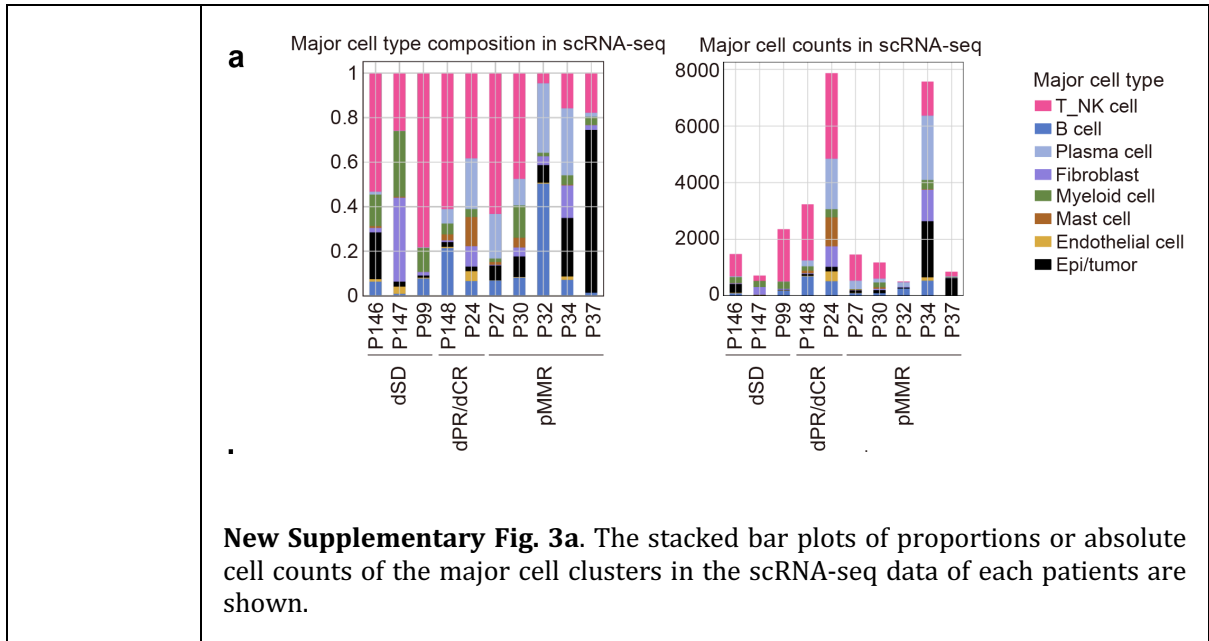
Ref 2.3 Revision of the Methods part

Reviewer Comment	The Material and Methods part needs to be revised thoroughly.
Author Response	We thank the reviewer for the comment and now have revised the Methods part thoroughly to make the statement clear and straight.
Excerpt from	Please see the revised Methods in the main text from page 26 to page 34.

revised manuscript	
--------------------	--

Ref 2.4 Revision of labelling and description of cell clusters in Fig. 2, Supplementary Fig. 2 and 3

Reviewer Comment (i)	<p>In general, the authors should make sure to carefully describe the labeling/characterization of all cell clusters.</p> <p>In Supplementary Figure 2a, the authors should show the major cell type instead of cell subtypes to better relate this to the conclusion drawn from Figure 1e.</p>
Author Response (i)	<p>We thank the reviewer for the comments and now have revised the labelling and descriptions of cell clusters in the mentioned figures accordingly.</p> <p>The revised Supplementary Fig. 2a now displays both major cell types and subtype plots.</p> <p>Revised Supplementary Fig. 2a. The spatial plots of the major spatial clusters, sub-clusters and H&E image in each specimen are shown.</p>
Reviewer Comment (ii)	<p>In Figure 2b, the authors should include a distribution plot of major cell types from scRNA-Seq in each patient and within dMMR, pMMR, dSD and dPR/dCR groups similar to the one shown in Supplementary Figure 4f.</p>
Author Response (ii)	<p>We have now included the cell numbers of the major cell types from each patient similar to Supplementary Fig. 4f as a new Supplementary Fig. 3a.</p>



New Supplementary Fig. 3a. The stacked bar plots of proportions or absolute cell counts of the major cell clusters in the scRNA-seq data of each patients are shown.

Excerpt from revised manuscript (ii)

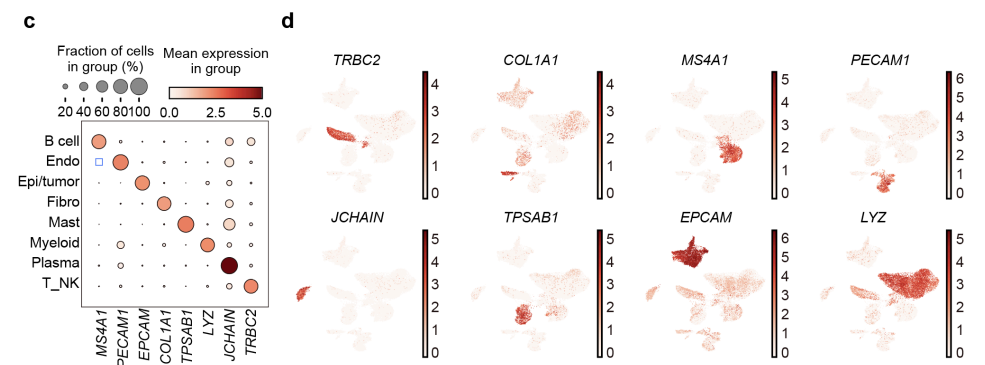
(P. 7:)
Result lane 173
 In total, we identified 8 major cell clusters (including 33 sub-clusters), covering 23 immune cell and 10 stromal cell subtypes (**Fig. 2a-c, table S2-3**). The cell counts were comparable in the patients except for patient #24 and #34 (**Supplementary Fig. 3a**).

Reviewer Comment (iii)

In Supplementary Figure 3, the author should include a dot plot showing the marker genes used to identify the major cell types shown in Figure 2b.

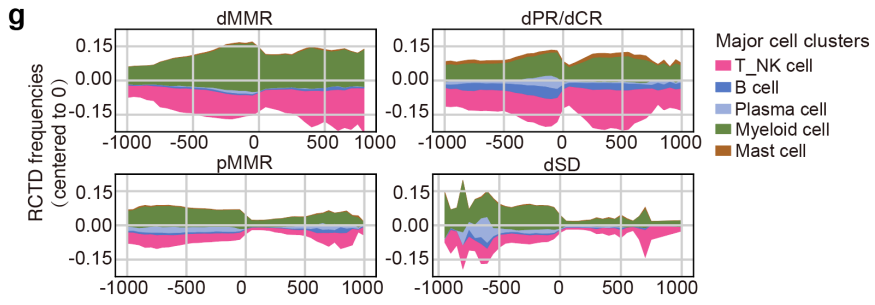
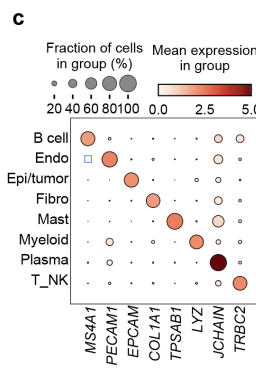
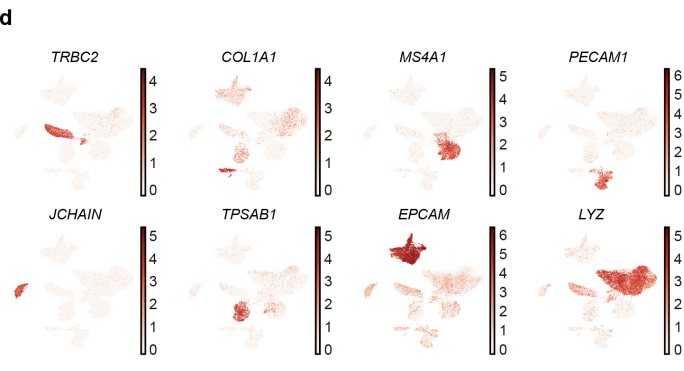
Author Response (iii)

We have now uniformed the color bar and revised the dot plot of the marker genes used to identify the major cell types in the revised Supplementary Figure 3c-d.



Revised Supplementary Figure 3c-d. **c** Bubble plots of marker gene expressions in major cell clusters from the scRNA-seq dataset are shown. The plots are sized by the fraction of cells with positive gene expression, while the color represents the gene expression level. **d** Expression level of canonical marker genes for each major cell cluster is shown in UMAP.

<p>Reviewer Comment (iv)</p>	<p>The color scale used in figures 2a and 2c is not easy to read. In figure 2c it is in particular difficult to grasp which is the dominating cell type (distinguishing hues of green colors).</p>		
<p>Author Response (iv)</p>	<p>We apologize for the confusion caused by the color labelling in Fig. 2. It is indeed extremely difficult to read more than 30 different colors on a single panel of the UMAP data. We therefore assigned a principal color to each major cell type: green for myeloid cell clusters, red for NK_T cell clusters, blue for B/plasma cell clusters, violet for fibroblasts, dark brown for mast cell, orange for endothelial cell and black for epi/tumor cell, in consistence with the main cell type labelling in the Fig. 2b. Next, we fine-tuned the shades to ensure that subsets within each major category are similar yet distinct in the revised Fig. 2a.</p> <div data-bbox="416 689 928 1355" style="text-align: center;"> <p>a Cell clusters (n=28223)</p> <p>b Major cell type</p> <p>c Patient ID</p> <table border="0" style="width: 100%; font-size: small;"> <tr> <td style="vertical-align: top;"> <p>Cell sub-clusters</p> <ul style="list-style-type: none"> CD8_Cyto CD8_CXCL13 CD8_HSP CD8_Teff CD8_Tem CD4_act CD4_Tem CD4_CXCL13 CD4_Treg NK_gdT Endo Epi/Tumor B_act B_naive Plasma_IgM Plasma_IgG cDC1 cDC2 pDC DC_LAMP3 Mac_M1 Mac_M2 Mac_SPP1 Monocyte_S100A8 Mast CAF_ADAMDEC1 CAF_CXCL8 CAF_CXCL14 CAF_KCNN3 CAF_PI16 Fibro_GPM6B Fibro_MYH11 Fibro_NOTCH3 </td> <td style="vertical-align: top;"> <p>Major cell type</p> <ul style="list-style-type: none"> T_NK cell B cell Plasma cell Fibroblast Myeloid cell Mast cell Endothelial cell Epi/tumor <p>Patient ID</p> <ul style="list-style-type: none"> P24 P27 P30 P32 P34 P37 P99 P146 P147 P148 </td> </tr> </table> </div> <p>Revised Fig. 2a-c. a Uniform manifold approximation and projection (UMAP) of the transcriptome of 28,223 single cells from 10 CRC patients (5 pMMR; 2 dPR/CR; 3 dSD). Cells are colored by single cell subclusters, b major cell types or c patient ID. The names of the cell of interests are highlighted in red.</p>	<p>Cell sub-clusters</p> <ul style="list-style-type: none"> CD8_Cyto CD8_CXCL13 CD8_HSP CD8_Teff CD8_Tem CD4_act CD4_Tem CD4_CXCL13 CD4_Treg NK_gdT Endo Epi/Tumor B_act B_naive Plasma_IgM Plasma_IgG cDC1 cDC2 pDC DC_LAMP3 Mac_M1 Mac_M2 Mac_SPP1 Monocyte_S100A8 Mast CAF_ADAMDEC1 CAF_CXCL8 CAF_CXCL14 CAF_KCNN3 CAF_PI16 Fibro_GPM6B Fibro_MYH11 Fibro_NOTCH3 	<p>Major cell type</p> <ul style="list-style-type: none"> T_NK cell B cell Plasma cell Fibroblast Myeloid cell Mast cell Endothelial cell Epi/tumor <p>Patient ID</p> <ul style="list-style-type: none"> P24 P27 P30 P32 P34 P37 P99 P146 P147 P148
<p>Cell sub-clusters</p> <ul style="list-style-type: none"> CD8_Cyto CD8_CXCL13 CD8_HSP CD8_Teff CD8_Tem CD4_act CD4_Tem CD4_CXCL13 CD4_Treg NK_gdT Endo Epi/Tumor B_act B_naive Plasma_IgM Plasma_IgG cDC1 cDC2 pDC DC_LAMP3 Mac_M1 Mac_M2 Mac_SPP1 Monocyte_S100A8 Mast CAF_ADAMDEC1 CAF_CXCL8 CAF_CXCL14 CAF_KCNN3 CAF_PI16 Fibro_GPM6B Fibro_MYH11 Fibro_NOTCH3 	<p>Major cell type</p> <ul style="list-style-type: none"> T_NK cell B cell Plasma cell Fibroblast Myeloid cell Mast cell Endothelial cell Epi/tumor <p>Patient ID</p> <ul style="list-style-type: none"> P24 P27 P30 P32 P34 P37 P99 P146 P147 P148 		
<p>Reviewer Comment (v)</p>	<p>In Figure 2d, it would be valuable if the authors provide the same plot with major cell type annotations to clearly show the abundance of those cells over tumor-stroma boundaries.</p>		
<p>Author Response (v)</p>	<p>We have now included the stream plot using major cell type distribution in a new Supplementary Fig.4g.</p>		

	<p>g</p>  <p>New Supplementary Fig. 4g. The stacked stream plots of major immune cell distribution patterns from distal stroma (-1000µm, left) to tumor center (1000µm, right) in indicated patient groups are shown. The mean RCTD frequencies of each immune cell in each 1mm interval was smoothed using slinger model and colored by cell clusters in accordance with Fig. 2b.</p>
<p>Reviewer Comment (vi)</p>	<p>Although the characterized clusters are nicely and convincingly shown on the UMAP plot (figure S3c), the mean gene expression of major cell type markers shown in figure Supplementary Figure 3b doesn't look convincing. Indeed, the average expression of each marker seems to reach the maximum value (of 1, coded as dark red / brown) in Supplementary Figure 3b. As the UMAP plot (Supplementary Figure 3c) suggests a higher variance (much more lighter dots are visible for every marker except JCHAIN), the mean will unlikely reach such a high value.</p>
<p>Author Response (vi)</p>	<p>We apologize for the confusion caused. We have now uniformed the color bar and revised the dot plot of the marker genes used to identify the major cell types in the revised Supplementary Figure 3c-d.</p> <div data-bbox="414 1198 1372 1568"> <p>c</p>  <p>d</p>  </div> <p>Revised Supplementary Figure 3c-d. c Bubble plots of marker gene expressions in major cell clusters from the scRNA-seq dataset are shown. The plots are sized by the fraction of cells with positive gene expression, while the color represents the gene expression level. d Expression level of canonical marker genes for each major cell cluster is shown in UMAP.</p>

Ref 2.5 Discussion of SPP1+macrophage and plasma/B cells

<p>Reviewer Comment</p>	<p>While a reduction in myeloid cells and in particular SPP1+ macrophages is visible in dCR and dPR in figure 2h, these patients show increased proportions of plasma cells and to a lesser extent B cells. The authors do not mention and interpret this</p>
-------------------------	---

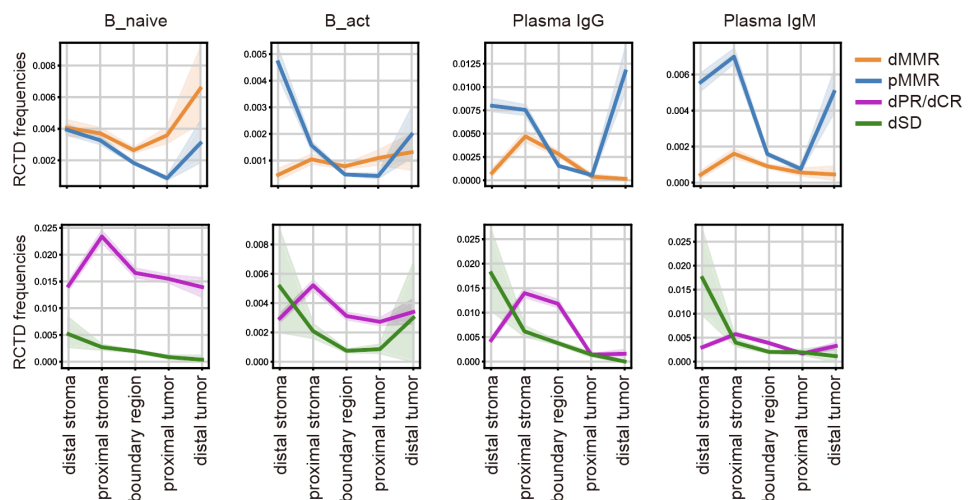
increase which of course affects the proportion of remainder cell types. Could the authors comment this observation and how this affects the proportion of the remaining ones?

Author Response

We thank the reviewer for highlighting these interesting points. We directed towards specific immune cell subsets of CD8_Teff, CD8_Tem, CD8_CXCL13, CD4_CXCL13, CD4_Treg, CD4_Tcm, cDC1 and DC_LAMP3, instead of others, based on their spatial distribution analysis indicated by the RCTD curve shown in the original Fig. 2f-g. In Fig. 2h, we then calculated the proportions of related immune cell subsets in the tumor-stroma boundary. As mentioned by the reviewer, the proportion of each cell type is indeed interconnected. For the SPP1+macrophages, they are widely studied and commonly recognized to function in promoting tumorigenesis and associate with lower immunotherapy response in CRC^{19,20}. Therefore, the abundance of SPP1+macrophages in the tumor-stroma boundary of CRC patients is expected. In addition, their higher RCTD frequency in the tumor-stroma boundary of dSD compared to dPR/dCR (**Fig. 2i**) is also consistent with previous reports²⁰. When we compared their RCTD frequencies in treatment-naïve patients, dMMR displayed a higher level of SPP1+macrophage in the tumor-stroma boundary compared to pMMR (**Fig. 2i**). This data suggested a possible role of SPP1+macrophage that might relate to the developmental differences in dMMR and pMMR, which would be interesting in further study. We have now included this information in our revised manuscript.

For the plasma and B cell clusters, the spatial distribution curve generated by calculating the RCTD frequencies suggested only marginal difference in the tumor-stroma boundary of treatment naïve dMMR and pMMR (**Fig. R5**). In comparison, the proportions of naïve and activated B cell clusters as well as IgG+ plasma cell cluster displayed higher levels in dPR/dCR compared to dSD (**Fig. R5**), suggesting that these B/plasma cells might be regulated by anti-PD1 treatment. To further study the relationship of B/plasma cells and anti-PD1 treatment, samples collected in CRC patients before and after anti-PD1 treatment will be important. As we focused on studying the cell types showing consistent difference between treatment naïve dMMR and pMMR, as well as anti-PD1-treated dPR/dCR and dSD, we did not explore the importance of B/plasma cells in our current study, which will be interested to further investigate in the future.

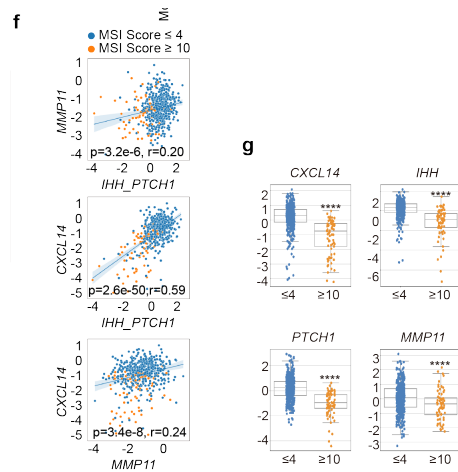
Fig R5



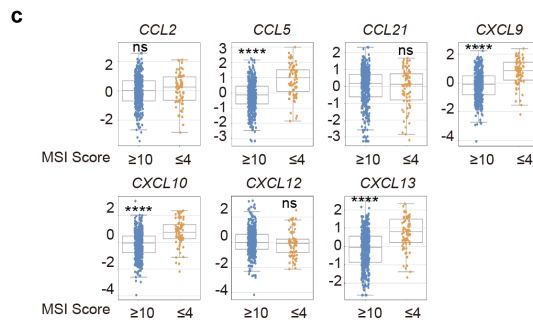
	<p>Fig R5. The distribution curve of the RCTD frequencies of plasma cell and B cell clusters in distal stroma (-500 to -1000µm), proximal stroma (-150 to -500µm), tumor-stromal boundary (-150 to +150µm), proximal tumor (+150 to +500µm), and distal tumor (+500 to +1000µm) in the spatial map.</p>
Excerpt from revised manuscript	<p>(P. 9:) Result lane 220 By dissecting the spatial distribution pattern of each immune cell subsets in details, we observed that immune cell subsets_of CD8_Teff, CD8_Tem, CD8_CXCL13, CD4_CXCL13, CD4_Treg, CD4_Tcm, cDC1 and DC_LAMP3, <u>but not other clusters</u> showed significant enrichment peaks within the tumor-stroma boundary <u>in treatment naïve dMMR compared to pMMR (Fig. 2f)</u>, which were also significantly higher in dPR/dCR compared to dSD (Fig. 2g). <u>Interestingly, when we compared the RCTD frequencies of these immune cell subsets in the centre of boundary (0 µm), we observed that the majority of immune cells were Mac SPP1 in both treatment naïve dMMR and pMMR (Fig. 2h).</u> In addition, <u>the proportion of Mac SPP1 was higher in treatment naïve dMMR compared to pMMR, while lower in dPR/CR compared to dSD (Fig. 2h-i).</u> Previous reports on the immune cell frequencies in CRC tumors have demonstrated that SPP1-expressing macrophages (SPP1, APOE, APOC1) (Supplementary Fig. 4c) <u>were commonly detected and their abundance are reported to correlate with less therapeutic benefit from anti-PD1 therapy^{10,11}.</u> This observation further supported the consistency and importance of immune cells in the tumor-stroma boundary.</p>

Ref 2.6 Clarification of the patient selection in TCGA dataset

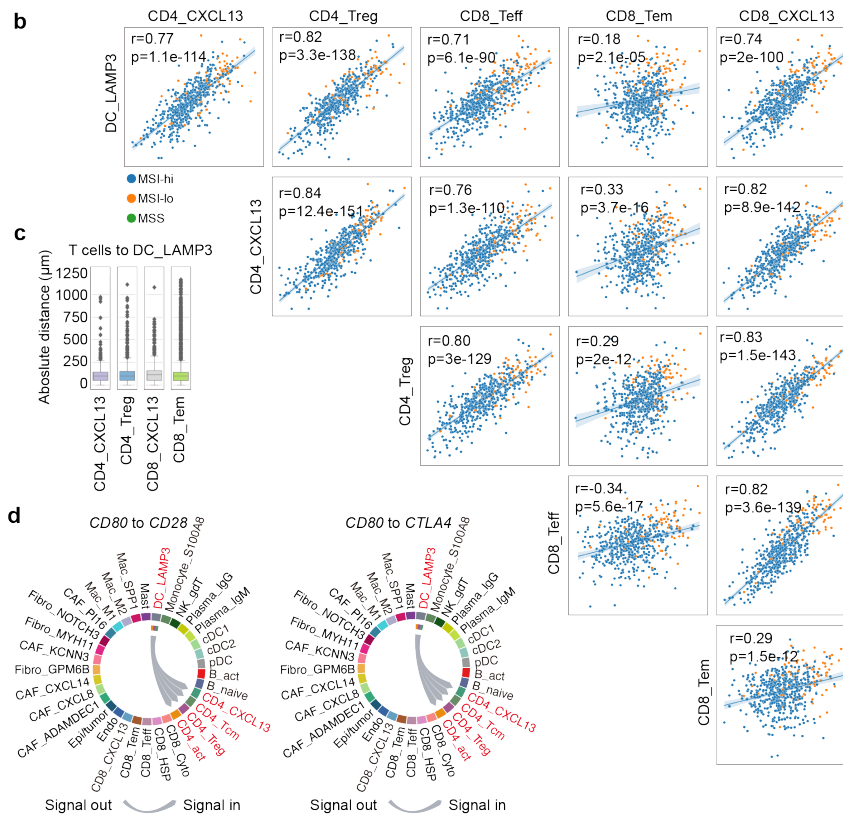
Reviewer Comment	<p>The authors use the COAD bulk RNA-Seq dataset from TCGA to support their findings. However, the manuscript does not provide any detail on how the data was fetched and processed. In particular, the number of reported COAD samples (n=275) highly deviates from the currently available participants in the COAD project on the TCGA/GDC portal (n=461). The authors should clearly state why they only used a subset of patients. What was the rationale?</p>
Author Response	<p>We agree with the reviewer that the rationale for patient sample selection is needed. We initially explored the potential use of different currently available datasets of COAD patients, including the TCGA/GDC portal (n=461) mentioned by the reviewer. However, we found incomplete clinical information of MMR status and MSI scores in the TCGA/GDC portal (n=461, https://portal.gdc.cancer.gov/projects/TCGA-COAD). Therefore, we generated our data in the original Fig 6f-g, Supplementary Fig. 6c and 7b based on the publication from Cancer Genome Atlas Network in 2012 (n=276) instead ²¹. As pointed by the reviewer, we further searched the COAD patient cohorts in cBioPortal (https://www.cbioportal.org/). We indeed found a larger COAD cohort from TCGA (n=594) and 572 of them had complete clinical information, which included additional patient numbers compared to the 2012 version we used previously. Therefore, we updated our analysis in the revised Fig. 6f-g, Supplementary Fig. 6c and 7a. Consistently, patients with low MSI score (< 4, n=494) displayed significantly lower expression of immune cell-trafficking chemokines (CCL5, CXCL9, CXCL10, CXCL13, Supplementary Fig. 6c) but higher levels of IHH, PTCH1, CXCL14, and MMP11 compared to those who with high MSI score (> 10, n=78) (revised Fig. 6g). The expressions of CXCL14, MMP11, and IHH_PTCH1 were also correlated (revised Fig. 6f).</p>



Revised Fig. 6f-g. f Pearson correlations and g expressions of *IHH_PTCH1*, *MMP11* and *CXCL14* from COAD TCGA dataset are shown. Patients are stratified to MSI-hi (MSI score ≥ 10 , n = 78) and MSI-lo (MSI score ≤ 10 , n = 494) accordingly. *IHH_PTCH1* scores are calculated as sum of *IHH* and *PTCH1* Z-scores. Data are represented as mean \pm SD and analyzed by unpaired Student-t test. ****, $p < 0.01$.



Revised Supplementary Fig. 6c. The expressions of indicated chemokines from MSI-hi (MSI score ≥ 10 , n = 78) and MSI-lo (MSI score ≤ 10 , n = 494) groups in COAD TCGA data are shown as dot plot graphs. Data are represented as mean \pm SD and analyzed by unpaired Student-t test. ns, not significant; ****, $p < 0.0001$.



Revised Supplementary Fig. 7b. Pearson correlation of the signature scores of DC_LAMP3 and T cell clusters from MSI-hi (MSI score ≥ 10 , $n = 78$) and MSI-lo (MSI score ≤ 4 , $n = 494$) groups in COAD TCGA data are shown. The signature Z-scores are calculated using the top10 DEGs from each cell cluster in our scRNA-seq data.

Excerpt from revised manuscript

(P. 11:)

Result lane 275

In parallel, consistent higher mRNA levels of *CCL5*, *CXCL9*, *CXCL10* and *CXCL13* were detected in MSI-hi (MSI score ≥ 10) compared to MSI-lo (MSI score ≤ 4) CRC from colorectal adenocarcinoma (COAD) TCGA dataset (**Supplementary Fig. 6c**).

(P. 12:)

Result lane 325

As the sample size of our in-house datasets was limited, we also validated these associations using the bulk-RNAseq datasets of 572 CRC patients with complete clinical information from COAD TCGA. Consistently, the DC_LAMP3 gene signature (top10 DEGs in RNA-seq datasets, **table S2**) was also positively associated with CD4_CXCL13, CD4_Treg, CD8_Tem and CD8_CXCL13 signatures (**Supplementary Fig. 7b**).

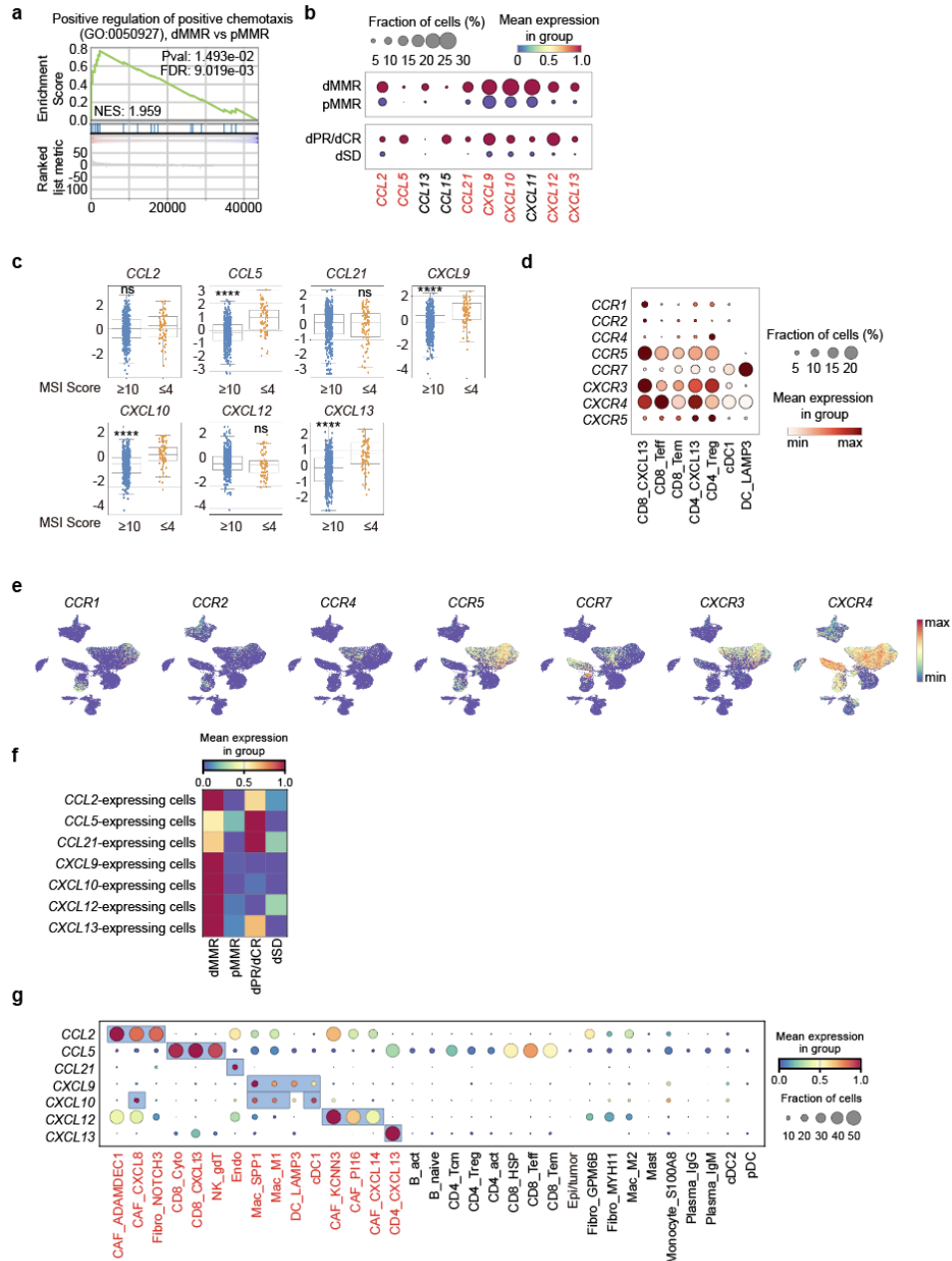
(P. 17:)

Result lane 471

Moreover, the expressions of *MMP11*, *IHH*, *PTCH1* and *CXCL14* were significantly higher in MSI-lo tumors (MSI score ≤ 4) compared to MSI-hi ones (MSI score ≥ 10) from the COAD TCGA dataset ($n=592$), which were also positively correlated (**Fig. 6f-g**).

Ref 2.7 Revision of figure legends and panel flow

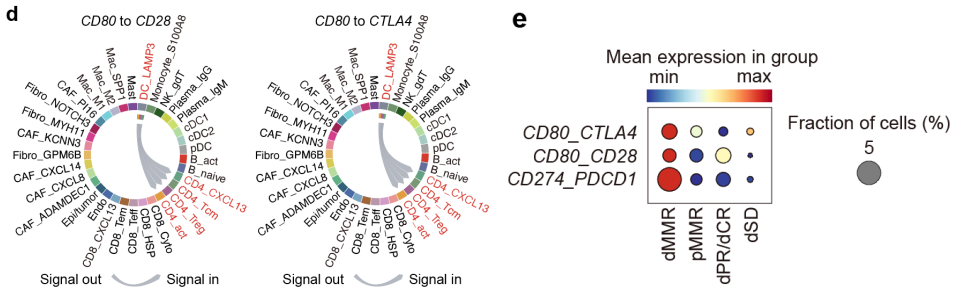
Reviewer Comment	Overall, figures are of good quality, but the authors should make sure to provide exhaustive legends. For example, Supplementary Figure 6f shows the mean expression as a scale but it is not clear if the values were normalized (capped to 1 and like the min/max scale shown in panel d?). The same Supplementary Figure 6g shows boxes which are not described in the legend nor in the manuscript and their purpose can only be guessed out of the main manuscript. In addition, the flow of Supplementary Figure 6 is misleading as the panels appear in the following order: a, b, d, c, f, e and g.
Author Response	We apologize for the unclear description of our figures and panel labeling. We have now revised our figure legends and double checked our panel flow to all our figures besides the Supplementary Fig. 6 thoroughly.
Excerpt from revised manuscript	Please see the thoroughly revised main figure legend in the main text from page 36 to page 39, and the revised supplementary figure legend in the in the supplementary file page 1 to page 19.



Revised Supplementary Fig. 6. **a** GSEA plot of the upregulated genes related to positive regulation of positive chemotaxis (GO:0050927) in the tumor-stroma boundary of treatment naïve dMMR compared to pMMR is shown. GSEA plot showing the up-regulation of the genes related to in dMMR boundaries (in comparison to pMMR boundaries). **b** Bubble plots of indicated chemokine expressions in the tumor-stroma boundary of indicated patient groups. The plots are sized by the fraction of cells with positive gene expression, while the color represents the gene expression level. The chemokines with higher expressions in treatment naïve dMMR compared to pMMR, as well as in anti-PD1-treated dPR/dCR compared to dSD are highlighted in red. **c** The expressions of indicated chemokines from MSI-hi (MSI score ≥ 10 , $n = 78$) and MSI-lo (MSI score ≤ 4 , $n = 494$) groups in COAD TCGA data are shown as dot plot graphs. Data are represented as mean \pm SD and analyzed by unpaired Student-t test. ns, not significant; ****, $p < 0.0001$. **d** Bubble plots of chemokine receptors of chemokines highlighted in **b** from indicated immune cell clusters are shown. The plots are sized by the fraction of cells with positive gene expression, while the color

represents the gene expression level. **e** UMAP of indicated chemokine receptor expressions from the scRNA-seq dataset. **f** Heatmap of chemokine-expressing cells in the tumor-stroma boundary of indicated patient groups. **g** Bubble plots of the chemokine expressions profiling in the cell clusters from the scRNA-seq dataset. The cells of interests are highlighted in red and framed.

Ref 2.8 Additional analysis of ligand-receptor pairs between DC and T cells

<p>Reviewer Comment</p>	<p>The authors suggest that DC and T-cells crosstalk to accumulate in the tumor-stroma boundary (line 291). While the correlation plots (albeit some exhibiting poor correlation coefficients) support the spatial co-occurrence, the analysis could benefit from a ligand receptor pair analysis (such as performed by the authors in figure 3) to identify potential crosstalk signaling pathways.</p>
<p>Author Response</p>	<p>We thank the reviewer for this good suggestion. First, we updated the correlation plots in the revised Supplementary Fig. 7b using the larger COAD cohort from TCGA (n=572), as mentioned in Ref 2.6. As suggested by the reviewer, we applied additional analysis to explore the potential crosstalk signaling pathways among the cell clusters we identified. Indeed, we found that LAMP3+DC and CD4+T cell subsets may also interact via CD80-CTLA4, CD80-CD28, besides CD274-PDCD1 (new Supplementary Fig.7d). In addition, the expression of CD80-CD28 in the tumor-stroma boundary exhibited a similarly elevated level in treatment naïve dMMR compared to pMMR, as well as higher level in dPR/dCR compared to dSD (new Supplementary Fig. 7e). As CD80 signal exhibits a regulatory effect on the CD274-PDCD1 pathway^{22,23}, this CD80-CD28 ligand-receptor pair might also play a possible role in regulating the immunotherapy response in CRC.</p>  <p>new Supplementary Fig 7d-e. d The chord plots show the ligand-receptor interaction of <i>CD80_CD28</i> (left) and <i>CD80_CTLA4</i> (right) between <i>DC_LAMP3</i> and <i>CD4+T</i> cell clusters. e Bubble plots of expression profiling of ligand-receptor pairs <i>CD80_CTLA4</i>, <i>CD80_CD28</i> and <i>CD274_PDCD1</i> in the tumor-stromal boundary of indicated patient groups are shown. The plots are sized by the fraction of cells with positive gene expression, while the color represents the gene expression level.</p>
<p>Excerpt from revised manuscript</p>	<p>(P. :13) Result lane 340 Of note, the ligand-receptor pair analysis of PD1-PD-L1 axis indicated the potential interactions of <i>DC_LAMP3</i> towards <i>CD4_CXCL13</i> and <i>CD8_CXCL13</i>, but not other cell types (Fig. 3b). <u>In parallel, <i>DC_LAMP3</i> may also interact with</u></p>

	<u>CD4 CXCL13 via CD80-CD28 axis in the tumor-stroma boundary of treatment naïve dMMR and dPR/dCR patients (Supplementary Fig 7d-e).</u>
--	--

Ref 2.9 Revision of typo errors

Reviewer Comment	Several typos subsist in the manuscript (batch: Bacth, line 152; bath line 153). Further language editing will improve the reading.
Author Response	We apologize for the typo errors in our manuscript. We have read the manuscript thoroughly and revised all the typo errors in the original version.
Excerpt from revised manuscript	<p>(P. 7:) Result lane 171 We integrated the cells by <u>Batch</u> Balanced K Nearest Neighbors (BBKNN) algorithm to correct the <u>batch</u> effect</p> <p>(P. 13:) Result lane 348 mIF staining data of specimens from treatment naïve dMMR CRC further verified the potential physical <u>juxtaposition</u> (mean distance <100µm) of PD1- and PD-L1-expressing cells in the tumor-stroma boundary (Fig. 3e and 3f).</p> <p>(P. 19:) Discussion lane 561 In consistent with our findings, previous study in HCC also showed that <i>LAMP3</i>+DCs highly expressed <i>CD274</i> (PD-L1) and exhibited the physical <u>juxtaposition</u> towards <i>PDCD1</i>-expressing T cell subsets ²⁵.</p>

Ref 2.10

Reviewer Comment	The raw sequencing data kindly provided for reviewing purposes is not accessible or likely outdated (pointing to a “Wrong share code OR this preview is Cancelled.” webpage).
Author Response	The raw sequencing data is now fully opened in Genome Sequence Archive (accession number: PRJCA020107 https://ngdc.cnca.ac.cn/gsa-human/browse/HRA005647). The processed matrix file could be accessed in STOmicsDB of China National GeneBank Datadase with accession number STT0000036.
Excerpt from revised manuscript	<p>(P. 26:) Method lane 801 Data and code availability</p> <p>The raw sequencing FASTQ files could be accessed on Genome Sequence Archive (accession number: PRJCA020107, https://ngdc.cnca.ac.cn/gsa-human/browse/HRA005647), <u>complying with the Chinese laws</u>. The processed</p>

	<p>h5ad <u>files of Stereo-seq and scRNAseq was deposited on STOmicsDB⁶⁴ of China National GenBank Database (accession number: STT0000036). All codes for data analysis and plotting are available upon request. <u>Please contact the lead author: Rongxin Zhang (zhangrx@sysucc.org.cn.)</u></u></p>
--	---

Reviewer 3#: expertise in colorectal cancer TME, immunogenomics, scRNAseq and ST

Overall comments	Feng and colleagues' manuscript, which integrates spatial and single-cell transcriptomics along with multiplex immunofluorescence to explore the factors influencing response to immune checkpoint blockade (ICB) in colorectal cancer, represents a significant effort. However, there are substantial concerns regarding the study's design and the occasionally overstated conclusions drawn from the data.
Author Response	We are grateful for the reviewer's insights and compliments on our study. We also acknowledge the shortcomings raised by the reviewer and have addressed them in the revised manuscript.
Summary of the revision	<ol style="list-style-type: none"> 1. Add new information to clarify the clinical features and ICB response assessment of our patient cohort. 2. Revise the description about the resolution of our stereo-seq platform by performing additional analysis and include discussion about the limitations of our study. 3. Add new experiments to support our analysis at least partially. 4. Revise the Methods thoroughly.

Ref 3.1 Clarification of sample size

Reviewer Comment (i)	The study's primary comparison between mismatch repair deficient (dMMR) and proficient (pMMR) colorectal cancer cases may not accurately reflect the nuances of ICB response. It would be more appropriate to analyze separate cohorts of dMMR and pMMR patients, further divided into responders and non-responders. Additionally, comparing treatment-naïve pMMR cases with treated dMMR cases introduces a confounding factor. A more focused analysis solely on dMMR cases in the current cohort may still not provide a sufficient sample size to draw robust conclusions.
Author Response (i)	<p>We agree with the reviewer that an equal sample size across all groups would be optimal for the analysis. For the treatment naïve cases, we have included comparable sample size of dMMR and pMMR for our stereo-seq analysis. However, collecting tissues from an equal sample size for the anti-PD1 treated dMMR and pMMR groups posed considerable challenges.</p> <p>The initial study on the relationship between MMR status and therapeutic response to anti-PD1 was conducted in 2015 ²⁴. Based on data from multiple clinical trials, the FDA subsequently approved anti-PD1 antibodies as a first-line treatment for unresectable or metastatic MSI-H/dMMR CRC. Recent advancements of utilizing anti-PD1 in neoadjuvant, pre-operative settings have yielded substantial improvements in the response rate and disease-free survival among dMMR patients with resectable CRC ²⁵. In contrast, ICB has exhibited limited efficacy in pMMR cases, with a 0% response rate to anti-PD1 monotherapy and up to 27% PR/SD rate reported in early-stage patients to combinatory approaches ^{24,26}. Instead, CRC patients with pMMR showed improved disease-free survival with neoadjuvant chemoradiotherapy, especially for stage III disease ²⁷. Therefore, neoadjuvant anti-PD1 therapy is infrequently employed in the clinical management of CRC patients with pMMR. As a consequence, we were unable to collect tissues from anti-PD1-treated pMMR patients.</p>

	<p>As MSI-hi/dMMR has emerged as a predictive biomarker for determining ICB response, we classified pMMR patients as a potential low-response group in our manuscript. To improve our clarity, we have revised the description in our result part thoroughly. We provided separate descriptions of the differences observed between treatment-naïve dMMR and pMMR patients, as well as between patients with dSD or dPR/CR from anti-PD1-treated dMMR patients. In addition, we have included the information of clinical disparities on ICB response in dMMR and pMMR in the introduction of revised manuscript.</p>
Reviewer Comment (ii)	<p>There's a lack of clarity regarding the equal number of responders and non-responders in dMMR cases, especially given the previously reported high response rates. Clarification is needed on whether the cohort was specifically enriched for non-responders.</p>
Author Response (ii)	<p>For the localized dMMR CRC cases, it demonstrated complete clinical and pathological response rates to 60%-100% to neoadjuvant anti-PD1 monotherapy²⁵. Data from our own neoadjuvant anti-PD1 study also showed that 1 out of 6 patients who underwent surgery after one cycle treatment did not have a pathological complete response³. Due to the scarcity of cases with progressive disease (PD) in dMMR patients received anti-PD1 neoadjuvant therapy, we grouped CR/PR (n=6) as responders and SD (n=5) as non-responders for the analysis accordingly²⁵. As suggested by the reviewer, we ensured a comparable sample size between groups for the analysis.</p>
Excerpt from revised manuscript	<p>(P. 4:) Introduction lane 56 We recently reported a 93.75% (15/16) overall response rate (12 were complete response) to anti-programme death 1 (PD1) monoclonal antibody (mAb, sintilimab) in the dMMR cohorts, which potentially spare these patients from radical surgeries⁵. <u>In contrast, ICB has exhibited limited efficacy in pMMR cases, with a 0% response rate to anti-PD1 monotherapy and up to 27% of stable disease (SD) or partial response (PR) reported in early-stage patients to combinatory approaches^{4,6}</u></p> <p>(P. 9:) Result lane 220 By dissecting the spatial distribution pattern of each immune cell subsets in details, we observed that immune cell subsets <u>of CD8_Teff, CD8_Tem, CD8_CXCL13, CD4_CXCL13, CD4_Treg, CD4_Tcm, cDC1 and DC_LAMP3, but not other clusters</u> showed significant enrichment peaks within the tumor-stroma boundary <u>in treatment naïve dMMR compared to pMMR (Fig. 2f), which were also significantly higher in dPR/dCR compared to dSD (Fig. 2g). Interestingly, when we compared the RCTD frequencies of these immune cell subsets in the centre of boundary (0 µm), we observed that the majority of immune cells were Mac SPP1 in both treatment naïve dMMR and pMMR (Fig. 2h). In addition, the proportion of Mac SPP1 was higher in treatment naïve dMMR compared to pMMR, while lower in dPR/CR compared to dSD (Fig. 2h-i).</u></p> <p>(P. 10:) Result lane 270 By comparing the gene expressions in the tumor-stroma boundary, we detected a significant enrichment of positive regulation of positive chemotaxis (GO:0050927) in <u>treatment naïve dMMR compared to pMMR by gene set</u></p>

enrichment analysis (GSEA) (FDR=0.009, p=0.015; **Supplementary Fig. 6a**). Specifically, the expressions of *CCL2/5/13/15/21* and *CXCL9/10/11/12/13* were significantly higher in the tumor-stroma boundary of treatment naïve dMMR compared to pMMR (**Supplementary Fig. 6b**).

(P. 11:)

Result lane 285

Next, we detected the expressions of corresponding receptors toward *CCL2/5/21* and *CXCL9/10/13* on the immune cells that displayed higher abundance in treatment naïve dMMR or dPR/dCR using scRNA-seq dataset.

Result lane 300

Of note, *CCL2*, *CCL5*, *CCL21*, and *CXCL13*-expressing cells but no other chemokine-expressing cells showed significant higher abundances in treatment naïve dMMR compared to pMMR, which were consistently higher in dPR/dCR compared to dSD (**Supplementary Fig. 6f**), indicating that the *CCL21-CCR7*, *CXCL13-CXCR5* and *CCL5-CCR5* may be the key chemotaxis pathways in controlling the recruitment of DC and T cell subsets in the tumor-stroma boundary of ICB responders.

(P. 12:)

Result lane 319

Next, we explored the potential crosstalk among *cDC1*, *DC_LAMP3*, *CD4_CXCL13*, *CD4_Treg*, *CD8_Teff*, *CD8_Tem* and *CD8_CXCL13* cells that presented at higher levels in the tumor-stroma boundary of treatment naïve dMMR by calculating their Pearson's correlations and spatial distances.

(P. 13:)

Result lane 354

When further applied these exhausted signatures and PD1-PD-L1 axis into our spatial transcriptomics FOV analysis, our data confirmed an elevation of *PDCD1/CD274* and T cell exhaustion signature in the tumor-stroma boundary of treatment naïve dMMR patients (**Fig. 3h-i**). Interestingly, we noticed that *DC_LAMP3* also highly expressed other co-inhibitory molecules, like *LGALS9*, and co-stimulatory molecules, including *CD80*, *CD86*, *ICOSLG*, *CD70*, *PVR* (**Supplementary Fig. 7f-h**).

(P. 15:)

Result lane 409

Of note, we found that the ratio of *CXCL14/CXCL8*-expressed fibroblasts was significantly higher in treatment naïve pMMR compared to dMMR, or dSD compared to dPR/CR (**Fig. 4h**), thus highlighting the potential role of fibroblast plasticity in ICB response of CRCs.

Result lane 431

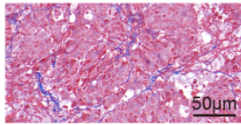
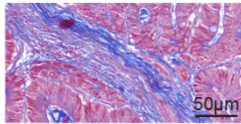
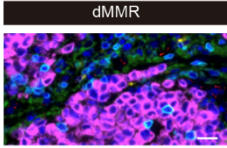
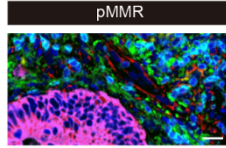
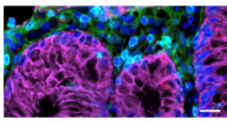
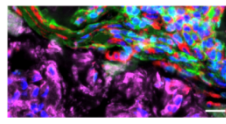
To further evaluate the distribution of collagen fiber and CAF *CXCL14*, Masson's trichrome staining and mIF staining were performed. As expected, a well-organized matrix structure and higher level of *COL1A1*⁺*CXCL14*⁺ cells were clearly observed in the tumor-stroma boundary of treatment naïve pMMR but not dMMR (**Fig. 5h-i**). In addition, higher frequency of *COL1A1*⁺*CXCL14*⁺ cells was also detected in the tumor-stroma boundary of dSD compared to dPR/dCR (**Fig. 5i**).

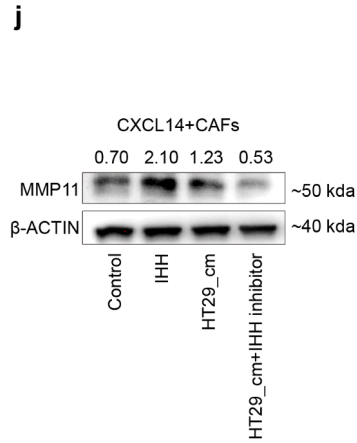
(P. 18:)

Discussion lane 520

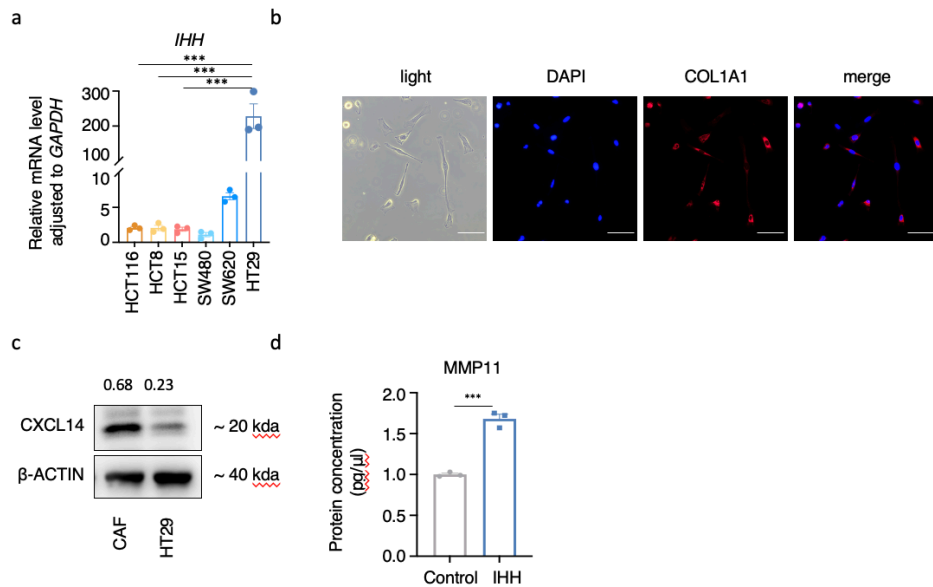
	In general, the tumor-stroma boundary of <u>treatment naïve dMMR patients</u> displayed an immune activation state (state 1 & 2) compared to an immune exclusive one (state 0) in pMMR patients. <u>This distinction was also observed in ICB-treated patients, where dPR/dCR displayed an immune activation state (state 1 & 2), whereas dSD demonstrated an immune exclusive state (state 0).</u>
--	---

Ref 3.2 Statement rephrase and experimental validation

Reviewer Comment	The use of the term "determinants of efficacy of immunotherapy" in the title and throughout the paper is misleading. Ideally, these determinants should be assessed before the administration of immunotherapy, not post-treatment.
Author Response	<p>We acknowledge the reviewer's comments regarding our inaccurate descriptions and lack of functional data support. We have now included new experimental data to support our bioinformatic analysis at least partially: 1) new sets of multiplex immunofluorescences staining of CXCL14+CAFs on patient specimens (new Fig. 5i); 2) new Masson's trichrome staining to indicate the collagen fibers deposition in dMMR and pMMR (new Fig. 5h); 3) <i>in vitro</i> assay to indicate the possible role of IHH/PTCH1 pathway on CAFs (new Fig. 6j and supplementary Fig. 9). These data are now included in the revised manuscript, respectively. In addition, we have revised our descriptions accordingly.</p> <div style="display: flex; justify-content: space-around; align-items: flex-start;"> <div style="text-align: center;"> <p>h</p> <p>Masson's staining</p> <div style="display: flex; flex-direction: column; gap: 10px;"> <div style="text-align: center;"> <p>dMMR</p>  </div> <div style="text-align: center;"> <p>pMMR</p>  </div> </div> </div> <div style="text-align: center;"> <p>i</p> <div style="display: grid; grid-template-columns: 1fr 1fr; gap: 5px;"> <div style="text-align: center;"> <p>dMMR</p>  </div> <div style="text-align: center;"> <p>pMMR</p>  </div> <div style="text-align: center;"> <p>dPR/dCR</p>  </div> <div style="text-align: center;"> <p>dSD</p>  </div> </div> <p style="font-size: small; margin-top: 5px;">Multi-plexed IF staining of tumor-stroma boundary: Pan-CK COL1A1 CD3 CXCL14 DAPI Scale bar : 20µm</p> </div> </div> <p>Fig. 5h-i. h Representative images of Masson's trichrome staining from treatment naïve dMMR and pMMR patients. Scale bar = 50µm. i Representative mIF images of panCK, COL1A1, CD3 and CXCL14 in indicated patient groups. DAPI was used as a positive control for cell nuclei staining. Scale bars, 50 µm.</p>



New Fig. 6j. Western blot analysis of MMP11 in indicated group is shown. β -actin serves as loading control. Number indicates the relative expression towards β -actin.



New Supplementary Fig. 9. **a** The relative expression of *IHH* to *GAPDH* in the 6 human CRC cell lines. Data are represented as mean \pm SD and analyzed by unpaired Student-t test. **b** The representative images of the morphology and IF staining of COL1A1 in the CAFs are shown. DAPI was used as a positive control for cell nuclei staining. Scale bars, 20 μ m. **c** Western blot analysis of CXCL14 in CAF and HT29 cell lines is shown. β -actin serves as loading control. Number indicates the relative expression towards β -actin. **d** The relative expression of *MMP11* to *GAPDH* in HT29 cells treated with PBS or IHH recombinant protein. Data are represented as mean \pm SD and analyzed by unpaired Student-t test. ***, $p < 0.001$.

Excerpt from revised manuscript

(P. 3:)

Abstract lane 43

Our results identified the spatial organization and immune status of the tumor-stroma boundary as a distinctive feature of dMMR and pMMR CRCs, which associates with ICB response.

Abstract lane 48

	<p>Our work therefore <u>points out the importance of</u> the molecular and cellular spatial structures of tumors <u>in</u> ICB response, raising the possibility of reprogramming tumor-stroma boundary for sensitizing immunotherapies in the majority of CRCs.</p> <p>(P. 5:) Introduction lane 101 In this microscopic structure of tumor-stroma boundary, the active interplays among tumor cells, fibroblasts, macrophage/dendritic cells (DCs) and T cell subsets <u>associated with</u> the distinctive immune status of dMMR and pMMR CRCs patients, <u>which may lead</u> to their diverse ICB responses.</p> <p>(P. 7:) Result lane 162 The proximity (Fig. 1e) and the correlation (Fig. 1f) between the boundary and epi/tumor clusters further indicated that the presence and spatial organization of tumor-stroma boundary may <u>associate with</u> ICB response in CRC patients.</p> <p>(P. 13:) Result lane 366 <i>The plasticity of CAF <u>correlates with</u> the immune status of tumor-stroma boundary in ICB non-responders</i></p> <p>Result lane 369 As we have pinpointed the importance of tumor-stroma boundary in <u>contributing to</u> ICB response, we next focused on analysing the spatial transcriptomic features of treatment-naïve pMMR and dSD.</p> <p>(P. 17:) Discussion lane 500 We identified spatially organized cell-cell interactions that contribute to a coordinated multi-cellular tumor-stroma boundary ($0\pm 150\mu\text{m}$) <u>in ICB response</u> of CRC patients.</p>
--	---

Ref 3.3 Clarification of scRNAseq and stereo-seq analysis on a per-patient basis

<p>Reviewer Comment</p>	<p>For methodological transparency, it's recommended to indicate in Table S1 or Figure 1 which patients underwent specific analytical processes. Were all patients analyzed with single-cell RNA sequencing also subject to spatial transcriptomics? And were RCTD analyses consistently performed on paired samples? If there's a mismatch in sample processing, this could affect the validity of the RCTD findings.</p>
<p>Author Response</p>	<p>We apologize for the unclear description in the methodology part about the analysis on a per-patient basis. We have now incorporated this information into the revised Table S1. We concur with the reviewer that, in theory, performing RCTD analysis with paired samples would enhance the accuracy of the results. However, technical disparities between scRNA-seq and spatial transcriptomics present significant challenges in acquiring compatible paired data for each experimental iteration. First, the dissociation process for generating single-cell suspension in scRNAseq would preferentially enrich immune cells²⁸. As a result, immune cells accounted for around 24.6%-97.1% in our scRNAseq analysis (Fig. R6 a-b). In contrast, immune cells only comprised 2.4% to 23.2% in the RCTD analysis (Supplementary Fig. 4f). This discrepancy led to a suboptimal</p>

resolution of the single-cell transcriptome for stromal cells. For example, a mere five fibroblasts were captured in the scRNA-seq data from Patient No. 27, and no endothelial cells were isolated from Patient No. 37. Moreover, the limited throughput of scRNA-seq technology poses another hurdle. Each scRNA-seq run yielded 506 to 7,861 single cells, while stereo-seq can encompass over 200,000 cells per slide ^{5,6,29}. The scRNA-seq, with its relatively lower cell count, cannot comprehensively represent all cell types found in the spatial transcriptome, thereby limiting subsequent bioinformatic analyses.

We acknowledge that integrating scRNA-seq with spatial transcriptomics remains a formidable task in the current scientific landscape. Deciding whether to deconvolute each spatial transcriptome using paired samples or to treat all samples as a collective entity can lead to different interpretations, each with its own subtle biases. Therefore, we opted to integrate the scRNA-seq data from all patients and use it as a unified reference for deconvoluting the spatial transcriptome. Post-data processing and manual annotation revealed that plasmacytoid dendritic cells (pDCs) were the subtype with the fewest cells, n=33, which still meets the minimum cell number requirement for RCTD analysis (minimum cell number = 25). Given that our key findings from the spatial transcriptome were further supported by multiplexed immunofluorescence, we are confident that our study delivers meaningful and reliable insights.

Table S1: Clinical information of the patients

Table S1. Clinical information of the patients.													
patients No.	age	gender	MMR status	MSI status	pre-surgery TNM stage	post-surgery TNM stage	stereo-seq				response on NCCN TRG	response on RECIST	group label in this study
							treatment	APD1 drug	course of treatment	timepoint for sampling			
24	69	F	dMMR	MSI-H	cT4N1M0	pT3N1M0	pPD1	Pembrolizumab	4	post-treatment	0	CR	dSCR
25	34	M	dMMR	MSI-H	cT4N2M0	pT3N2M0	pPD1	Pembrolizumab	8	post-treatment	0	CR	dSCR
99	55	F	dMMR	MSI-H	cT4N2M1	pT4N2M1	NA	NA	NA	treatment-naive	NA	NA	dMMR
61	51	F	dMMR	MSI-H	cT4N2M0	pT3N2M0	pPD1	Camrelizumab	4	post-treatment	1	nCR	dSCR
55	71	M	dMMR	MSI-H	cT3N2M0	pT3N2M0	pPD1	Camrelizumab	4	post-treatment	0	CR	dSCR
99	39	M	dMMR	MSI-H	cT4N2M0	pT4N2M0	NA	NA	NA	treatment-naive	NA	NA	dMMR
100	55	M	dMMR	MSI-H	cT4N2M0	pT3N2M0	NA	NA	NA	treatment-naive	2	SD	dMMR
104	53	F	dMMR	undetermined	cT3N1M0	pT3N1M0	pPD1	Sintilimab	4	post-treatment	1	PR	dSCR
157	79	F	dMMR	undetermined	cT4N1M0	pT3N2M0	NA	NA	NA	treatment-naive	NA	NA	dMMR
113	54	F	dMMR	MSI-H	cT4N1M1	pT3N1M0	pPD1	Sintilimab	8	post-treatment	1	PR	dSCR
50	57	F	pMMR	MSS	cT3N2M0	pT3N1M0	NA	NA	NA	treatment-naive	NA	NA	pMMR
55	46	F	pMMR	MSS	cT3N2M0	pT3N2M0	NA	NA	NA	treatment-naive	NA	NA	pMMR
99	74	F	dMMR	MSS	cT4N2M0	pT3N2M0	NA	NA	NA	treatment-naive	NA	NA	pMMR
67	74	F	pMMR	MSS	cT3N2M0	pT3N1M0	NA	NA	NA	treatment-naive	NA	NA	pMMR
71	51	M	dMMR	MSS	cT3N2M0	pT3N2M0	NA	NA	NA	treatment-naive	NA	NA	pMMR

scRNA-seq													
patients No.	age	gender	MMR status	MSI status	pre-surgery TNM stage	post-surgery TNM stage	treatment	APD1 drug	course of treatment	timepoint for sampling	response on NCCN TRG	response on RECIST	group label in this study
146	76	F	dMMR	MSI-H	cT4N1M0	pT3N1M0	pPD1	Pembrolizumab	3	post-treatment	2	SD	dSD
147	38	M	dMMR	MSI-H	cT4N2M1	pT4N2M1	pPD1+themo	Nivolumab	8	post-treatment	2	SD	dSD
149	34	F	dMMR	MSI-H	cT4N2M0	pT3N1M0	pPD1	Tislelizumab	3	post-treatment	1	PR	dSCR
99	39	M	dMMR	MSI-H	cT4N2M0	pT4N2M0	pPD1	Camrelizumab	8	post-treatment	2	SD	dSD
24	69	F	dMMR	MSI-H	cT4N1M0	pT3N1M0	pPD1	Pembrolizumab	4	post-treatment	0	CR	dSCR
77	61	F	pMMR	MSS	cT3N1M0	pT3N1M0	NA	NA	NA	treatment-naive	NA	NA	pMMR
30	67	M	pMMR	MSS	cT3N1M0	pT3N2M0	NA	NA	NA	treatment-naive	NA	NA	pMMR
32	56	F	dMMR	MSS	cT3N2M0	pT3N2M0	NA	NA	NA	treatment-naive	NA	NA	pMMR
34	70	M	pMMR	MSS	cT3N2M0	pT3N2M0	NA	NA	NA	treatment-naive	NA	NA	pMMR
37	63	M	pMMR	MSS	cT3N2M0	pT3N1M0	NA	NA	NA	treatment-naive	NA	NA	pMMR

nCR: near complete response

Fig. R6

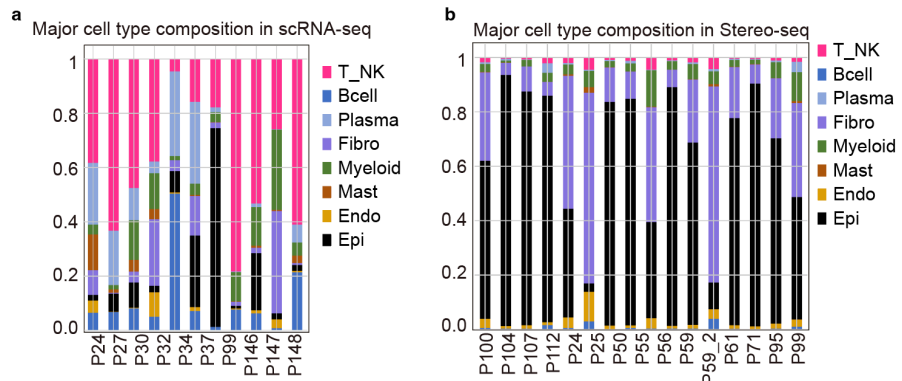


Fig R6. a Stacked box plot showing proportion or RCTD frequencies of the major cell types in scRNAseq and **b** stereo-seq in each patient, respectively.

Minor comments:

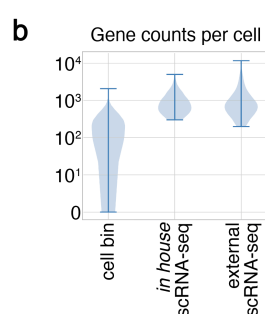
Ref M3.1 Statement rephrase

Reviewer Comment (i)	Certain claims, such as those in the abstract about unraveling the "black box" of ICB response, should be moderated. The primary known determinant in this context is the mutational burden, particularly in distinguishing between MMRd and MMRp CRCs. The term "black box" seems to oversimplify the current understanding of these mechanisms.
Author Response (i)	We acknowledge the reviewer's comment and have revised the description accordingly.
Excerpt from revised manuscript (i)	(P. 3:) Abstract lane 48 Our work therefore <u>points out the importance of</u> the molecular and cellular spatial structures of tumors <u>in</u> ICB response, raising the possibility of reprogramming tumor-stroma boundary for sensitizing immunotherapies in the majority of CRCs.
Reviewer Comment (ii)	The claim of treatment-induced changes (line 346) lacks a pre-treatment comparative analysis, which is crucial for substantiating such conclusions.
Author Response (ii)	We agree with the reviewer that direct comparison between pre- and post-treatment samples is necessary for these conclusions. We have now revised the description accordingly.
Excerpt from revised manuscript (ii)	(P. 14:) Result lane 376 In addition, anti-PD1 treatment <u>was associated with the reduction</u> of state 1 and expansion of state 2 in dPR/dCR, <u>but an elevation</u> of state 0 in dSD (Fig. 4a and 4b).

Ref M3.2 Clarification of spatial resolution of stereo-seq platform

Reviewer Comment	<p>In the Results section, the authors' claim about the resolution of spatial transcriptomic data requires further justification, especially when compared to similar technologies like Visium. The significance of choosing this particular technology for its resolution, as stated in the introduction, remains unclear.</p> <p>In the Results section the authors claim that they are able to analyse the spatial transcriptomic data at 50 um resolution, which is not that different from technologies like Visium. I therefore do not understand the significance of the last paragraph from the introduction where the authors claim that they have opted for this technology because of its resolution.</p>
Author Response	We acknowledge the issue of inconsistent description of the spatial resolution in our previous study and the current one raised by the reviewer. As mentioned in the introduction, the Stereo-seq platform we developed indeed could achieve high sensitivity and single-cell resolution (500nm) analysis <i>in situ</i> when studying mouse embryos ⁵ and axolotl brain ⁶ . We therefore applied the stereo-seq to

analyze the tumor tissues collected from CRC patients in the current study. Unfortunately, when we set the cell bin for single-cell segmentation, we could only generate fewer than 300 genes per bin (**new Supplementary Fig. 1b**). Compared to scRNA-seq datasets generated from CRC patients in our in-house dataset and the literature (**new Supplementary Fig. 1b**)⁷, ~300 genes/cell was insufficient for cell type annotation and follow-up analysis. One probable explanation may be the difference on the average cell size and the complexity among different tissues. This observation indicated the limitation of our Stereo-seq platform, which may not be universally applicable, particularly in tissues enriched with small-sized immune cells, such as tumors, spleen and thymus. Therefore, we set the bin size to bin100 (50µm x 50µm) in our stereo-seq data analysis. In addition, we employed parallel scRNA-seq analysis alongside Stereo-seq in our current study. This combination allowed us to distinguish transcriptionally similar cell types and analyze their spatial localization. We have now revised our manuscript and incorporated this information to clarify the resolution problem.



New Supplementary Fig. 1b. Violin plots of the gene counts per cell in cell bin segmented of Stereo-seq data from a representative patient #59, our in house scRNA-seq data and a representative public scRNA-seq data (GSE178341) are shown.

Excerpt from revised manuscript

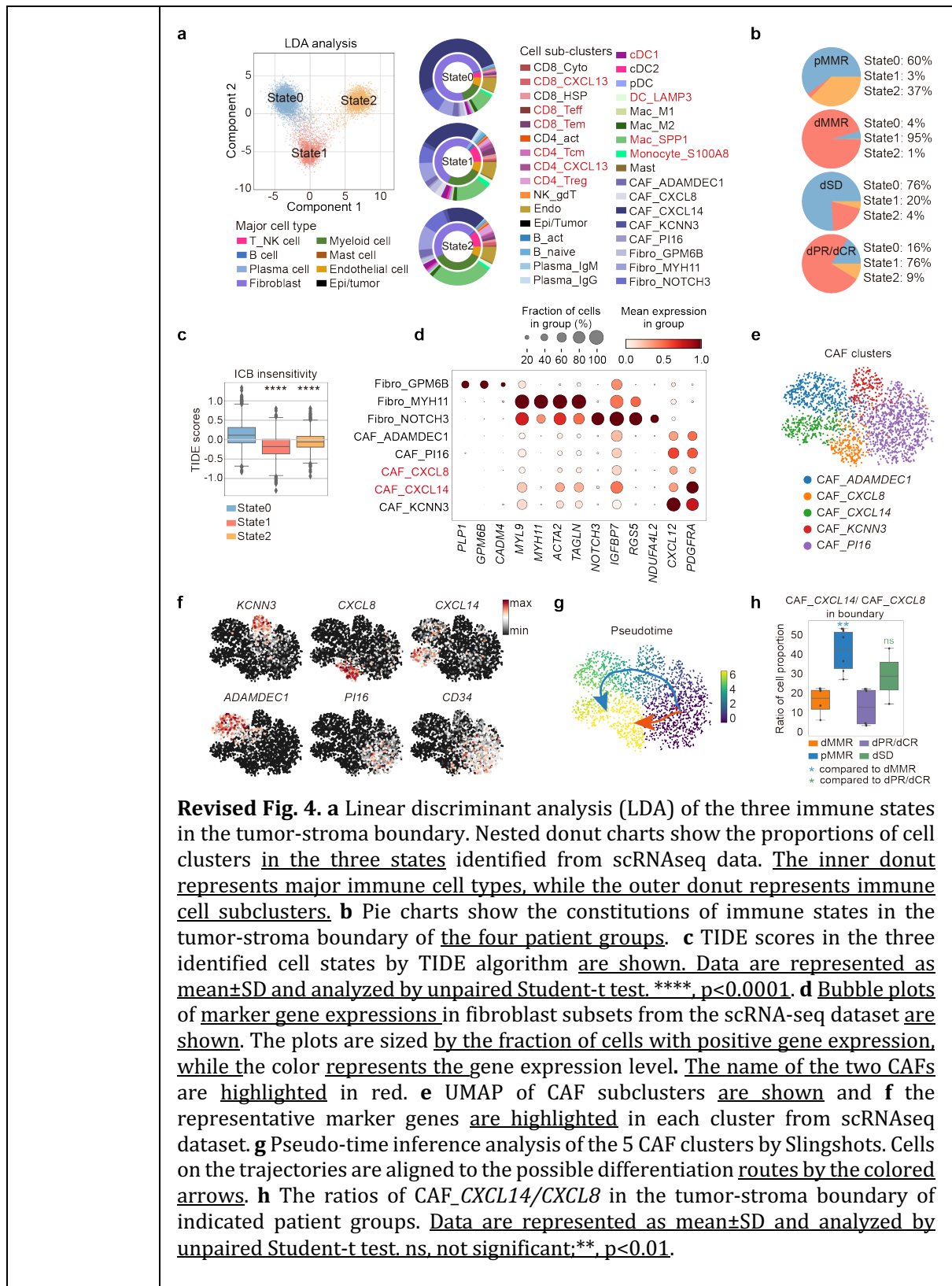
(P. 5:)
Introduction lane 88
We therefore developed the spatial enhanced resolution omics-sequencing (Stereo-seq). It is a DNA nanoball (DNB)-patterned array embedded with coordinate identity¹³ and unique molecular identifiers (MID) co-barcoded poly-T probe, capable of capturing mRNA *in situ* at a resolution of 500 nanometer (nm). Using this platform, we successfully constructed 2-dimensional (2D) spatial transcriptomic maps at single cell level in mouse embryos and axolotl brain^{13,14}. Considering the complexity and smaller size of immune cells in the tumors, here we applied integrative analysis of scRNA-seq and Stereo-seq to in-depth dissect the gene regulatory programs and cell-cell interactions underlying ICB response in CRC patients. Through analysis in 25 tumor specimens from CRC patients of treatment naïve dMMR, pMMR and anti-PD1-treated dMMR patients that included responders (complete response (CR)/PR) and non-responders (stable disease, SD), we generated a CRC spatial transcriptomic atlas and uncovered a 300 micrometer (µm) boundary region (0±150 µm) that regulated immune cell influx to the tumor center region (>150 µm).

(P. 6:)
Results lane 118
 After pre-processing on the raw data generated by Stereo-seq (see Methods), the spatial transcriptome map was lassoed out and matched to the tissue edge

	<p>(https://www.stomics.tech/sap/home.html). <u>As the single-cell resolution was insufficient to generate an adequate number of genes per bin for cell type annotation and follow-up analysis in tumor tissues (Supplementary Fig. 1b), we adjusted the bin size to bin100, which allowed us to obtain a sufficient gene count for transcriptomic analysis at a resolution of 50µm (Supplementary Fig. 1b-d).</u></p> <p>(P. 21:) Discussion lane 601 <u>Secondly, the Stereo-seq technique has not reached the single-cell resolution when analyzing heterogenous and complex tumor specimens in the current study. The nanoscale resolution (capture spot diameter: 220 nm; center-to-center distance: 500 nm) of Stereo-seq merely supported an estimate of 1-10 cells in each bin in CRC tumor tissues compared to previous analysis in mouse embryos and axolotl brain^{13,14,63}. One probable explanation may be the difference on the average cell size and the complexity among different tissues. This observation indicated the limitation of our Stereo-seq platform, which may not be universally applicable, particularly in tissues enriched with small-sized immune cells, such as tumors, spleen and thymus. A more precise spatial map, if we can develop in the future, will be essential for better understanding of how to therapeutically target the spatiotemporal heterogeneity of the complex TME of CRCs, as well as other cancers. For example, enrichment of the variable regions of T and B cell receptor mRNA accompanied with the current Stereo-seq platform would present a compelling strategy for mapping the immune cells, at least T cell and B cells at single cell resolution in tumors <i>in situ</i>.</u></p>
--	---

Ref M3.3 Data interpretation of dCR patients

Reviewer Comment (i)	The interpretation of immune cell infiltration patterns in dSD versus dCR patients (line 183) appears speculative, especially in the absence of a tumor border in dCR patients. The observed patterns might simply reflect the presence of tumor cells, which inherently limits immune cell infiltration.
Author Response (i)	We thank the reviewer for pointing out this speculation. Accordingly, we have revised our description to solely focus on describing the situation in dSD patients.
Excerpt from revised manuscript (i)	(P. 8:) Result lane 208 Of note, after anti-PD1 treatment, a clearer discontinuous curve that reflected limited immune cell infiltration was noticed in dSD patients (Fig. 2d, Supplementary Fig. 4g).
Reviewer Comment (ii)	The discrepancy in the classification of responders between Figures 2 and 4 needs clarification. Why are only dPR patients considered responders in Figure 4, whereas dCR patients are also included in Figure 2?
Author Response (ii)	We apologize for the inconsistency of grouping information in Fig. 2 and Fig. 4 . We now updated our analysis in revised Fig. 4 by including data from both dPR and dCR.

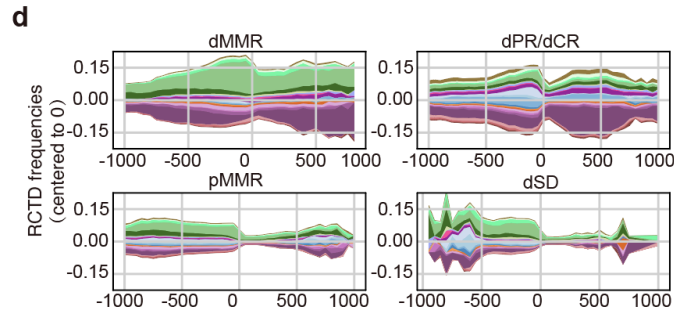


Ref 3.4 Uniform Y-axis in figure 2D

Reviewer Comment	For consistency in data presentation, Figure 2D should have a uniform Y-axis.
------------------	---

Author
Response

We apologize for the inconsistency in data presentation in **Fig. 2d**. We now have revised the Y-axis using a uniform scale bar.



Revised Fig. 2d. The stacked stream plots of immune cell distribution patterns from distal stroma (-1000 μ m, left) to tumor center (1000 μ m, right) in indicated patient groups are shown. The mean RCTD frequencies of each immune cell in each 1mm interval was smoothed using slinger model and colored by cell sub-clusters in accordance with **a**.

Reference

- 1 Kim, S. H. *et al.* What Is the Ideal Tumor Regression Grading System in Rectal Cancer Patients after Preoperative Chemoradiotherapy? *Cancer Res Treat* **48**, 998-1009, doi:10.4143/crt.2015.254 (2016).
- 2 Benson, A. B. *et al.* Rectal Cancer, Version 2.2022, NCCN Clinical Practice Guidelines in Oncology. *J Natl Compr Canc Netw* **20**, 1139-1167, doi:10.6004/jnccn.2022.0051 (2022).
- 3 Chen, G. *et al.* Neoadjuvant PD-1 blockade with sintilimab in mismatch-repair deficient, locally advanced rectal cancer: an open-label, single-centre phase 2 study. *Lancet Gastroenterol Hepatol* **8**, 422-431, doi:10.1016/S2468-1253(22)00439-3 (2023).
- 4 Eisenhauer, E. A. *et al.* New response evaluation criteria in solid tumours: revised RECIST guideline (version 1.1). *Eur J Cancer* **45**, 228-247, doi:10.1016/j.ejca.2008.10.026 (2009).
- 5 Chen, A. *et al.* Spatiotemporal transcriptomic atlas of mouse organogenesis using DNA nanoball-patterned arrays. *Cell* **185**, 1777-1792 e1721, doi:10.1016/j.cell.2022.04.003 (2022).
- 6 Wei, X. *et al.* Single-cell Stereo-seq reveals induced progenitor cells involved in axolotl brain regeneration. *Science* **377**, eabp9444, doi:10.1126/science.abp9444 (2022).
- 7 Pelka, K. *et al.* Spatially organized multicellular immune hubs in human colorectal cancer. *Cell* **184**, 4734-4752. e4720 (2021).
- 8 Wang, M. *et al.* High-resolution 3D spatiotemporal transcriptomic maps of developing *Drosophila* embryos and larvae. *Dev Cell* **57**, 1271-1283 e1274, doi:10.1016/j.devcel.2022.04.006 (2022).
- 9 McGinnis, C. S., Murrow, L. M. & Gartner, Z. J. DoubletFinder: Doublet Detection in Single-Cell RNA Sequencing Data Using Artificial Nearest Neighbors. *Cell Syst* **8**, 329-337 e324, doi:10.1016/j.cels.2019.03.003 (2019).
- 10 Xun, Z. *et al.* Reconstruction of the tumor spatial microenvironment along the malignant-boundary-nonmalignant axis. *Nat Commun* **14**, 933, doi:10.1038/s41467-023-36560-7 (2023).
- 11 Traag, V. A., Waltman, L. & van Eck, N. J. From Louvain to Leiden: guaranteeing well-connected communities. *Sci Rep* **9**, 5233, doi:10.1038/s41598-019-41695-z (2019).
- 12 Zhang, R. *et al.* Spatial transcriptome unveils a discontinuous inflammatory pattern in proficient mismatch repair colorectal adenocarcinoma. *Fundamental Research* **3**, 640-646 (2023).
- 13 Joanito, I. *et al.* Single-cell and bulk transcriptome sequencing identifies two epithelial tumor cell states and refines the consensus molecular classification of colorectal cancer. *Nat Genet* **54**, 963-975, doi:10.1038/s41588-022-01100-4 (2022).
- 14 Shen, K. *et al.* Resolving cancer-stroma interfacial signalling and interventions with micropatterned tumour-stromal assays. *Nat Commun* **5**, 5662, doi:10.1038/ncomms6662 (2014).
- 15 Verginadis, I *et al.* A stromal Integrated Stress Response activates perivascular cancer-associated fibroblasts to drive angiogenesis and tumour progression. *Nat Cell Biol* **24**, 940-953, doi:10.1038/s41556-022-00918-8 (2022).
- 16 Sahai, E. *et al.* A framework for advancing our understanding of cancer-associated fibroblasts. *Nat Rev Cancer* **20**, 174-186, doi:10.1038/s41568-019-0238-1 (2020).
- 17 Feig, C. *et al.* Targeting CXCL12 from FAP-expressing carcinoma-associated fibroblasts synergizes with anti-PD-L1 immunotherapy in pancreatic cancer. *Proc Natl Acad Sci U S A* **110**, 20212-20217, doi:10.1073/pnas.1320318110 (2013).
- 18 Li, J. *et al.* Remodeling of the immune and stromal cell compartment by PD-1 blockade in mismatch repair-deficient colorectal cancer. *Cancer Cell* **41**, 1152-1169 e1157, doi:10.1016/j.ccell.2023.04.011 (2023).

- 19 Zhang, L. *et al.* Single-cell analyses inform mechanisms of myeloid-targeted therapies in colon cancer. *Cell* **181**, 442-459. e429 (2020).
- 20 Qi, J. *et al.* Single-cell and spatial analysis reveal interaction of FAP+ fibroblasts and SPP1+ macrophages in colorectal cancer. *Nature communications* **13**, 1-20 (2022).
- 21 Cancer Genome Atlas, N. Comprehensive molecular characterization of human colon and rectal cancer. *Nature* **487**, 330-337, doi:10.1038/nature11252 (2012).
- 22 Sugiura, D. *et al.* Restriction of PD-1 function by cis-PD-L1/CD80 interactions is required for optimal T cell responses. *Science* **364**, 558-566, doi:10.1126/science.aav7062 (2019).
- 23 Zhao, Y. *et al.* PD-L1:CD80 Cis-Heterodimer Triggers the Co-stimulatory Receptor CD28 While Repressing the Inhibitory PD-1 and CTLA-4 Pathways. *Immunity* **51**, 1059-1073 e1059, doi:10.1016/j.immuni.2019.11.003 (2019).
- 24 Le, D. T. *et al.* PD-1 Blockade in Tumors with Mismatch-Repair Deficiency. *N Engl J Med* **372**, 2509-2520, doi:10.1056/NEJMoa1500596 (2015).
- 25 Emiloju, O. E. & Sinicrope, F. A. Neoadjuvant Immune Checkpoint Inhibitor Therapy for Localized Deficient Mismatch Repair Colorectal Cancer: A Review. *JAMA Oncol* **9**, 1708-1715, doi:10.1001/jamaoncol.2023.3323 (2023).
- 26 Chalabi, M. *et al.* Neoadjuvant immunotherapy leads to pathological responses in MMR-proficient and MMR-deficient early-stage colon cancers. *Nat Med* **26**, 566-576, doi:10.1038/s41591-020-0805-8 (2020).
- 27 Ye, S. B. *et al.* Association of mismatch repair status with survival and response to neoadjuvant chemo(radio)therapy in rectal cancer. *NPJ Precis Oncol* **4**, 26, doi:10.1038/s41698-020-00132-5 (2020).
- 28 Andrews, T. S. *et al.* Single-Cell, Single-Nucleus, and Spatial RNA Sequencing of the Human Liver Identifies Cholangiocyte and Mesenchymal Heterogeneity. *Hepatol Commun* **6**, 821-840, doi:10.1002/hep4.1854 (2022).
- 29 Chen, A. *et al.* Single-cell spatial transcriptome reveals cell-type organization in the macaque cortex. *Cell*, doi:10.1016/j.cell.2023.06.009 (2023).

Reviewers' comments:

Reviewer #1 (Remarks to the Author):

In the revised manuscript the authors addressed all concerns raised and added additional data and changed the manuscript accordingly that I have no concerns for publishing the manuscript in NCOMMS

Reviewer #2 (Remarks to the Author):

The authors addressed most comments but some still remain.

The comments of the authors explaining why they were not able to use their spatial sequencing at the maximum resolution are convincing in the result and discussion sections. The introduction section should nevertheless make clear that the high resolution which was previously achieved by this technique does not apply to this study. Line 88 states for example that a higher resolution than 50 μm is required suggesting that the proposed technique will lead to this goal in the current study (which is not the case). It is not obvious for a reader to conclude that the authors will fallback to a reduced resolution from the updated lines 94-95 introducing the scRNA-Seq integration in particular as they state earlier that a higher resolution is a prerequisite. As a consequence, the authors should still rephrase this part of the section to avoid the feeling of overselling their technique in the context of this study.

In supplementary figure 3, the color scale bars updated by the authors indeed help to further interpret the shown intensities. However, it still shows and underlines an apparent discrepancy between the heatmap and the UMAP plot. For instance, Epithelial cells appear as an intermediate mean expression (~ 2.5) while the UMAP suggests a very strong EPCAM expression for the whole cluster ($\sim 5-6$). Similarly, Plasma cells appear as highly expressing JCHAIN on the heatmap (average of ~ 5) while the UMAP plot suggests a much lower expression (< 4). Could the authors check again for this? Could it be related to an overlaying issue on the UMAP plot? (darker/lighter dots hiding underlying dots). If this is the case using a hexbin or nebulosa density plot for the UMAP representation might improve the rendering.

In the sup fig 6 + FIGURE 6 the legend MSI-low patients are reported as patients with a MSI score ≥ 10 while it is likely a score < 4 . The handling of the TCGA data is still missing in the material and method section (origin of the processed data including the clinical data). I suppose that the MSI score refers to the MANTIS score which should be clearly stated including the origin of the score (obtained from elsewhere + reference or computed yourself).

Reviewer #3 (Remarks to the Author):

I thank the authors for their efforts in addressing my comments. However, I still have a major conceptual reservation regarding this paper. The authors state at the beginning of the abstract:

“Colorectal cancer (CRC) patients with mismatch repair (MMR)-deficient (dMMR) but not MMR-proficient (pMMR) tend to benefit from immune checkpoint blockade (ICB) therapy. To uncover the rules governing these varied therapeutic responses, we integrated spatial enhanced resolution omics-sequencing (Stereo-seq), single-cell RNA sequencing, and multiplexed imaging analysis to create high-definition spatial maps of tumors from treatment-naïve and ICB-treated CRC patients.”

The difference between MMR-p and MMR-d in terms of response to ICB is already well known in the field: MMR-d respond because of the heightened mutation burden and, in particular, the presence of frameshift mutations. What the field wants to know are the determinants of response within MMR-d cancers in the advanced setting and the determinants of response within MMR-p cancers in the primary setting (about one-third of patients respond to neoadjuvant ICB). Furthermore, what are the differences in response rates between the primary and metastatic settings? None of these questions are addressed by the present manuscript.

The manuscript frequently relies on comparing MMR-d and MMR-p in the context of ICB response, but this comparison is fundamentally flawed. Additionally, the authors often overinterpret their observations to extract biological significance where there is none. For example:

“Interestingly, dMMR patients who experienced lower clinical benefit towards anti-PD1 therapy, i.e., dSD, displayed a well-organized tumor-stroma boundary structure similar to pMMR, commonly recognized as an ICB insensitive group (Fig. 1d). Moreover, dCR patients displayed significantly lower proportions of tumor-stroma boundary and proliferative tumor clusters (tumor_MIK67) compared to dSD (Fig. 1c).”

This conclusion is problematic because, obviously, there are fewer tumor cells in cases of complete response (CR), resulting in a less defined tumor-stroma boundary.

Thank you for considering these concerns.

Point-to-point response letter to NCOMMS-23-41464B

Reviewer #1:

In the revised manuscript the authors addressed all concerns raised and added additional data and changed the manuscript accordingly that I have no concerns for publishing the manuscript in NCOMMS.

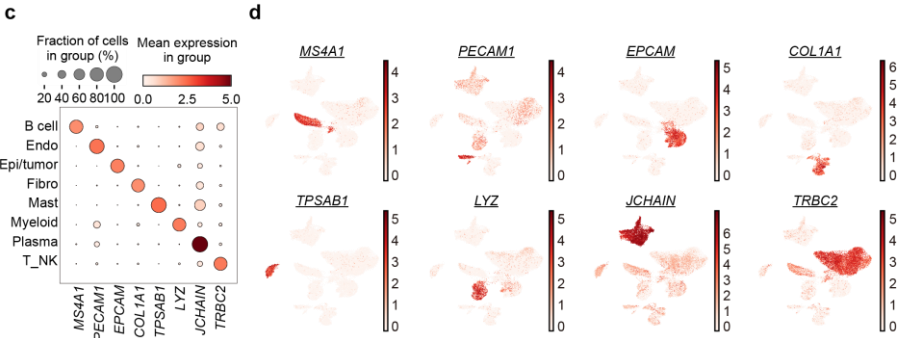
Author response: We are grateful for the time and the compliments provided by the reviewer.

Reviewer #2:

Ref 2.1 Clarification of spatial resolution of the stereo-seq platform

Reviewer comments	The comments of the authors explaining why they were not able to use their spatial sequencing at the maximum resolution are convincing in the result and discussion sections. The introduction section should nevertheless make clear that the high resolution which was previously achieved by this technique does not apply to this study. Line 88 states for example that a higher resolution than 50 μm is required suggesting that the proposed technique will lead to this goal in the current study (which is not the case). It is not obvious for a reader to conclude that the authors will fall back to a reduced resolution from the updated lines 94-95 introducing the scRNA-Seq integration in particular as they state earlier that a higher resolution is a prerequisite. As a consequence, the authors should still rephrase this part of the section to avoid the feeling of overselling their technique in the context of this study.
Author response	We acknowledge the issue of spatial resolution used in this study raised by the reviewer. We amended our statement accordingly to avoid the feeling of overselling our technique as followed.
Excerpt from revised manuscript	(P. 4:) Introduction lane 83 Several high throughput spatial transcriptomic technologies are therefore developed to dissect the detailed information of molecular and cellular features in tissues in situ, including commercialized Visium by 10X Genomics, CosMx SMI and DBiT-seq ¹² , <u>as well as the spatial enhanced resolution omics-sequencing (Stereo-seq) developed by us^{13,14}. The stereo-seq provides customized resolution by binning neighboring nanoballs as a minimal spot for further analysis, e.g., at anatomical level with square bins or at single cell level with cell bins^{13,14}. However, the resolution is often compromised by the tissue nature in practice, because smaller spots contain fewer detected transcripts. Considering the smaller size of immune cells and their physical overlay on the stromal cells in the tumors, here we applied an integrative analysis of scRNA-seq and Stereo-seq at 50μm resolution to in-depth dissect the gene regulatory programs and cell-cell interactions underlying ICB response in CRC patients.</u>

Ref 2.2 Discrepancy in the scale bars of UMAP plot and the dot plot.

<p>Reviewer comments (i)</p>	<p>In supplementary figure 3, the color scale bars updated by the authors indeed help to further interpret the shown intensities. However, it still shows and underlines an apparent discrepancy between the heatmap and the UMAP plot. For instance, Epithelial cells appear as an intermediate mean expression (~2.5) while the UMAP suggests a very strong EPCAM expression for the whole cluster (~5-6). Similarly, Plasma cell appear as highly expressing JCHAIN on the heatmap (average of ~5) while the UMAP plot suggests a much lower expression (<4). Could the authors check again for this? Could it be related to an overlaying issue on the UMAP plot? (darker/lighter dots hiding underlying dots). If this is the case using a hexbin or nebulosa density plot for the UMAP representation might improve the rendering.</p>
<p>Author response (i)</p>	<p>We thank the reviewer for pointing out the inconsistent bar in supplementary figure 3d. We double checked the expression level in our source code and found that the incorrect information was actually delivered by the misposition of the gene symbols when editing the font. We apologize for the misleading information and correct it accordingly.</p>  <p>Revised Supplementary Figure 3c-d. c Bubble plots of marker gene expressions in major cell clusters from the scRNA-seq dataset are shown. The plots are sized by the fraction of cells with positive gene expression, while the color represents the gene expression level. d Expression level of canonical marker genes for each major cell cluster is shown in UMAP.</p>
<p>Reviewer comments (ii)</p>	<p>In the sup fig 6 + FIGURE 6 the legend MSI-low patients are reported as patients with a MSI score ≥ 10 while it is likely a score < 4. The handling of the TCGA data is still missing in the material and method section (origin of the processed data including the clinical data). I suppose that the MSI score refers to the MANTIS score which should be clearly stated including the origin of the score (obtained from elsewhere + reference or computed yourself).</p>
<p>Author response (ii)</p>	<p>We agree with the reviewer that more detailed information about the handling of the TCGA data needs to be included. First, instead of the MANTIS score mentioned by the reviewer, we used the MSI sensor score method¹. The performance of MSI sensor score is very similar with MANTIS score in evaluating MSI level using the TCGA data (Fig R1). The TCGA data, including</p>

the Z-scored gene expression matrix and the clinical information (with MSI sensor and MANTIS score), was directly downloaded from cBioPortal (https://www.cbioportal.org/study/summary?id=coadread_tcga_pan_can_atlas_2018). Since we did not generate inhouse code for MSI evaluation, we add this information to **Data and code availability** part as stated below.

Fig R1

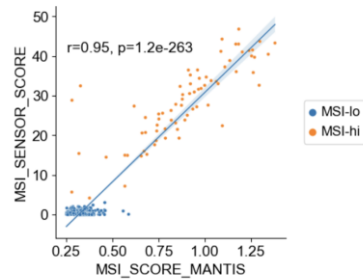


Fig R1. The correlation of MSI sensor score and MSI MANTIS score in the TCGA cohort (MSI score \geq 10, n = 78; MSI score $<$ 4 n = 494, r=0.95, p=1.2e⁻²⁶³).

Excerpt from revised manuscript

(P. 26:)

Methods lane 798

Data and code availability

The raw sequencing FASTQ files could be accessed on Genome Sequence Archive (accession number: PRJCA020107, <https://ngdc.cncb.ac.cn/gsa-human/browse/HRA005647>), complying with the Chinese laws. The processed h5ad files of Stereo-seq and scRNAseq was deposited on STOmicsDB64 of China National GenBank Database (accession number: STT0000036, <https://db.cngb.org/stomics/project/STT0000036>). The external TCGA with Z-scored gene expression matrix and the MSI scores could be downloaded through https://www.cbioportal.org/study/summary?id=coadread_tcga_pan_can_atlas_2018. All codes for data analysis and plotting are available upon request. Please contact the lead author: Rongxin Zhang (zhangrx@sysucc.org.cn.)

(P. 17:)

Result lane 468

Moreover, the expressions of *MMP11*, *IHH*, *PTCH1* and *CXCL14* were significantly higher in MSI-lo tumors (MSI sensor scores \leq 4) compared to MSI-hi ones (MSI sensor score \geq 10) from the COAD TCGA dataset (n=572), which were also positively correlated (**Fig. 6f-g**).

(P. 39:)

Figure legend lane 1170

Patients are stratified to MSI-hi (MSI sensor score \geq 10, n = 78) and MSI-lo (MSI sensor score \geq 10, n = 494)

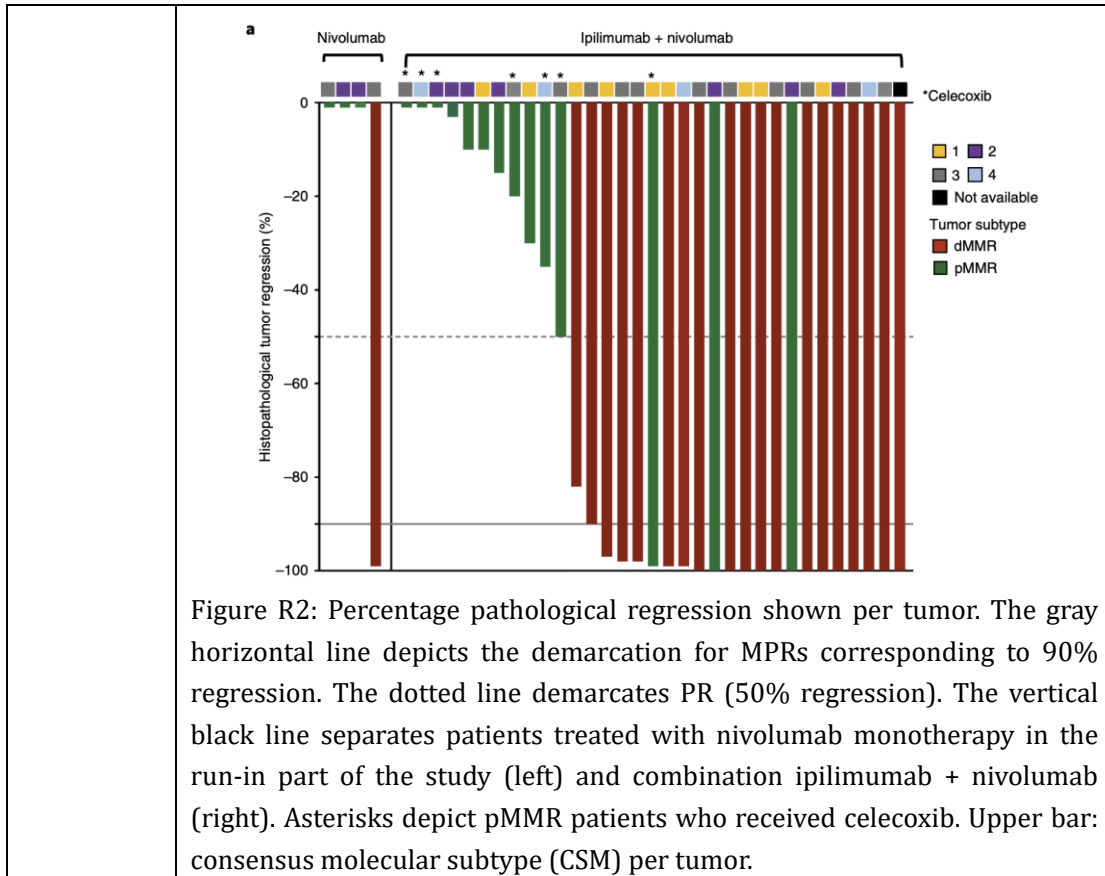
Reviewer #3:

Ref 3.1 Major conceptual reservation on the findings of this study.

Reviewer comments	<p>I thank the authors for their efforts in addressing my comments. However, I still have a major conceptual reservation regarding this paper. The authors state at the beginning of the abstract:</p> <p>“Colorectal cancer (CRC) patients with mismatch repair (MMR)-deficient (dMMR) but not MMR-proficient (pMMR) tend to benefit from immune checkpoint blockade (ICB) therapy. To uncover the rules governing these varied therapeutic responses, we integrated spatial enhanced resolution omics-sequencing (Stereo-seq), single-cell RNA sequencing, and multiplexed imaging analysis to create high-definition spatial maps of tumors from treatment-naïve and ICB-treated CRC patients.”</p> <p>The difference between MMR-p and MMR-d in terms of response to ICB is already well known in the field: MMR-d respond because of the heightened mutation burden and, in particular, the presence of frameshift mutations. What the field wants to know are the determinants of response within MMR-d cancers in the advanced setting and the determinants of response within MMR-p cancers in the primary setting (about one-third of patients respond to neoadjuvant ICB). Furthermore, what are the differences in response rates between the primary and metastatic settings? None of these questions are addressed by the present manuscript.</p>
Author response	<p>We thank the reviewer for pointing out the attractive questions beyond this study. However, we believe our study is equivalently important to both clinical practitioners and fundamental science researchers.</p> <p>First of all, the reviewer pointed out that “The difference between MMR-p and MMR-d in terms of response to ICB is already well known in the field: MMR-d respond because of the heightened mutation burden and, in particular, the presence of frameshift mutations. According to the clinical data as we mentioned in the introduction, MMR status is indeed one of the biomarkers used clinically for patient stratification on ICB treatment. Nevertheless, studies using scRNA-seq analysis have revealed that the immune and stromal features of the tumor microenvironment also significantly contribute to variable ICB response across CRC patient populations ^{2,3}. Specifically, a publication by Qi J et al demonstrated that the accumulation of FAP1+fibroblast and SPP1+macrophages in tumor-stroma boundary correlated with poorer ICB response, even in CRC patients with substantially higher non-silent mutation rates ³. These findings underscore the importance of characterizing the spatial organization and cellular interactions within the CRC tumor microenvironment to understand and potentially overcome therapeutic resistance. To this end, we have generated high-definition spatial maps of the immune, stromal, and malignant cell networks in tumors from</p>

treatment-naïve dMMR and pMMR CRC patients. We believe these data provide critical insights to demonstrate a path to advancing treatment in pMMR patients.

Secondly, we agree with the reviewer that elucidating the determinants of response within MMR-d cancers in the advanced setting, and in MMR-p in the primary setting, or across primary and metastatic settings of CRC, represents an important and unsolved research question in the field. Nevertheless, the clinical context of our current investigation was the neoadjuvant monotherapy with ICB in early-stage primary CRC patients (Table S1), as per the approved human ethics protocol. We also have interests in continuing to study the immune features of tumors from MMR-d in the advanced setting or across primary and metastatic settings, building upon the insights gained from our current study. Regarding MMR-p CRC patients in the primary setting, the reviewer mentioned that approximately one-third of MMR-p patients exhibit a favorable response to neoadjuvant ICB. Unfortunately, this observation does not align with the broader literature on ICB efficacy in pMMR CRC. Studies have consistently demonstrated limited efficacy of ICB monotherapy in pMMR cases, with a 0% response rate to anti-PD1 monotherapy and up to 27% PR/SD rate reported in early-stage patients to combinatory approaches (e.g. anti-PD1 plus anti-CTLA4) ^{4,5}. We adopted the graph published by Myriam C et al (Fig. R2), which clearly showed low response to ICB monotherapy (Nivolumab) in pMMR CRC patients. In addition, as pMMR CRC patients have been shown to respond more favorably to neoadjuvant chemoradiotherapy⁶, we mainly used neoadjuvant chemoradiotherapy for pMMR CRC patients according to the clinical guidelines. Consequently, we were unable to obtain tissue samples from anti-PD1-treated pMMR CRC patients. Moving forward, we are eager to investigate the immune features of tumors in pMMR CRC patients in the context of combination immunotherapies, should such opportunities arise.



Ref 3.2 Fundamentally flawed comparison of MMR-d and MMR-p in the context of ICB response.

Reviewer comments	The manuscript frequently relies on comparing MMR-d and MMR-p in the context of ICB response, but this comparison is fundamentally flawed.
Author response	The reviewer expressed concern regarding the comparison between MMR-d and MMR-p CRCs in the context of ICB response. However, we respectively disagree with the reviewer's comment that "this comparison is fundamentally flawed". We have further clarified the separate analyses by comparing the differences between treatment-naïve dMMR and pMMR CRCs, as well as between anti-PD1-treated dMMR responders and non-responders, in the revised manuscript. We identified that the spatial organization and immune status of the tumor-stroma boundary were distinct in tumors from treatment-naïve dMMR and pMMR CRCs. Additionally, we observed that dSD, the non-responders in the anti-PD1-treated dMMR patient group, also displayed a well-organized tumor-stroma boundary structure (Fig. 1d). Considering the clinical observation that most pMMR CRCs exhibit a lower response to anti-PD1 monotherapy, we speculated that the spatial organization and immune status of the tumor-stroma boundary in pMMR CRCs may be one of the reasons for their reduced responsiveness, and this could be further studied to identify therapeutic targets for overcoming ICB resistance in the majority of pMMR CRCs. Therefore, we believe that these two-step comparisons could provide insights into the importance of the

	tumor-stromal boundary structure in ICB response in CRC, and we cannot agree with the reviewer's comment that "this comparison is fundamentally flawed".
--	--

Ref 3.3 Less defined tumor-stroma boundary

Reviewer comments	<p>Additionally, the authors often overinterpret their observations to extract biological significance where there is none. For example:</p> <p>“Interestingly, dMMR patients who experienced lower clinical benefit towards anti-PD1 therapy, i.e., dSD, displayed a well-organized tumor-stroma boundary structure similar to pMMR, commonly recognized as an ICB insensitive group (Fig. 1d). Moreover, dCR patients displayed significantly lower proportions of tumor-stroma boundary and proliferative tumor clusters (tumor_MIK67) compared to dSD (Fig. 1c).”</p> <p>This conclusion is problematic because, obviously, there are fewer tumor cells in cases of complete response (CR), resulting in a less defined tumor-stroma boundary.</p>
Author response	<p>We acknowledge the reviewer’s concern about the definition of tumor-stroma boundary. We therefore make further clarification on the definition of the tumor-stromal boundary.</p> <p>First of all, the tumor-stroma physically surrounded the epi/tumor spatial cluster in the spatial transcriptomic map (Fig 1e, absolute distance =0 μm). Therefore, the shrinkage of the tumor volume in cases of CR shall be surrounded by decreased surface, which is exactly the tumor-stroma boundary. In this regard, the statement quoted by the reviewer shall support the definition of tumor-stroma boundary, instead of undermining it.</p> <p>Secondly, the CRC tumors bear frameshift mutations as mentioned by the reviewer. We thus assessed the copy number variation (CNV) score in the spatial transcriptomic data ^{7,8} (https://github.com/broadinstitute/infercnv). As a result, we found the boundary defined by us (distance=0) separated the stroma and tumors as regions with low CNV scores and high CNV scores (Fig. S2b). In addition, the epi/tumor region exhibited significantly elevated CNV alterations over other 4 spatial clusters (Fig. S2b-c), which further supported that the tumor-stroma boundary defined by us was physically located at the tumor border.</p> <p>Thirdly, the tumor-stroma boundary is commonly recognized as a niche composed of malignant cells in the outermost circle of solid tumor and non-malignant cells that are closely adjacent in spatial architecture, bridging these distinct spatial regions⁹. To further clarify the definition of tumor-stroma boundary, we added the analysis of the tumor-stroma interface-</p>

associated gene expression curves based on the publication from Shen et al.¹⁰. Using the 11 pertinent genes identified in the tumor-stroma interface in breast cancer, our data consistently showed that 8 out of 11 genes (MKI67, PTEN, FOXC1, MMP11, RRP2, INHBA, TWIST1, GREM1) were significantly enriched at the boundary region (**new Supplementary Fig. 2d**), further supporting that our boundary definition is robust.

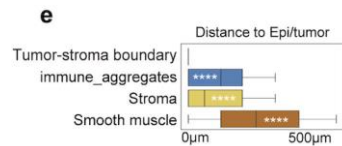


Figure 1e. The average distance from epi/tumor cluster to the clusters of tumor-stroma boundary, immune aggregates, stroma and smooth muscle. Data are represented as mean±SD and analyzed by Unpaired Student-t test. ns, not significant; *, p<0.05; **, p<0.01.

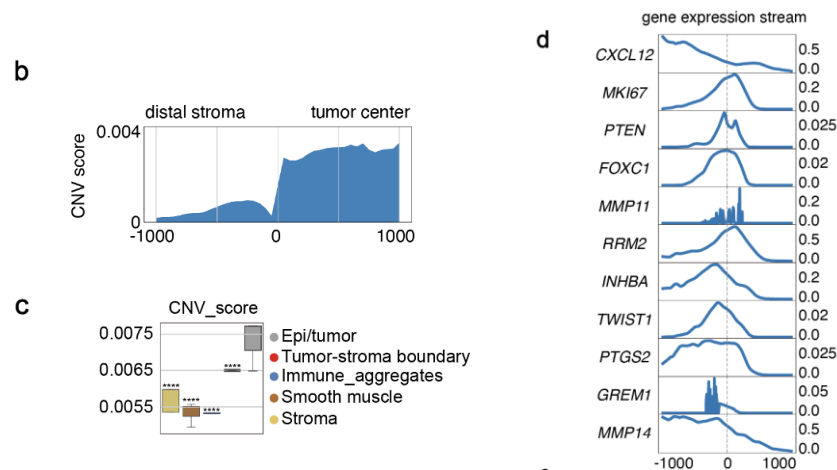


Fig. S2b-c. **b** The stacked stream plot of the CNV scores from the distal stroma (-1000µm, left) to the tumor center (1000µm, right) is shown. The mean CNV score in each 1mm interval is smoothed using slinger model. The distance of boundary was set to 0µm. **c** The box plots of the CNV scores in each major spatial cluster are shown. The asterisk represents the comparison of the epi/tumor clusters towards other spatial clusters. Data are represented as mean±SD and analyzed by unpaired Student-t test. ****, p<0.0001. **d** The stacked stream plots of the indicated gene expressions from the distal stroma (-1000µm, left) to the tumor center (1000µm, right) are shown. The mean expression level in each 1mm interval is smoothed using slinger model. The distance of boundary was set to 0µm.

Reference

- 1 Niu, B. *et al.* MSIsensor: microsatellite instability detection using paired tumor-normal sequence data. *Bioinformatics* **30**, 1015-1016, doi:10.1093/bioinformatics/btt755 (2014).
- 2 Pelka, K. *et al.* Spatially organized multicellular immune hubs in human colorectal cancer. *Cell* **184**, 4734-4752. e4720 (2021).
- 3 Qi, J. *et al.* Single-cell and spatial analysis reveal interaction of FAP+ fibroblasts and SPP1+ macrophages in colorectal cancer. *Nature communications* **13**, 1-20 (2022).
- 4 Le, D. T. *et al.* PD-1 Blockade in Tumors with Mismatch-Repair Deficiency. *N Engl J Med* **372**, 2509-2520, doi:10.1056/NEJMoa1500596 (2015).
- 5 Chalabi, M. *et al.* Neoadjuvant immunotherapy leads to pathological responses in MMR-proficient and MMR-deficient early-stage colon cancers. *Nat Med* **26**, 566-576, doi:10.1038/s41591-020-0805-8 (2020).
- 6 Ye, S. B. *et al.* Association of mismatch repair status with survival and response to neoadjuvant chemo(radio)therapy in rectal cancer. *NPJ Precis Oncol* **4**, 26, doi:10.1038/s41698-020-00132-5 (2020).
- 7 Zhang, R. *et al.* Spatial transcriptome unveils a discontinuous inflammatory pattern in proficient mismatch repair colorectal adenocarcinoma. *Fundamental Research* **3**, 640-646 (2023).
- 8 Joanito, I. *et al.* Single-cell and bulk transcriptome sequencing identifies two epithelial tumor cell states and refines the consensus molecular classification of colorectal cancer. *Nat Genet* **54**, 963-975, doi:10.1038/s41588-022-01100-4 (2022).
- 9 Xun, Z. *et al.* Reconstruction of the tumor spatial microenvironment along the malignant-boundary-nonmalignant axis. *Nat Commun* **14**, 933, doi:10.1038/s41467-023-36560-7 (2023).
- 10 Shen, K. *et al.* Resolving cancer-stroma interfacial signalling and interventions with micropatterned tumour-stromal assays. *Nat Commun* **5**, 5662, doi:10.1038/ncomms6662 (2014).

REVIEWERS' COMMENTS

Reviewer #2 (Remarks to the Author):

Dear authors

Thanks for addressing my comments.

Could you please look whether the numbers are correct here?

Figure legend line 1170

MSI-hi ≥ 10 and MSI-lo ≥ 10 , should this not be ≤ 4

Reviewer #3 (Remarks to the Author):

Dear Authors,

I appreciate your efforts to address my criticism. Unfortunately, I still disagree with your interpretation of the data, particularly its clinical significance. The substantial biological differences between MMR-d and MMR-p tumors seem to be used to find correlates of response to checkpoint blockade therapy, which I believe is not a valid comparison. In my opinion, this study would only be clinically relevant if it explores factors associated with response specifically within MMR-d or MMR-p cancers.

Specific comments regarding your rebuttal:

1. "First of all, the reviewer pointed out that 'The difference between MMR-p and MMR-d in terms of response to ICB is already well known in the field: MMR-d respond because of the heightened mutation burden and, in particular, the presence of frameshift mutations. According to the clinical data as we mentioned in the introduction, MMR status is indeed one of the biomarkers used clinically for patient stratification on ICB treatment. Nevertheless, studies using scRNA-seq analysis have revealed that the immune and stromal features of the tumor microenvironment also significantly contribute to variable ICB response across CRC patient populations 2,3."

R: References 2 and 3 do not include samples that have been treated with immunotherapy. Therefore, the statement that immune and stromal features contribute to variable ICB response across CRC patient populations is not supported by those references. Even if this statement were true, these features would need to be investigated specifically within MMR-d or MMR-p sample groups due to their significant biological differences. Thus, the conceptual issue remains unresolved.

2. "Regarding MMR-p CRC patients in the primary setting, the reviewer mentioned that approximately one-third of MMR-p patients exhibit a favorable response to neoadjuvant ICB. Unfortunately, this observation does not align with the broader literature on ICB efficacy in pMMR CRC"

R: I was indeed referring to the study by Chalabi et al., where approximately one-third of MMR-p patients respond to ICB in the neoadjuvant setting. To my knowledge, this is the only study that included a significant number of patients with early-stage MMR-p colon cancers, so I do not understand the authors' objection to my statement. This study also perfectly highlights the conceptual issue I have with this manuscript. The NICHE trial demonstrates nearly 100% responses in MMR-d cases and 27% responses in MMR-p. The scientific question to be addressed here is the comparison between responders and non-responders in the MMR-p tumors, not the differences between MMR-p and MMR-d.

3. "We identified that the spatial organization and immune status of the tumor-stroma boundary were distinct in tumors from treatment-naïve dMMR and pMMR CRCs. Additionally, we observed that dSD, the non-responders in the anti-PD1-treated dMMR patient group, also displayed a well-organized tumor-stroma boundary structure (Fig. 1d)."

"First of all, the tumor-stroma physically surrounded the epi/tumor spatial cluster in the spatial transcriptomic map (Fig 1e, absolute distance =0 μm). Therefore, the shrinkage of the tumor volume in cases of CR shall be surrounded by decreased surface, which is exactly the tumor-stroma boundary. In this regard, the statement quoted by the reviewer shall support the definition of tumor-stroma boundary, instead of undermining it."

R: I do not understand the authors' response. My argument is that the tumor-stromal boundary cannot be accurately evaluated in the post-therapy setting because complete responders will have no boundary or a diminished one, which will obviously differentiate responders from non-responders. The statement that the tumor-stromal boundary impacts response could only be proven in pre-treatment samples.

Point-to-point response letter to NCOMMS-23-41464Z

Reviewer #2:

Ref 2.1 Wrong numbers in the figure legend

Reviewer comments	Thanks for addressing my comments. Could you please look whether the numbers are correct here? Figure legend lane 1170 MSI-hi ≥ 10 and MSI-lo ≥ 10 , should this not be ≤ 4
Author response	We are grateful for the reviewer for pointing out our typo and we have amended it accordingly
Excerpt from revised manuscript	Figure legend lane 1173 Patients are stratified to MSI-hi (MSI sensor score ≥ 10 , n = 78) and MSI-lo (MSI sensor score ≤ 4 , n = 494) accordingly.

Reviewer #3:

Ref 3.1 Misleading reference insertion and conceptual issue.

Reviewer comments	<p>1. "First of all, the reviewer pointed out that "The difference between MMR-p and MMR-d in terms of response to ICB is already well known in the field: MMR-d respond because of the heightened mutation burden and, in particular, the presence of frameshift mutations. According to the clinical data as we mentioned in the introduction, MMR status is indeed one of the biomarkers used clinically for patient stratification on ICB treatment. Nevertheless, studies using scRNA-seq analysis have revealed that the immune and stromal features of the tumor microenvironment also significantly contribute to variable ICB response across CRC patient populations 2,3."</p> <p>R: References 2 and 3 do not include samples that have been treated with immunotherapy. Therefore, the statement that immune and stromal features contribute to variable ICB response across CRC patient populations is not supported by those references. Even if this statement were true, these features would need to be investigated specifically within MMR-d or MMR-p sample groups due to their significant biological differences. Thus, the conceptual issue remains unresolved.</p>
Author response	<p>We thank the reviewer for the comments and agree with the reviewer that the comparison within MMR-d or MMR-p groups under ICB treatment is one of the key questions remaining to be further investigated in the field.</p> <p>We apologize for mislabeling the reference in our last rebuttal letter as mentioned by the reviewer. The reference 2¹ shall be replaced by the paper published in Cancer Cell². In this study, 19 patients with MMR-d CRC who</p>

	<p>received neoadjuvant PD-1 blockade were included for scRNAseq analysis. The data showed that the abundance and dynamics of immune and stromal cells, like CD4+ Th and CXCL12+CAF correlated with ICB efficacy. In parallel, although the study that we mentioned by Qi J et al ³ only included in house sequencing data from treatment naïve CRC patients, they used online available dataset from CRC and urothelial carcinoma patients with ICB treatment (UC, IMvigor210 cohort) to validate the importance of FAP+ fibroblasts and SPP1+ macrophages in ICB response. Their analysis suggested that the tumors enriched with FAP+ fibroblasts and SPP1+ macrophages was immune-exclusive and thus less sensitive to immunotherapy, even though the CRC tumor with FAP+ fibroblasts and SPP1+ macrophages exhibited a relatively high rate of non-silent mutations and single-nucleotide variant (SNV)-predicted neoantigens. Therefore, these studies strengthened an important opinion that the immune features of the tumor microenvironment and mutation burden are both important in determining the ICB response. Furthermore, we notice that this phenomenon could also be extended to other cancers, like HCC, melanoma, NSCLC ^{4,5}.</p>
--	---

Ref 3.2 Discrepancy in interpreting the NICHE trial data.

<p>Reviewer comments (i)</p>	<p>2. "Regarding MMR-p CRC patients in the primary setting, the reviewer mentioned that approximately one-third of MMR-p patients exhibit a favorable response to neoadjuvant ICB. Unfortunately, this observation does not align with the broader literature on ICB efficacy in pMMR CRC"</p> <p>R: I was indeed referring to the study by Chalabi et al., where approximately one-third of MMR-p patients respond to ICB in the neoadjuvant setting. To my knowledge, this is the only study that included a significant number of patients with early-stage MMR-p colon cancers, so I do not understand the authors' objection to my statement. This study also perfectly highlights the conceptual issue I have with this manuscript. The NICHE trial demonstrates nearly 100% responses in MMR-d cases and 27% responses in MMR-p. The scientific question to be addressed here is the comparison between responders and non-responders in the MMR-p tumors, not the differences between MMR-p and MMR-d.</p>
<p>Author response (i)</p>	<p>We apologize for the confusion in the data description. As mentioned by the reviewer, the NICHE trial data reported by Chalabi et al., indeed included a significant number of patients with early-stage MMR-p colon cancers under immunotherapy treatment. As shown in Fig.R1 below, the NICHE trial data demonstrated nearly 100% responses in MMR-d cases and 27% responses in MMR-p under the treatment by combinatory anti-PD1 plus anti-CTLA4 treatment (i.e. Ipilimumab+nivolumab, Fig. R1 on the right) in the neoadjuvant setting. In comparison, the CRC patients recruited in our study only received monotherapy, i.e. anti-PD1 treatment. The responding rate of MMR-p under monotherapy, as shown in the NICHE trial in Fig. R1 (i.e. the</p>

nivolumab treatment group on the left), is very limited, which aligns with the broader literature on ICB efficacy in pMMR CRC under ICB monotherapy.

We agree with the reviewer that the comparison between ICB responders and non-responders in MMR-p tumors is important to investigate in the field. We also value the message delivered by the NICHE trial that some pMMR CRCs may potentially respond to combinatory immunotherapies in the neoadjuvant setting, which makes similar analyses in pMMR responders and non-responders, like our current experimental setting, possible. In parallel, the NICHE trial first pinpointed the discrepant immunotherapeutic efficacy in dMMR and pMMR CRC patients, which initiated follow-up studies to understand the immune features and molecular mechanisms underlying their potential differences. As one of the follow-up studies, our data further pointed out the importance of the spatial organization and immune status of the tumor-stroma boundary in dMMR and pMMR CRC patients, which may at least partially contribute to their difference in ICB responsiveness. Follow-up studies on analyzing the spatial features of tumor microenvironment in MMR-p CRC patients under combinatory immunotherapy treatment would be necessary to consolidate our speculation.

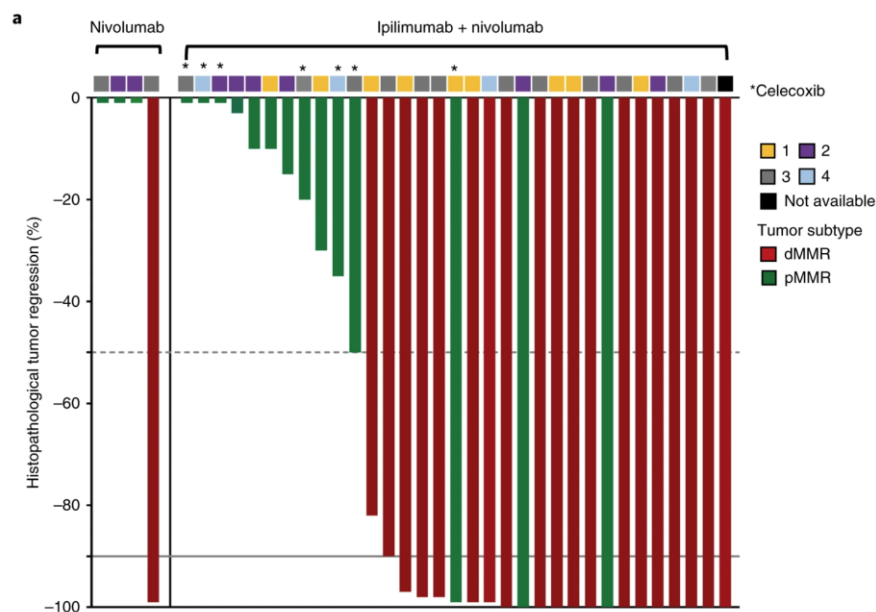


Fig. R1. Percentage pathological regression shown per tumor. The gray horizontal line depicts the demarcation for MPRs corresponding to 90% regression. The dotted line demarcates PR (50% regression). The vertical black line separates patients treated with nivolumab monotherapy in the run-in part of the study (left) and combination ipilimumab + nivolumab (right). Asterisks depict pMMR patients who received celecoxib. Upper bar: CMS subtyping per tumor. Adopted from Chalabi et al., 2020 ⁶.

Reviewer comments	<p>3. “We identified that the spatial organization and immune status of the tumor-stroma boundary were distinct in tumors from treatment-naïve dMMR and pMMR CRCs. Additionally, we observed that dSD, the non-responders in the anti-PD1-treated dMMR patient group, also displayed a well-organized tumor-stroma boundary structure (Fig. 1d).”</p> <p>“First of all, the tumor-stroma physically surrounded the epi/tumor spatial cluster in the spatial transcriptomic map (Fig 1e, absolute distance =0 μm). Therefore, the shrinkage of the tumor volume in cases of CR shall be surrounded by decreased surface, which is exactly the tumor-stroma boundary. In this regard, the statement quoted by the reviewer shall support the definition of tumor-stroma boundary, instead of undermining it.”</p> <p>R: I do not understand the authors' response. My argument is that the tumor-stromal boundary cannot be accurately evaluated in the post-therapy setting because complete responders will have no boundary or a diminished one, which will obviously differentiate responders from non-responders. The statement that the tumor-stromal boundary impacts response could only be proven in pre-treatment samples.</p>										
Author response	<p>We acknowledge the reviewer’s concern about the definition of tumor-stroma boundary. As shown in figure 1c, the reviewer’s concern that “complete responders will have no boundary or a diminished one” may be partially supported. Nevertheless, the clinical definition of CR needs to be supported by H&E staining in tissues together with follow-up CT scan and Colonoscopy as we provided in supplementary table 1. Therefore, we can still identify the boundary spots from the spatial transcriptomics data from dCR specimens, although the proportion was lower compared to dSD. As shown below about the number of boundary spots (bin50, 25 μm x25 μm) in each group, the numbers in dCR were still enough for comparison analysis.</p> <table data-bbox="424 1406 638 1592"> <tr> <td>pMMR</td> <td>11324</td> </tr> <tr> <td>dMMR</td> <td>2635</td> </tr> <tr> <td>dNR</td> <td>2244</td> </tr> <tr> <td>dPR</td> <td>765</td> </tr> <tr> <td>dCR</td> <td>671</td> </tr> </table>	pMMR	11324	dMMR	2635	dNR	2244	dPR	765	dCR	671
pMMR	11324										
dMMR	2635										
dNR	2244										
dPR	765										
dCR	671										

In addition, as mentioned by the reviewer, the comparison between pre- and post-treatment samples in patients under ICB treatment would be perfect for analyzing the importance and dynamic changes of the tumor-stromal boundary, which is quite difficult due to ethics and clinical issues.

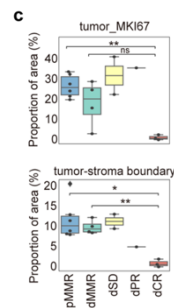


Figure 1c Proportions of spatial clusters tumor_MKI67 and tumor-stroma boundary in indicated patient groups. The smooth muscle is not included to remove sampling bias. Data are represented as mean±SD and analyzed by Unpaired Student-t test. ns, not significant; *, p<0.05; **, p<0.01.

Reference

- 1 Pelka, K. *et al.* Spatially organized multicellular immune hubs in human colorectal cancer. *Cell* **184**, 4734–4752. e4720 (2021).
- 2 Li, J. *et al.* Remodeling of the immune and stromal cell compartment by PD-1 blockade in mismatch repair-deficient colorectal cancer. *Cancer Cell* **41**, 1152–1169 e1157, doi:10.1016/j.ccell.2023.04.011 (2023).
- 3 Qi, J. *et al.* Single-cell and spatial analysis reveal interaction of FAP+ fibroblasts and SPP1+ macrophages in colorectal cancer. *Nature communications* **13**, 1–20 (2022).
- 4 Magen, A. *et al.* Intratumoral dendritic cell-CD4(+) T helper cell niches enable CD8(+) T cell differentiation following PD-1 blockade in hepatocellular carcinoma. *Nat Med* **29**, 1389–1399, doi:10.1038/s41591-023-02345-0 (2023).
- 5 Litchfield, K. *et al.* Meta-analysis of tumor- and T cell-intrinsic mechanisms of sensitization to checkpoint inhibition. *Cell* **184**, 596–614 e514, doi:10.1016/j.cell.2021.01.002 (2021).
- 6 Chalabi, M. *et al.* Neoadjuvant immunotherapy leads to pathological responses in MMR-proficient and MMR-deficient early-stage colon cancers. *Nat Med* **26**, 566–576, doi:10.1038/s41591-020-0805-8 (2020).